Eocene nappe tectonics and late-Alpine extension in the central Anatolide belt, western Turkey — structure, kinematics and deformation history

Dissertation zur Erlangung des Grades
"Doktor der Naturwissenschaften"

am Fachbereich Geowissenschaften
der Johannes Gutenberg-Universität in Mainz

Klaus Gessner, geboren am 14.04.1967 in Schlitz

Mainz, im Mai 2000

Erklärung

Ich versichere hiermit, die vorliegende Arbeit selbständig und nur unter Verwendung der angegebenen Quellen und Hilfsmittel verfaßt zu haben.

Mainz, im Mai 2000 Klaus Rossner

Datum der Prüfung: 21. Juni 2000

Ruins of the Belevi mausoleum, a structure inferred to date back to the 3rd Century BC. Its base is an outcrop of marble from the Selçuk mélange displaying L_{A2} lineations.

‘It is a fascinating country, with a character of its own.’

George E. Bean in ’Turkey beyond the Maeander’, Ernest Benn Ltd., London 1972

Abstract

Structural analysis reveals that the Anatolide belt of western Turkey was assembled in the Eocene by top-to-S out-of-sequence thrusting of the Cycladic blueschist unit onto the Menderes nappes during greenschist-facies metamorphism.

The Cycladic blueschist unit in western Turkey contains relics of a prograde Alpine fabric (D_{A1}), which was overgrown by poikiloblastic chloritoid and kyanite during high-pressure metamorphism. This high-pressure mineral growth stage temporally overlapped with the onset of a consecutive deformation event (D_{A2}), which was associated with top-to-NE shearing during initial decompression. The subsequent greenschist-facies deformation (D_{A3}) is the first event that affected both the Cycladic blueschist unit and the Menderes nappes. The thrust contact between the Cycladic blueschist unit and the Menderes nappes is a D_{A3} shear zone, the Cycladic-Menderes thrust (CMT). Along the CMT, the Cycladic blueschist unit was juxtaposed with different thrust sheets of the Menderes nappes and thus defines the CMT as an out-of-sequence ramp structure, which cuts up-section towards the south. In the Cycladic blueschist unit, deformation fabrics associated with the CMT crosscut high-pressure structures.

In the Menderes nappes in the footwall, D_{A3} is well constrained by a regionally coherent deformation fabric with top-to-S kinematic indicators in the internal parts of the nappes and in shear zones, which define the nappe boundaries. Within the Çine nappe Proterozoic/Cambrian granitic rocks can be subdivided into older orthogneisses and younger metagranites. The deformation history of these granitic rocks documents two major deformation events. An early deformation event (D_{PA}) during amphibolite-facies metamorphism only affected the orthogneisses and predominantly top-to-NE shear-sense indicators associated with a NE-trending stretching lineation developed. The younger metagranites are deformed both by isolated D_{A3} shear zones, and by a major D_{A3} shear zone along the southern boundary of the Çine massif. D_{A3} shear zones are associated with a N-trending stretching lineation, which formed during greenschist-facies metamorphism. Kinematic indicators associated with this stretching lineation reveal a top-to-S sense of shear. The greenschist-facies shear zones cut the amphibolite-facies structures in the orthogneisses. Magmatic zircons from a metagranite, which crosscuts orthogneiss containing amphibolite-facies top-to-NE shear-sense indicators yielded an $^{207}Pb/^{206}Pb$ age of 547.2±1.0 Ma, which suggests that D_{PA} is of Proterozoic age. Such an age is corroborated by the observation that mid-Triassic granites of the Çine and Bozdag nappes lack D_{PA} structures. The younger, top-to-S fabrics are likely to be coeval with the first deformation event in the Bayındır nappe.

The lack of Alpine high-pressure fabrics below the CMT implies ~35 km of exhumation of the Cycladic blueschist prior to its Eocene emplacement on top of the Menderes nappes. The substantial differences in the pre-assembly tectonometamorphic histories of the Cycladic blueschist unit and the Menderes nappes contradict the model of a laterally continuous orogenic zone, in which the Menderes nappes are interpreted as the eastern extension of the Cycladic blueschist

unit.
Structural analysis of late Alpine brittle faulting and cooling age patterns provided by low-temperature thermochronological data reveal that the geometry of the Eocene nappe pile in the central Anatolide belt has been dramatically modified by Miocene to Recent core-complex formation. A large syncline structure in the central part of the Anatolide belt is related to rotation of two symmetrically arranged detachment system from an initially steep to a presently shallow orientation by a rolling-hinge mechanism. The bivergent detachment system delimits the Central Menderes metamorphic core complex (CMCC). According to the regional pattern of apatite fission-track ages, the CMCC started to form in the middle Miocene. Back-rotation of time lines of apatite-fission track ages and the regional foliation shows that upwarping of the footwalls to the detachments produced the syncline structure. Detachment faulting caused considerable topography across the CMCC, which suggests that the upper mantle was involved in this process.

Zusammenfassung

Strukturgeologische Untersuchungen belegen, daß die Anatoliden der Westtürkei im Eozän durch die Plazierung der Kykladischen Blauschiefereinheit entlang einer durchbrechenden Überschiebung auf die Menderes-Decken unter grünschieferfaziellen Metamorphosebedingungen entstanden.

Die kykladischen Blauschiefer in der Westtürkei enthalten Relikte eines prograden alpinen Gefüges (D_{A1}), welches hochruckmetamorph von Disthen und Chloritoid poikiloblastisch überwachsen wurde. Dieses Mineralstadium dauerte noch während des Beginns des nachfolgenden Deformationsereignisses (D_{A2}) an, welches durch NE-gerichtete Scherung und Dekompression charakterisiert ist. Die nachfolgende Deformation (D_{A3}) war das erste Ereignis, das beide Einheiten, sowohl die kykladische Blauschifereinheit als auch die Menderes-Decken, gemeinsam erfaßte. Der Überschiebungskontakt zwischen der kykladischen Blauschiefereinheit und den Menderes-Decken ist eine D_{A3}-Scherzone: die ‘Cycladic-Menderes Thrust’ (CMT). Entlang der CMT-Überschiebungsbahn wurden die kykladischen Blauschiefer gegen veschiedene Einheiten der MN plaziert. Die CMT steigt nach S zum strukturell Hangenden hin an und kann daher als eine durchbrechende Überschiebung entlang einer nach S ansteigenden Rampe betrachtet werden. In den kykladischen Blauschiefern überprägen D_{A3}-Strukturen, die im Zusammenhang mit der CMT stehen, hochdruckmentamorphe Gefüge.

In den Menderes-Decken, dem Liegenden der CMT, wird D_{A3} durch regional vebreitete Gefügeelemente dokumentiert, die im Zusammenhang mit S-gerichteten Schersinnindikatoren stehen. D_{A3}-Gefüge haben die Decken intern deformiert und bilden jene Scherzonen, welche die Decken untereinander abgrenzen. In der Çine-Decke können granitische Gesteine in Orthogneise und Metagranite unterteilt werden. Die Deformationsgeschichte dieser Gesteine dokumentiert zwei Ereignisse. Ein frühes amphibolitfazielles Ereignis erfaßte nur die Orthogneise, in denen vorwiegend NE-SW orientierte Lineare und NE-gerichtete Schersinnindikatoren entstanden. Die jüngeren Metagranite wurden sowohl durch vereinzelte D_{A3}-Scherzonen, als auch in einer großmaßstäblichen D_{A3}-Scherzone am Südrand des Çine-Massivs deformiert. In D_{A3}-Scherzonen sind die Lineare N-S orientiert und die zugehörigen Schersinnindikatoren zeigen S-gerichtete Scherung unter grünschieferfaziellen Bedingungen an. Diese grünschieferfaziellen Scherzonen überprägen die amphibolitfaziellen Gefüge in den Orthogneisen. Magmatische Zirkone aus einem Metagranit, der einen Orthogneiss mit Top-NE Gefügen durchschlägt, ergaben ein $^{207}Pb/^{206}Pb$-Alter von 547,2±1,0 Ma. Dies deutet darauf hin, daß D_{PA} proterozoischen Alters ist. Dies wird auch durch die Tatsache gestützt, daß triassische Granite in der Çine- und der Bozdag-Decke keine D_{PA}-Gefüge zeigen. Die jüngeren Top-S-Gefüge sind wahrscheinlich zur gleichen Zeit entstanden wie die ältesten Gefüge der Bayındır-Decke.

Das Fehlen von Hochdruck-Gefügen im Liegenden der CMT impliziert eine Exhumierung der kykladischen Blauschiefer von mehr ca. 35 km, bevor diese im Eozän auf die Menderes-Decken

aufgeschoben wurden. Die substantiellen Unterschiede bezüglich in der tektonometamorphen Geschichte der kykladischen Blauschiefer und der Menderes-Decken widersprechen der Modellvorstellung eines lateral kontinuierlichen Orogengürtels, nach der die Menderes-Decken als östliche Fortsezung der kykladischen Blauschiefer angesehen werden.

Die Analyse spröder spätalpiner Deformationsstrukturen und das regionale Muster mit Hilfe von Spaltspurdatierung modellierter Abkühlalter deuten darauf hin, daß die Struktur des Eozänen Deckenstapels durch miozäne bis rezente Kernkomplex-Bildung stark modifiziert wurde. Eine großmaßstäbliche Muldenstruktur im zentralen Teil der Anatoliden hat sich als Folge zweier symmetrisch angeordneter Detachment-Systeme von initial steilen zu heute flachen Orientierungen im Einflußbreich von 'Rolling Hinges' gebildet. Die Detachment-Störungen begrenzen den 'Central Menderes metamorphic core complex' (CMCC). Das Muster der Apatit-Spaltspuralter belegt, daß die Bildung des CMCC im Miozän begann. Durch die Rück-Deformierung von parallel zur Foliation konstruierten Linien gleicher Abkühlalter kann gezeigt werden, daß die Aufwölbung im Liegenden der Detachments zur Entstehung der Muldenstruktur führte. Das hohe topographische Relief im Bereich des CMCC ist eine Folge der Detachment-Störungen, was darauf hindeutet daß der obere Mantel in den Prozeß mit einbezogen gewesen ist.

Foreword

(i) Scope and layout of thesis

The work presented in this thesis aims to resolve the structure and kinematic evolution of the central Anatolide belt in western Turkey. The approach taken has been to systematically map and analyse deformation fabrics with respect to overprinting and cross-cutting relations. Wherever possible, fabric analysis has been linked to a framework of absolute ages provided by fossil evidence, lead isotope dating and fission-track thermochronology.

This thesis is divided into six Chapters: the introductory Chapter 1 is followed by three Chapters which each represent self-consistent research manuscripts, which have been submitted to scientific journals. A fifth Chapter summarises the conclusions of Chapters 2 through 4; Chapter 6 lists the references cited in the text.

In the Chapter 1 earlier work is reviewed which is considered to be relevant to the regional tectonic framework of central western Turkey. As the consecutive Chapters contain detailed introductory sections themselves, only a general picture is given to avoid unneccessary repetition.

Chapter 2 deals with fabric overprint and cross-cutting in the granitiod rocks of the central Anatolide belt and provides constraints on the age of pre-Alpine deformation. Chapter 2 is largely identical with the revised version of a manuscript submitted to ‘International Journal of Earth Science (Geologische Rundschau)’ entitled ‘Tectonic significance of deformation patterns in granitoid rocks of the Menderes nappes, Anatolide belt, southwest Turkey.’ Co-authors are Sandra Piazolo, Talip Güngör, Uwe Ring, Alfred Kröner and Cees W. Passchier.

The subject of Chapter 3 is to constrain the sequence of the multiphase Alpine deformation and the contact between the Cycladic blueschist unit with the Menderes nappes. This Chapter has been submitted to ‘Tectonics’ in March 2000 as a manuscript entitled ‘The Cyclades in Turkey: Evidence for Eocene post-high-pressure emplacement of the Cycladic blueschist unit onto the Menderes nappes, Anatolide belt, western Turkey’. Co-authors are Uwe Ring, Cees W. Passchier and Talip Güngör.

Chapter 4 addresses structural overprint during late Alpine core complex formation and the cooling history of the Anatolide belt and is largely identical with a manuscript entitled ‘An active bivergent rolling-hinge detachment system: The Central Menderes metamorphic core complex in western Turkey’, which has been submitted to ‘Geology’ in May 2000.

It should be noted that all of the above manuscripts have been prepared together with co-authors and some of the data presented have not been produced by the author of this thesis. This is the case for the $^{207}Pb/^{206}Pb$ zircon-age of Chapter 2, which has been produced by Alfred Kröner (Johannes Gutenberg-Universität Mainz), as well as for the low-temperature thermochronological data and modeling in Chapter 4, which is the work of Christopher Johnson (Imperial College, London). Additional field work in the central Çine Massif has been carried out by Sandra Piazolo and Arno Wamsler.

(ii) Acknowledgements and dedication

My special thanks go to my supervisors who have been there when I needed them - in the field and in Mainz. Without the help of my turkish colleagues I would have been lost in many ways in western Turkey. It has been suspected that the slaughtering of ca. 20 million Turkish rams at Kurban Bayramı in 1998 signifiantly helped the discovery of the D_{A2} and D_{A1} events, but don't take my word for it!

Many thanks to all my colleagues in Mainz. My parents as well as my mother and father-in-law are thanked for assitance in a great many ways.

This thesis is dedicated to my wife and son, which are thanked for a million *really* important things *beyond* Geology.

Index

Chapter 1

Introduction

The Anatolide belt of western Turkey, which is part of the Alpine-Himalayan orogenic system, formed as a consequence of Eocene collision tectonics. The lowermost tectonic units of the Anatolide belt are the Menderes nappes [*Ring et al.,* 1999a], overlain by the Cycladic Blueschist unit, the Lycian nappes [*de Graciansky*, 1972] and the Vardar-Izmir-Ankara zone [*Sengör and Yilmaz*, 1981]. The Vardar-Izmir-Ankara zone is the suture of the northern branch of Neotethys. To the north the suture zone is overlain by the Sakarya continent, which together with the Rhodope Massif and the Pontides forms the Internal zone (the 'Pontide arc system' of *Sengör and Yilmaz* [1981]) of the Hellenide-Anatolide orogen.

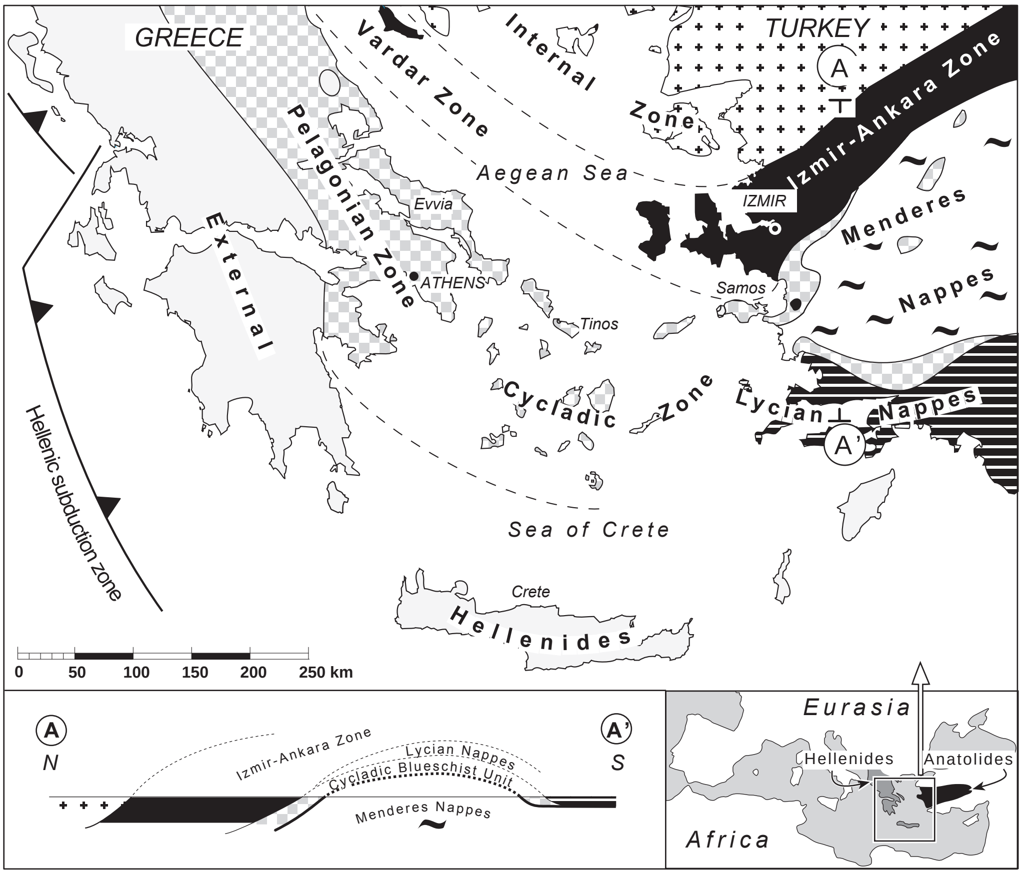

Figure 1.1:
Map and cross-section showing the major tectonometamorphic units of the Hellenide-Anatolide orogenic belt. The Cycladic blueschist unit makes up the largest part of the Cycladic zone in the Hellenidesand extends into the upper levels of the Anatolide belt. Cross section A-A' shows the window character of the Anatolide belt. Inset shows location of main map in the Mediterranean and regional extent of the Hellenides and the Anatolides.

1.1 Terminology

The term 'Anatolide belt' refers to the 'Anatolides' of *Ketin* [1966] (see also *Sengör and Yilmaz* [1981]), and is used in this thesis for a part of the Turkish Alpides, which formed during Eocene thrusting of the Cycladic blueschist unit onto the Anatolian microcontinent. The widely used term 'Menderes Massif' [*Paréjas*, 1941], (the 'Menderes Massif *s. str.*' of *Sengör et al.* [1984]) has been avoided, because in a genetic sense it misleadingly implies a coherent basement complex rather than a pile of nappes with very different tectonometamorphic histories. The term 'massif' is instead used with respect to the late-Alpine extension in order to outline the rigid and 'passive' character of the Çine Massif and the Gördes Massif, which frame the Central Menderes metamorphic core complex (Chapter 4; see also Fig. 2.1, Fig. 4.2).

1.2 Earlier work on the architecture and tectonic evolution of the Anatolide belt

The window character of the Anatolide belt (Fig. 1.1) had first been stressed by *Dürr* [1975], who suggested that, like the Cycladic islands, the 'Menderes-Kristallin' was characterised by a tri-partite onion-shaped architecture consisting of a 'gneissic core', a 'Palaeozoic inner cover' of mica-schist and a 'Mesozoic outer marble cover'. Based on the apparent regional similarity, *Dürr et. al.* [1978] incorporated the metamorphics of Attica, the Cyclades and western Turkey into a continuous 'Median Aegean Crystalline belt' with a basement of inferred Precambrian age remobilised during Alpine deformation. Following the correlation of *Dürr et al.* [1978], *Sengör and Yilmaz* [1981] and *Sengör et al.* [1984] postulated an Anatolide-Tauride microcontinent, which during the Permo-Mesozoic had been continuous with Apulia and was connected to Africa through Sicily. According to the palaeogeographic reconstruction of *Sengör and Yilmaz* [1981] the Anatolide-Tauride microcontinent was bounded by a northern and a southern branch of Neotethys which had opened in the Triassic. Incipient Alpine convergence is documented by late Cretaceous ophiolite obduction [*de Graciansky*, 1972; *Bernoulli et al.*, 1974] and according to *Sengör and Yilmaz* [1981] resulted in south-propagating imbrication of the Anatolide-Tauride microcontinent during its Eocene collision with the Sakarya continent. In this context *Sengör and Yilmaz* [1981] and *Sengör et al.* [1984] have attributed an Eocene to late Oligocene 'Main Menderes Metamorphism' to burial of the Anatolide belt during collision-related thrusting of the Lycian nappes. The gneisses and granitoids of the 'gneissic core' were inferred to display relics of Pan-African collision tectonics and it was argued that these rocks had been continuous with the Pan-African basement of Egypt and the Levantine coast [*Sengör et al.*, 1984]. *Sengör et al.* [1984] further suggested that the protolith of the Palaeozoic 'cover schist' [*Dürr*, 1975] had been sedimented onto this Pan-African basement and suggested the existence of a main supra-Pan-African unconformity between core and cover.

In studies focused on a large-scale south-dipping shear zone along the contact between granito-

id gneisses and schist in the southern part of the Anatolide belt (hereafter named 'Selimiye shear zone'), *Bozkurt et al.* [1993a, 1993b] as well as *Bozkurt and Park* [1994] questioned the existence of the main supra-Pan-African unconformity. Furthermore, these authors along with *Erdogan* [1992] argued against the core-cover interpretation of *Dürr* [1975], because along the southern margin of the 'gneissic core' the protolith of the granitoid gneiss intruded schists, which by lithostratigraphic correlation were generally assumed to be Paleozoic in protolith age. Taking into account the present orientation of the Selimiye shear zone, its generally down-dip top-to-S kinematic indicators and a presumed ductile-through-brittle evolution, *Bozkurt et al.* [1993a, 1993b] and *Bozkurt and Park* [1994] interpreted the Selimiye shear zone to be extensional and the granitoid protoliths to have been emplaced during an Oligocene post-orogenic collapse.
Isotopic dating of the granite and the schist in the Selimiye shear zone by *Hetzel and Reischmann* [1996] however indicated that the granite intruded at ~546 Ma and that both the granite and the gneiss had cooled through the muscovite cooling temperature between 43-37 Ma. This intrusion age inferred the existence of Proterozic schists. *Hetzel and Reischmann* [1996] also questioned the ductile-through-brittle evolution in the Selimiye shear zone of *Bozkurt et al.* [1993a, 1993b] and *Bozkurt and Park* [1994] for which they found no supportive evidence. *Collins and Robertson* [1998] considered Eocene thrusting within the Lycian nappes to be coeval with the peak metamorphism of the Anatolide belt and the development of the Selimiye shear zone for which they consequently favoured a contractive over an extensional setting. The extensional versus contractional interpretation of this shear zone is an important keystone to the tectonometamorphic evolution of the Anatolide belt and will be discussed in more detail in Chapters 2 and 3.

An Alpine contractional event associated with top-to-N kinematic fabric elements under greenschist to amphibolite facies conditions which had imbricated 'core' and 'cover' was suggested by *Hetzel et al.* [1998]. These authors claimed that fabrics in granitoid gneisses of the 'gneissic core' may be as old as Proterozoic, as these were intruded by an undeformed granite which yielded an intrusion age of 551 Ma. Meanwhile for many granitoid gneisses and metapelites of the Anatolide belt Proterozoic/Cambrian intrusion ages have been determined (e.g. *Dannat* [1997]; *Reischmann and Loos* [1999]; *Hetzel et al.* [1998]). Intrusion relationships and crosscutting of kinemtic fabric elements in the granitoid rocks are the main subject of Chapter 2, which also contains a more detailed review of recently published isotopic age data. Alpine contraction was also evident from an inverted metamorphic field gradient across the northern central area of the Anatolide belt [*Izdar*, 1971; *Dora et al.*, 1995; *Hetzel*, 1995; *Hetzel et al.*, 1995a; *Lackmann,* 1997; *Gessner et al*., 1998; *Partzsch et al.,* 1998]. *Gessner et al*. [1998] furthermore argued that marble-bearing micaschists occur in two different structural levels, above and below the granitoid gneisses, and questioned the existence of a continuous 'cover' in the sense of *Dürr* [1975] and *Dora et al*. [1997].

The recent discovery of high-pressure metamorphic relics in the Anatolide belt further complicated the pictue. The high-pressure rocks occur in two structural levels. Granitic gneisses contain eclogitic metabasites, which are likely to be pre-Alpine in age [*Oberhänsli et al*., 1997] (see also Chapter 2). Blueschist facies metapelites [*Candan et al.*, 1998] and eclogitic relics in a metaolistostrome [*Oelsner et al.*, 1999] occur in the upper structural levels of the nappe pile, which are likely to be continuous with the Cycladic blueschists on Samos [*Candan et al.*, 1998; *Ring et al.*, 1999b]. These similarities have led *Ring et al.* [1999a] to propose that the upper levels of the Anatolide belt (roughly identical with the 'marble cover' of Dürr, 1975] were an overthrust part of the Cycladic blueschist belt, while the lower level, which they named 'Menderes nappes', represented an exotic block within the Eastern Mediterranean area. Structural and metamorphic evidence for this subdivision and implications for regional tectonic reconstructions are discussed at length in Chapter 3.

Late Alpine extension in the Aegean and western Turkey has been attributed to a westward expulsion (e.g. *MacKenzie* [1972, 1978]; *Dewey and Sengör* [1979]) or counter-clockwise rotation [*Le Pichon*, 1995] of the Anatolian microplate towards the rapidly extending Aegean region following the early to middle Miocene collision of Arabia and Eurasia [*Sengör and Yilmaz*, 1981]. *Gautier et al.* [1996] and *Hatzfeld et al.* [1996] further consider gravitational collapse of the Aegean to play an important role.

Extensional unroofing of the Anatolide belt commenced in the early Miocene, which is documented by volcanic rocks, which unconformably overlie the Menderes nappes [*Becker-Platen*, 1971]. *Hetzel et al.* [1995a, 1995b] constrained extension and cooling for the northern central Anatolide belt to the early Miocene by isotopic dating of a syn-extensional granitoid intrusion into a large scale normal-sense ductile shear zone. The line of evidence presented by *Hetzel et al.* [1995a, 1995b] includes overprinting relations of kinematic fabric elements, which led the authors to propose symmetric crustal extension expressed by a bivergent down-dip shear zone geometry within the northern central part of the Anatolide belt. This interpretation is questioned by the interpretation of overprinting of microstructures presented in Chapter 3 of this thesis, which strongly suggests that the greenschist facies top-to-S kinematic indicators in the area are related to Eocene contraction rather than representing the southern leg of a Miocene bivergent extension structure. There is agreement, however, about the bivergent nature of late Alpine extension and it will be shown in Chapter 4 that its influence on the structure of the Alpine nappe pile has been quite dramatic since the middle Miocene.

Chapter 2

Pan-African deformation fabrics and their Alpine overprinting in granitic rocks of the Menderes nappes

This Chapter is largely identical with the revised version of a manuscript submitted to 'International Journal of Earth Science (Geologische Rundschau)' entitled 'Tectonic significance of deformation patterns in granitoid rocks of the Menderes nappes, Anatolide belt, southwest Turkey.' Co-authors are Sandra Piazolo, Talip Güngör, Uwe Ring, Alfred Kröner and Cees W. Passchier.

2.1 Abstract

Deformation fabrics in Proterozoic/Cambrian granitic rocks of the Çine nappe, and mid-Triassic granites of the Çine and Bozdag nappes constrain aspects of the tectonometamorphic evolution of the Menderes nappes of southwest Turkey. Based on intrusive contacts and structural criteria, the Proterozoic/Cambrian granitic rocks of the Çine nappe can be subdivided into older orthogneisses and younger metagranites. The deformation history of the granitic rocks documents two major deformation events. An early deformation event (D_{PA}) during amphibolite-facies metamorphism only affected the orthogneisses and predominantly top-to-NE shear-sense indicators associated with a NE-trending stretching lineation developed. The younger metagranites are deformed both by isolated shear zones, and by a major shear zone along the southern boundary of the Çine submassif. This deformation event is referred to as D_{A3}. D_{A3} shear zones are associated with a N-trending stretching lineation, which formed during greenschist-facies metamorphism. Kinematic indicators associated with this stretching lineation reveal a top-to-S sense of shear. The greenschist-facies shear zones cut the amphibolite-facies structures in the orthogneisses. $^{207}Pb/^{206}Pb$ dating of magmatic zircons from a metagranite, which crosscuts orthogneiss containing amphibolite-facies top-to-NE shear-sense indicators testifies that D_{PA} occurred before 547.2±1.0 Ma. Such an age is corroborated by the observation that mid-Triassic granites of the Çine and Bozdag nappes lack D_{PA} structures. The younger, top-to-S fabrics formed most likely as a result of top-to-S Alpine nappe stacking during the collision of the Sakarya continent with Anatolia in the Eocene.

2.2 Introduction

During the last decade, tectonic studies in the Anatolide belt of southwest Turkey have focussed on late Alpine N-S-oriented extensional deformation, which dominates all older structures and accomplished part of the exhumation of the Menderes nappes [*Hetzel and Ring,* 1993; *Bozkurt and Park,* 1994, 1997a, 1997b; *Hetzel et al.,* 1995a, 1995b; *Verge*, 1995; *Hetzel and Reischmann,* 1996; *Emre and Sözbilir*, 1997; *Isik and Tekeli*, in press]. Structures that predate late-orogenic extension [*Lackmann*, 1997; *Collins and Robertson*, 1998; *Gessner et al.,* 1998; *Hetzel et al.,* 1998; *Partzsch et al.,* 1998; *Ring et al.*, 1999a] suggest a complex history of crustal shortening, the timing of which is largely unknown. *Lackmann* [1997], *Gessner et al.* [1998] and *Hetzel et al.* [1998] stressed the regional importance of top-to-NE kinematic indicators in the central part of the Menderes nappes and attributed them to early Tertiary nappe stacking. Nonetheless, this interpretation is in contrast to existing regional tectonic models [*Sengör and Yilmaz,* 1981; *Sengör et al.*, 1984; *Collins and Robertson*, 1998]. *Sengör et al.* [1984] argued that the Menderes nappes had been deformed and metamorphosed during the early Tertiary collision of the Sakarya continent with Anatolia and interpreted the Menderes nappes to lie in the footwall of the southward propagating Lycian nappes. The Lycian nappes consist of carbonate platform sediments of Neotethys, which are situated tectonically beneath ophiolitic rocks. The Lycian nappes are interpreted to root in the Izmir-Ankara suture zone to the north of the Menderes nappes [*Collins and Robertson*, 1997] (Fig. 2.1). *Collins and Robertson* [1998] defined the Lycian nappes as a large-scale, thin-skinned thrust system and showed that within the Lycian nappes, polyphase, top-to-S thrust-sheet translation at upper crustal levels occurred from the late Cretaceous to the early Miocene. Following *Sengör et al.* [1984] and *Collins and Robertson* [1998], any major tectonic event related to Tertiary crustal convergence in the Menderes nappes should be characterised by top-to-S shearing.

As an attempt to reconcile the regional model of *Sengör et al.* [1984] with field evidence, a sequence of deformation structures in orthogneisses and metagranites is described from the central and southern Menderes nappes. These rocks are especially suitable for distinguishing pre-Alpine from Alpine tectonic events because their age is well constrained by radiometric dating [*Hetzel and Reischmann*, 1996, Dannat, 1997, *Reischmann and Loos*, 1999] (Table 1.1) and the deformation fabrics are then interpreted by suggesting a chronology of tectonometamorphic events and their corresponding kinematics.

2.3 Setting

A number of late Tertiary to Recent graben divide the Anatolide belt of southwest Turkey into the Gördes Massif, the Central Menderes metamorphic core complex and the Çine Massif. This study focuses on the latter two (Fig. 2.1).

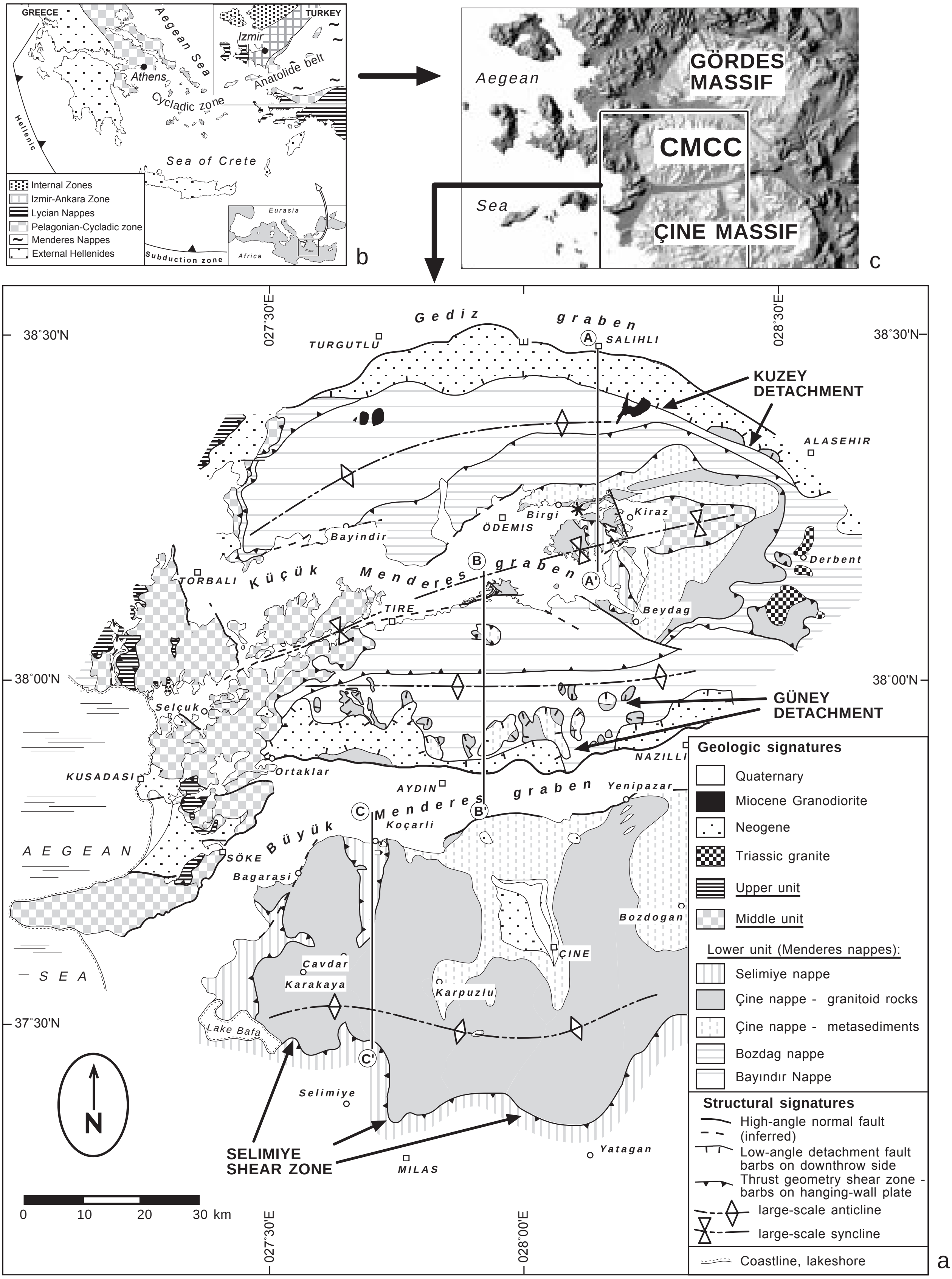

Figure 2.1: (a) Geologic map of the Anatolide belt of southwest Turkey based on *Candan and Dora* [1998], *Scotford* [1969], *Güngör* [1998], *Hetzel et al.* [1998] and own observations. (b) Generalised tectonic map of the Aegean and adjacent mainlands showing major tectonic units, present-day Hellenic subduction zone and location of main map. (c) Alternation of narrow E-W trending graben and 'massifs' resulting from neotectonic block faulting within the western Anatolian extensional province [*Hancock and Barka*, 1987; *Cohen et al.*, 1995]. Three graben cut the metamorphic complex in the area, the Gediz graben, the Küçük Menderes graben and the Büyük Menderes graben.

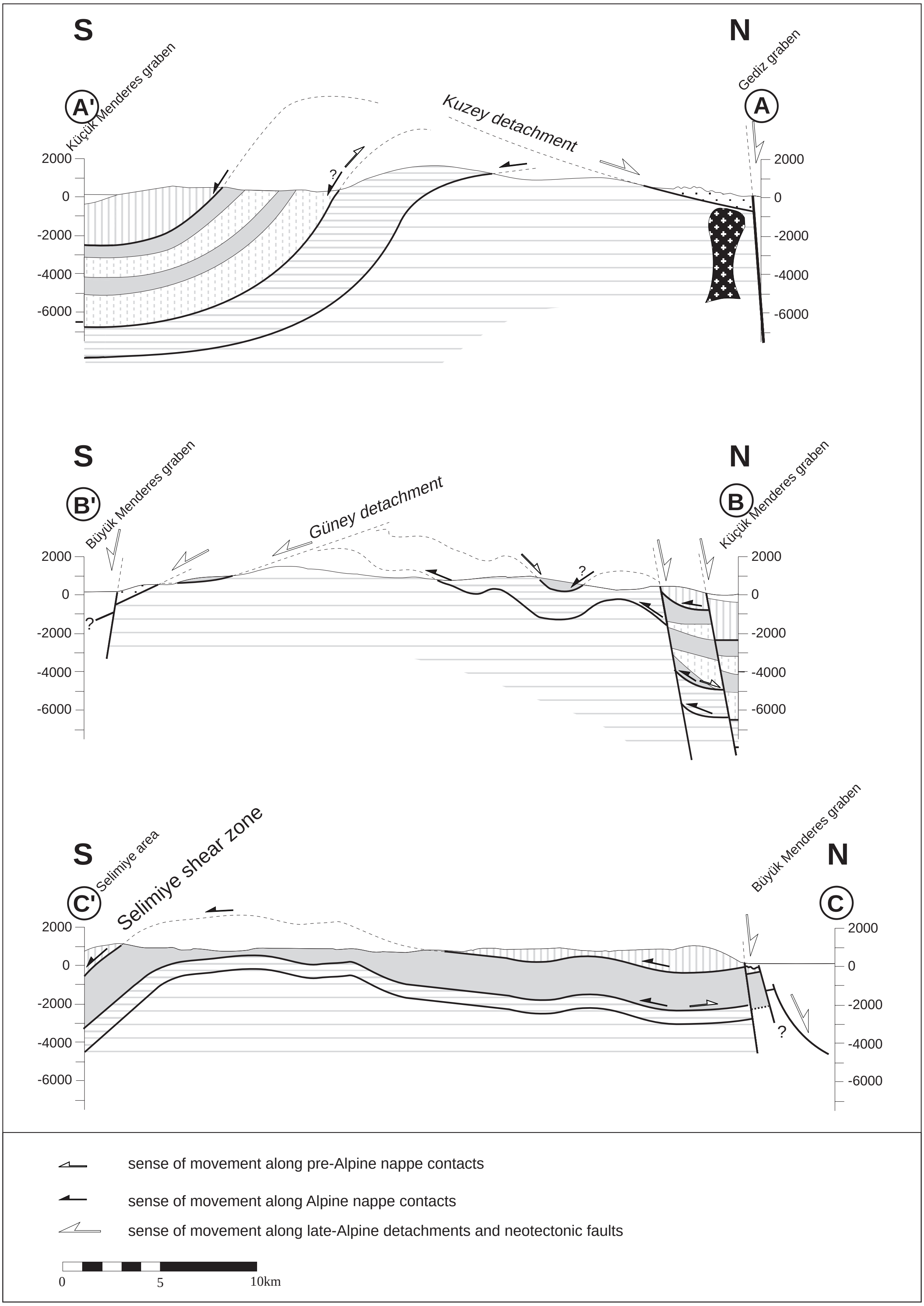

Figure 2.2: Geologic cross sections along section lines A—A', B—B' and C—C' as illustrated in Figure 2.1. Foliation planes and fold axes are projected into the section plan in order to extrapolate large-scale surface structures to greater depths, which enhances the geometric viability. Fill patterns correspond to Figure 2.1.

Table 2.1: Age data of granitic rocks from the Menderes nappes

Lithology and locality	Age [Ma]	Method	Authors
Metagranites and orthogneisses, entire Menderes nappes, Izmir-Ankara Zone	2555-1740;	$^{207}Pb/^{206}Pb$ single zircon evaporation	Reischmann et al. (1991)
Weakly deformed granite in Selimiye shear zone, southern Çine submassif	546.2±1.2	$^{207}Pb/^{206}Pb$ single zircon evaporation	Hetzel and Reischmann (1996)
Metagranites and orthogneisses, entire Menderes nappes	528±4.3 —541.4±2.5 659±7, 563±3 —546±5	$^{207}Pb/^{206}Pb$ single zircon evaporation $^{207}Pb/^{206}Pb$ single zircon evaporation	Dannat (1997), Reischmann and Loos (1999)
Weakly deformed granite, Birgi area, Ödemis submassif	551±1.4	$^{207}Pb/^{206}Pb$ single zircon evaporation	Hetzel et al. (1998)
Granites, Derbent area, Ödemis submassif	240.3±2.2; 226.5±6.8 ~240-250	^{207}Pb-^{206}Pb single zircon evaporation ^{207}Pb-^{206}Pb single zircon evaporation	Dannat (1997), Koralay et al. (1998)
Egrigöz granite, Gördes submassif	~20	$^{207}Pb/^{206}Pb$ single zircon evaporation	Reischmann et al. (1991)
Turgutlu and Salihli granodiorites, Ödemis submassif	19.5±1.4; 12.2±0.4 - 13.1±0.2	$^{40}Ar/^{39}Ar$ – amphibole isochron; $^{40}Ar/^{39}Ar$ – biotite plateau age	Hetzel et al. (1995a)

Table 2.2: Zircon morphology and Pb isotopic data from zircon evaporation

Sample	Zircon colour and morphology	Mass scans[1]	Evaporation temperature	Mean $^{207}/Pb/^{206}Pb$ ratio and 2σm error	$^{207}Pb/^{206}Pb$ age and 2σm error[3]
MM99-26	clear, euhedral, long-prismatic	227	1595 °C	0.05846±0.0002	547.2±1.0[3]

[1]Number of $^{207}Pb/^{206}Pb$ ratios evaluated for age assessment.

[2]Observed mean ratio corrected for non-radiogenic Pb; error based on uncertainties in counting statistics.

[3]Error enhanced to reproducibility of internal standard (for details see Kröner and Hegner 1998).

2.3.1 Architecture of the Anatolide belt in southwest Turkey

Traditionally the Anatolide belt has been interpreted as the eastern lateral continuation of the Cycladic zone [*Dürr et al.*, 1978]. These authors based their regional-scale correlation on litho-stratigraphic comparisons, proposing that an old crystalline core is overlain by Paleozoic and Mesozoic cover series with metamorphic grade decreasing up section in both the Anatolide belt and the Cycladic zone. This long-standing view has been challenged by recent geochronologic studies, which show marked differences in the age of the basement of the Anatolide belt and the Cycladic zone, indicating that the basement of the Cycladic zone and the Anatolide cannot be correlated. *Ring et al.* [1999a] proposed that two different units, the Cycladic blueschist unit and the underlying Menderes nappes make up the Anatolide belt.

In the Menderes nappes, pronounced magmatic activity occurred at the Proterozoic/Cambrian boundary [*Hetzel and Reischmann*, 1996; *Dannat*, 1997; *Reischmann and Loos*, 1999]. Minor magmatic events took place in the middle Triassic [*Dannat*, 1997; *Koralay et al.*, 1998] and the Miocene [*Hetzel et al.*, 1995a]. In the Cycladic zone, the granitic basement is of Carboniferous age [*Reischmann*, 1997; Engel and Reischmann, 1998]. In addition, there are Triassic intrusions [Reischmann, 1997, *Ring et al.*, 1999b] and prominent Miocene to recent magmatic activity in the Cycladic zone [*Altherr et al.*, 1982; *Dixon and Robertson*, 1984]. *Ring et al.* [1999a] (also see Chapter 3) supplied further evidence for major differences between the Anatolide belt and the Cycladic zone by showing that only the upper parts of the Anatolide belt can be correlated with the Cycladic zone. *Ring et al.* [1999a] proposed to subdivide the Anatolide belt into three major tectonic units (Fig. 2.1). (1) The Izmir-Ankara Zone and the Lycian nappes form the upper unit. (2) The Dilek nappe and the Selçuk melange form the middle unit. The upper and middle units can be correlated with tectonic units in the Cycladic zone. (3) The lower unit, referred to as the Menderes nappes, consists in ascending order of a lower metasedimentary succession, the Bayındır nappe, a metapelitic succession with abundant amphibolite and few marble lenses named the Bozdag nappe, a Proterozoic/Cambrian basement succession named the Çine nappe and an upper metasedimentary succession of intercalated marble and calcschist, the Selimiye nappe. The Menderes nappes have no counterpart in the adjacent Cycladic zone.

According to this subdivision the structurally lowest unit exposed in the Menderes nappes, the Bayındır nappe, is only deformed by one major Alpine tectonometamorphic event, whereas in the overlying Bozdag, Çine and Selimiye nappes pre-Alpine and Alpine events are documented. The subdivision of *Ring et al.* [1999a] is used in this study and illustrated in Figures 2.1 and 2.2.

2.3.2 Tectonic contacts within the Menderes nappes

Tertiary greenschist-facies shear zones separate individual nappes within the Menderes nappes (Figs. 2.1 and 2.2). The contact of the Bayındır nappe and the Bozdag nappe will be described in detail in Chapter 3. The few good outcrops along this contact are characterised by chlorite-bearing phyllitic to phyllonitic lithologies with complex refolded fabrics and a top-to-S sense of shear. The shear-sense indicators are overgrown by albite porphyroblasts, which commonly obscure earlier mylonitic fabrics.

Within the Bozdag nappe, a penetrative foliation and a NE-trending stretching lineation formed under prograde amphibolite-facies metamorphic conditions [*Lackmann*, 1997; *Hetzel et al.*, 1998]. Kinematic indicators associated with this stretching lineation show a top-to-NE sense of shear [*Hetzel et al.*, 1998]. The amphibolite-facies fabrics are cut by isolated greenschist facies shear zones [*Hetzel et al.*, 1998]. These shear zones produced a shear-band foliation and a N-trending stretching lineation. Associated with this stretching lineation are asymmetric fabric elements indicating a top-to-S sense of shear. The retrograde fabrics dominate over the prograde fabrics towards the contact between the Bozdag nappe and the overlying Çine nappe. In the Derbent area, this contact is characterised by asymmetric greenschist-facies top-to-S shear-bands in the Çine and Bozdag nappes. In the Bozdag nappe in the vicinity of the nappe contact, no relics of the earlier amphibolite-facies fabric are preserved. In contrast, an early amphibolite-facies schistosity is preserved in orthogneisses of the Çine nappe. A mid-Triassic granite in the Derbent area (Fig. 2.1a), shows a stitching relationship with the nappe contact between the Bozdag and Çine nappes. This suggests that the Bozdag/Çine nappe contact originally formed before the intrusion of the mid-Triassic granite under amphibolite-facies conditions and was reworked during Tertiary greenschist-facies deformation.

The Selimiye nappe tectonically overlies the Çine nappe in the central and southern Anatolide belt (Figs 2.1 and 2.2). This is well documented along the southern margin of the Çine Massif where the large-scale south-dipping ‘Selimiye shear zone’ (see below) of pre-late Eocene age [*Hetzel and Reischmann*, 1996] is exposed. In the Selimiye shear zone, asymmetric fabric elements indicate a top-to-S sense of shear [*Hetzel and Ring*, 1993; *Bozkurt and Park*, 1994; *Hetzel and Reischmann*, 1996]. Within the Selimiye nappe, *Bozkurt* [1996] reported relics of an earlier deformation event, which was characterised by a top-to-NE sense of shear. *Bozkurt and Park* [1994] and *Hetzel and Reischmann* [1996] interpreted the Selimiye shear zone as a crustal-scale extensional shear zone, whereas *Collins and Robertson* [1998] and *Ring et al.* [1999a] argued that the Selimiye shear zone is a thrust.

2.3.3 Late Alpine detachments

Southeast of Salihli and north of Aydın, isolated klippen of the Çine nappe occur in the hangingwall of two low-angle normal-fault systems related to late-orogenic extension (Fig. 2.1). These fault systems are exposed at the northern and southern margins of the Ödemis submassif and were named 'Kuzey detachment' and 'Güney detachment', respectively by *Ring et al.* [1999a] Late Alpine brittle faulting will be treated in detail in Chapter 4.

2.4 Granitic rocks of the Menderes nappes

The age of granitic intrusions in the Menderes nappes has been constrained by various geochronologic studies [*Reischmann et al.*, 1991; *Hetzel et al.*, 1995a; *Hetzel and Reischmann*, 1996; *Dannat*, 1997; *Hetzel et al.*, 1998; *Reischmann and Loos*, 1999] (Table 2.1). The data show that Proterozoic/Cambrian magmatic activity occurred in two distinct pulses at 550-570 Ma and at about 530 Ma, respectively. The Proterozoic/Cambrian intrusives occur only in the Çine and the Selimiye nappe; they will be referred to as the Proterozoic/Cambrian granitoids in the remainder of the thesis. According to *Dannat* [1997], these granitoids are peraluminous, strongly differentiated S-type granodiorites, tonalites and diorites. A subdivision of the granitic rocks into orthogneisses and metagranites will be introduced below.

Triassic granites occur in the eastern part of the Ödemis submassif and intrude rocks of the Çine and Bozdag nappes, respectively. The geochemistry of these granites classifies them also as highly differentiated, peraluminous granites [*Dannat*, 1997]. Furthermore, Miocene granites occur in the Ödemis and Gördes submassifs [*Hetzel et al.* 1995b].

2.4.1 Intrusive contacts

In the Çine nappe, the Proterozoic/Cambrian granitoids show abundant intrusive contacts towards metapelitic and migmatic gneisses, and with quartzofeldspathic metasediments (Fig. 2.3). Furthermore, intrusive relationships exist between different granitoid lithologies in the Çine nappe. Intrusive contacts between Proterozoic/Cambrian granitoids and garnet-bearing metapelite of the Selimiye nappe are known from the Lake Bafa area [*Erdogan and Güngör*, 1992; *Hetzel and Reischmann*, 1996].

The mid-Triassic granites show intrusive contacts with metapelites of the Bozdag nappe in the Derbent area (Fig. 2.4). *Candan* [1998, pers. comm.] also reported intrusive contacts of the granites with orthogneisses of the Çine nappe. The Miocene granites of the Ödemis submassif intruded into the Bayındır nappe [*Hetzel et al.*, 1995a].

2.4.2 Subdivision of the Proterozoic/Cambrian granitic rocks in the Çine nappe

The subdivision of granitic rocks in the Çine nappe in 'older' orthogneisses and 'younger' metagranites is based on structural characteristics and on intrusion relations. A discrimination between orthogneisses and metagranites represents a simplification of the overall appearance of the granitoid protoliths. The terms 'orthogneiss' and 'metagranite' are used in a categorical rather than a descriptive sense. The typical appearance of an orthogneiss in the Menderes nappes is that of a protomylonite to mylonite with 'augen'-shaped feldspar porphyroclasts. However, due to heterogeneous deformation, some orthogneisses are only weakly deformed. Some of these orthogneisses have been dated at 563-546 Ma [*Reischmann and Loos*, 1999]. The metagranites on the other hand are, in general, much less deformed than the orthogneisses and only display isolated greenschist-facies shear zones, which formed during metamorphism. As will be shown below, the orthogneisses of the Çine nappe are, like the mica schists of the Bozdag nappe, deformed by two consecutive sets of deformation fabrics. In contrast, the metagranites characteristically show only the second set of structures.

Both sets of granitoids of the Çine nappe formed during a series of intrusion stages. This is documented in the field by intrusive contacts between granitoids or xenoliths of earlier granitoids in later ones. It is beyond the scope of this study to resolve the number of intrusive stages within the granitoids, but it is important to note that the metagranites do not show the early structures and in places definetely intrude the orthogneisses.

2.5 Deformation of the Proterozoic/Cambrian granitoids

It is possible to distinguish structures, that formed during amphibolite-facies metamorphism from structures, which formed under greenschist-facies conditions. This distinction is based on overprinting criteria and the different degree of metamorphism under which the structures formed. The metamorphic criterion can be used because the individual nappes do not show pronounced regional variations in metamorphic grade. To constrain the metamorphic conditions during deformation, temperature-sensitive reaction textures within the foliation and the deformation behaviour of potassium feldspar have been used. Fabrics in which potassium feldspar dynamically recrystallised are likely to have been formed above 500°C [*Voll*, 1976; *Tullis and Yund*, 1985, 1987, 1991].

The amphibolite-facies structures are associated with kinematic indicators, which show a dominantly top-to-NE shear sense, although there are regional variations in the sense of shear. For reasons introduced above, this deformation will be referred to as D_{PA} (where the suffix 'PA' denotes pre-Alpine). The greenschist-facies event will be referred to as the D_{A3} deformation (the suffix A3 denotes a third Alpine deformation event; note that D_{A1} and D_{A2} refer to Alpine high-pressure fabric elements in the middle unit). A more detailed description of the Alpine deformation history is given in Chapter 3. Kinematic indicators of the greenschist-facies D_{A3} structures show a consistent top-to-S shear sense.

2.5.1 Amphibolite-facies structures (D_{PA})

The orthogneisses have a protomylonitic to mylonitic foliation (S_{PA}) consisting of biotite and/or white mica. Originally magmatic potassium feldspar and plagioclase form porphyroclasts, which are up to several centimetres in diameter, are deformed by dynamic recrystallisation and frequently form core-and-mantle structures. Biotite grains are recrystallised with their [001]-planes oriented subparallel to S_{PA}. Less frequent, kinked relic grains of biotite with minor recrystallised rims exist with [001]-planes oriented at high angles to the foliation. In aluminium-rich orthogneisses, S_{PA} is formed by biotite that grows at the expense of millimetre to centimetre-size garnets (Fig. 2.5).

In S_{PA} a regionally consistently NE-trending stretching lineation (L_{PA}) is developed (Fig. 2.6). Foliation and lineation form LS- or L-type tectonites. Elongated aggregates of recrystallised feldspar, quartz rods and elongated aggregates of recrystallised biotite grains form the stretching lineation. Recrystallised K-feldspar grains grew parallel to L_{PA} between boudinaged and displaced porphyroclasts (Fig. 2.7). These recrystallised grains range from tens to hundreds of microns in diameter.

Asymmetric deformation fabrics useful for kinematic analysis are frequently developed in the orthogneisses. This includes asymmetric recrystallised tails around feldspar porphyroclasts (sigma-type objects sensu *Passchier and Simpson* [1986]) and C- and C'-type shear bands [*Berthé et al.*, 1979] at the decimetre scale. The kinematic interpretation of asymmetric fabric elements [*Passchier and Simpson*, 1986; *Hanmer and Passchier*, 1991] reveals regional variations in shear sense (Fig. 2.8). North of the Büyük Menderes graben, top-to-NE shear-sense indicators (Fig. 2.9) dominate. At the northwestern margin of the Çine submassif, symmetric fabric elements, like symmetric strain shadows around feldspar and symmetric foliation boudinage with 'fish-mouth' quartz pods occur (Fig. 2.10 and 2.11) together with minor top-to-NE kinematic indicators (Fig. 2.8). In the central Çine submassif, both top-to-NE and top-to-SW kinematic indicators have been mapped.

There is no evidence that the top-to-NE and top-to-SW kinematic indicators are of different generations and no evidence that they developed during different metamorphic conditions. However, locally the top-to-SW indicators are inverted top-to-NE kinematic indicators due to later recumbent tight to isoclinal folding about axes parallel to the NE-trending D_{PA} stretching lineation.

Figure 2.3:
Deformed intrusive contact between granite and sillimanite-bearing metapelite of the Çine nappe at the northeastern shore of Lake Bafa. Location of outcrop: 37°29‘27N; 27°32‘13E.

Figure 2.4:
Folded vein of mid-Triassic granite in mica schist of the Bozdag nappe approximately 5 km southwest of Derbent.

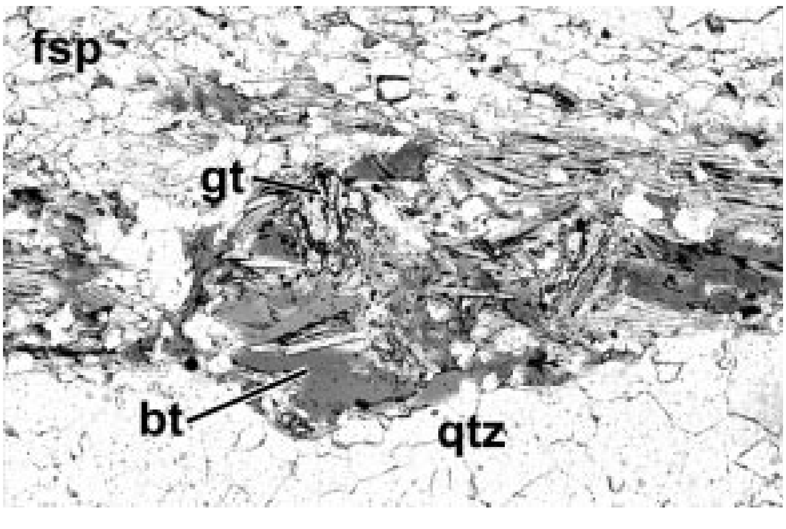

Figure 2.5:
Photomicrograph of biotite grains growing at the expense of garnet in orthogneiss of the Çine nappe. The biotite grains mimic the shape of the resorbed garnet grain. Location of outcrop: 37°56‘19N; 28°00‘47E.

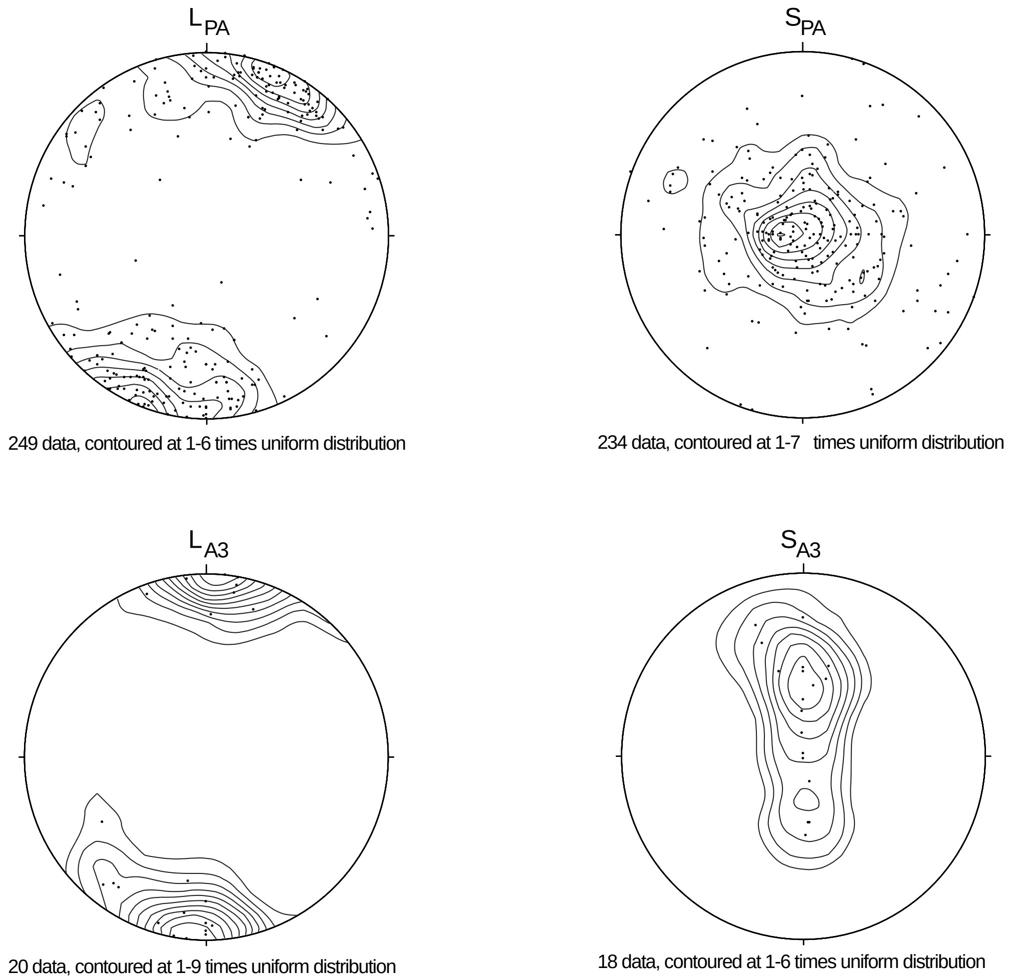

Figure 2.6:
Lower hemisphere equal-area projections of stretching lineations in granitic rocks of the Menderes nappes. Upper row: NE-trending stretching lineations formed during amphibolite-facies metamorphism in orthogneisses of the Çine nappe. Lower row: N-trending stretching lineations formed during greenschist-facies metamorphism in orthogneisses and metagranites of the Çine nappe.

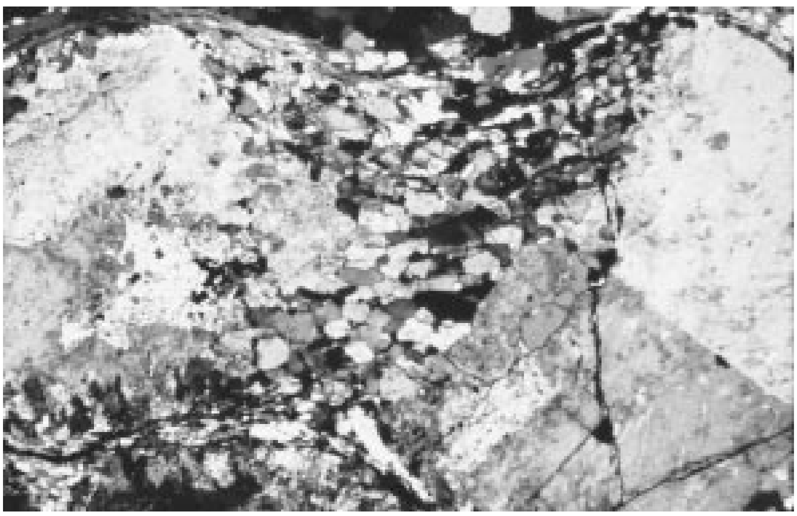

Figure 2.7:
Photomocrograph of boudinaged potassium feldspar porphyroclast with recrystallised grains of smaller grain size forming the boudin neck. Field of view is 16x11 mm. Location of outcrop: 38°07‘03N; 28°09‘21E.

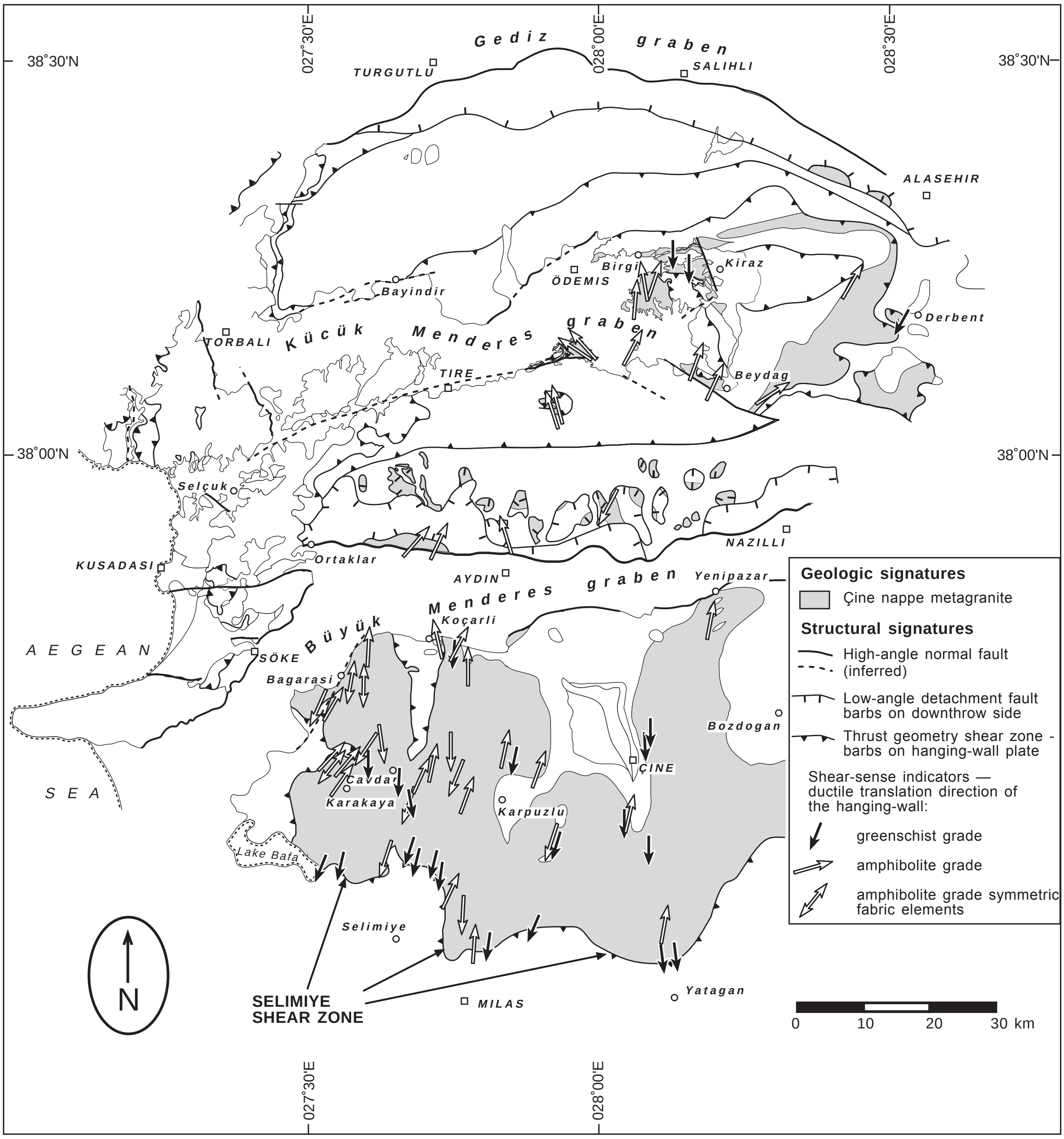

Figure 2.8:
Map showing D_{PA} (white) and D_{A3} (black) kinematic indicators in the Çine nappe granitoids. Arrowheads point to relative movement direction of the hangingwall.

Fig. 2.9:
C'-type shear-band foliation [*Berthé et al.*, 1979] indicating top-to-N sense of shear in orthogneiss of the Ödemis submassif. Note that the material in the strain shadows is mainly recrystallised potassium feldspar. Location of outcrop: 38°11'23N; 28°03'57E.

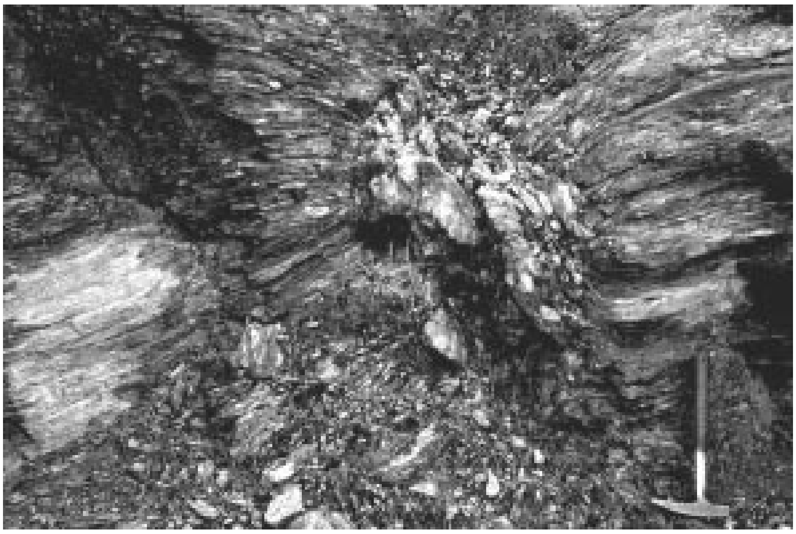

Fig. 2.10:
Foliation boudinage with quartz in the boudin neck. Symmetric foliation boudinage is typical for the northwestern part of the Çine submassif. Location of outcrop: 37°39'33N; 27°34'14E.

Fig. 2.11:
Foliation boudinage in orthogneiss southeast of Bagarası with symmetric 'fish-mouth'-type quartz pods in the neck of the boudin. Location of outcrop: 37°39'33N; 27°34'14E.

2.5.2 Greenschist-facies structures (D_{A3})

Greenschist-facies deformation structures (D_{A3}) are the second set of fabrics in the orthogneiss, where they crosscut the amphibolite-facies D_{PA} structures, and are the only set of structures in the metagranites. In orthogneisses in the Çine Massif and the CMCC D_{PA} fabrics are locally cut by isolated, centimetre to metre-thick, retrograde shear zones (Fig. 2.12) (see also *Hetzel et al.* [1998]). In these shear zones a new foliation (S_{A3}) formed. The development of S_{A3} is characterised by the breakdown of garnet, potassium feldspar and biotite and the new growth of chlorite, albite and white mica. In S_{A3}, a N-trending stretching (L_{A3}) lineation formed and is expressed by stretched aggregates of quartz (Fig. 2.6), chlorite and white mica.

In metagranites and orthogneisses of the Çine submassif, the greenschist-facies shear zones increase in number towards the Selimiye shear zone. In the Selimiye shear zone, the greenschist-facies structures obliterated all earlier fabrics in the orthogneisses. Across the Selimiye shear zone, kinematic indicators provide a consistent top-to-S sense of shear [*Hetzel* and *Ring*, 1993; *Bozkurt and Park*, 1994, 1997a, 1997b; *Hetzel and Reischmann*, 1996].

The formation of the greenschist-facies structures probably took place at temperatures below 400-500°C because feldspar porphyroclasts and biotite are commonly not recrystallised, but brittlely deformed (Fig. 2.13) [*Bozkurt and Park*, 1997a].

In the footwall of the Selimiye shear zone, metagranites and orthogneisses locally display networks of ultracataclasites and pseudotachylites, which cut ductile greenschist-facies structures. In contrast, D_{A3} structures in the hangingwall of the Selimiye shear zone are ductile and available data suggests that the D_{A3} structures formed during prograde greenschist-facies metamorphism.

2.5.3 Deformation of the Triassic granites and their wallrocks

In the Triassic granites of the Derbent area (Fig. 2.1) white mica, flattened quartz and K-feldspar grains define a well-developed foliation. Biotite is rare; small poikiloblastic garnets, which are tens of microns in diameter, locally occur. Elongate quartz and feldspar grains and aligned white mica form a N-trending stretching lineation. Deformation fabrics in the granites are largely symmetrical; foliation boudinage is locally observed.

In the surrounding mica schists of the Bozdag nappe, granitic dikes are folded together with their wallrock. In these mica schists, a greenschist-facies foliation is associated with a N-trending stretching lineation. Foliation and stretching lineation are associated with millimetre-spaced shear-band cleavages formed by chlorite and biotite. Poikiloblastic garnets, which are tens of microns in size, are locally observed. The shear bands indicate a top-to-S sense of shear (Fig. 2.14). In intercalated amphibolite lenses, an earlier foliation is cut by biotite-bearing shear-bands that also show a top-to-S sense of shear.

South of Derbent, the top-to-S fabrics in the mica schists of the Bozdag nappe can be followed across its upper nappe contact into the overlying Çine nappe. Asymmetric shear bands indicating a top-to-S sense of shear overprint the D_{PA} fabrics in both the Çine and Bozdag nappes.

2.5.4 Granites crosscutting D_{PA} structures and their zircon age

In a series of outcrops along a minor road from Eskiçine to Akçaova (southeast of Çine; Fig. 2.1), a suite of metagranites intruded an orthogneiss which depicts well-developed D_{PA} structures. Because the intrusion age of this metagranite provides a minimum age for the D_{PA} structures in this part of the Çine submassif, magmatic zircons of this rock have been dated using the zircon evaporation technique (Fig. 2.15, Fig. 2.16).
The zircon evaporation technique, which is based on $^{207}Pb/^{206}Pb$ isotope relations, has been described by *Kober* [1986, 1987]. The method involves repeated evaporation and deposition of Pb isotopes from chemically untreated single grains in a double-filament arrangement [*Kober*, 1987]. The analytical procedures and instrumental conditions used in this study are detailed in *Kröner and Hegner* [1998]. Repeated evaporation and deposition during the analytical procedure yielded $^{206}Pb/^{204}Pb$ ratios in excess of 40,000 with errors of 10% or less. Only zircons yielding such ratios were used for age assessment. Common lead was corrected, where necessary, using the model of *Stacey and Kramers* [1975].
No significant changes in the $^{207}Pb/^{206}Pb$ ratios were recorded on progressive heating; a feature suggesting that the zircons analysed contained only one stable radiogenic lead phase. The calculated age and uncertainty are based on the mean of all ratios evaluated. Mean age and error are presented as weighted means of the entire population (Table 2.2). The $^{207}Pb/^{206}Pb$ spectra are shown in a histogram, which permits visual assessment of the data distribution from which the age is derived (Fig. 2.16).
Since the evaporation technique only provides Pb isotopic ratios, there is no a priori way to determine whether a measured $^{207}Pb/^{206}Pb$ ratio reflects a concordant age. Thus, principally, the $^{207}Pb/^{206}Pb$ ages determined by this method are necessarily minimum ages. *Kröner and Hegner* [1998] discussed this problem and provided reliability criteria for evaporation analyses. Comparative studies by single-grain evaporation, conventional U-Pb dating and ion-microprobe analysis have shown excellent agreement [*Kröner et al.*, 1991; *Cocherie et al.*, 1992; *Jaeckel et al.*, 1997; *Karabinos*, 1997].
The analysed metagranite contained clear, euhedral, long-prismatic zircons of typical igneous habit (Fig. 2.9a). Analysis of one fraction of three grains yielded a mean age of 547.2±1.0 Ma (Fig. 2.9) which can be interpreted as dating the time of protolith crystallisation. This must be considered with caution since it is only one analysis, but it agrees well with zircon ages of other granitods within the area (cf. Table 2.1).

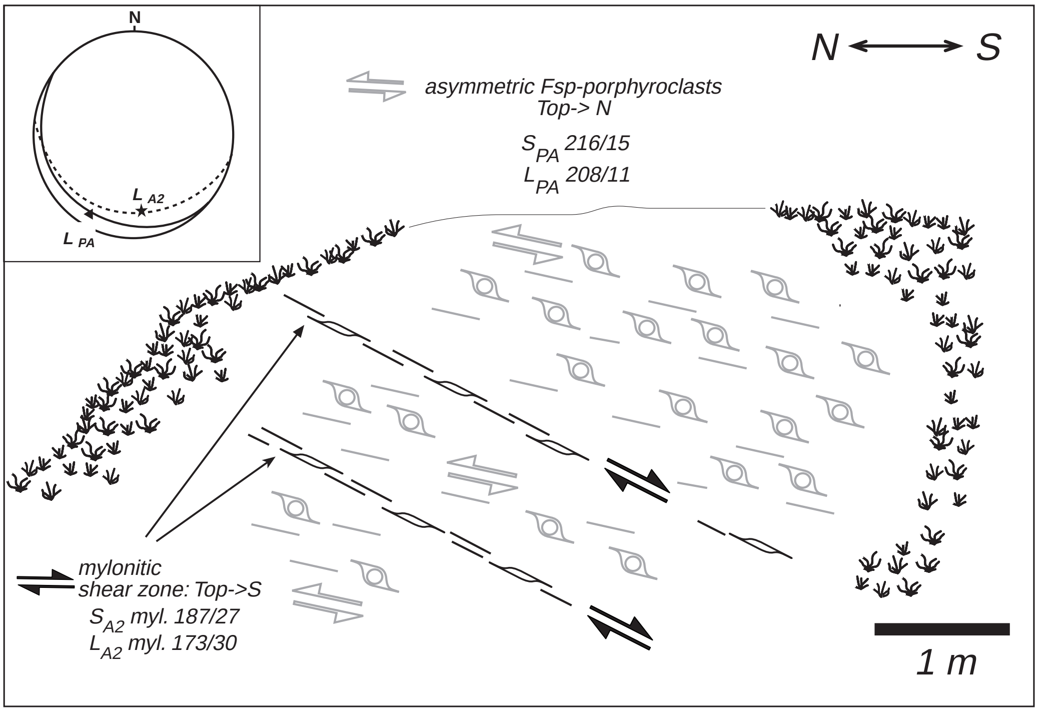

Fig. 2.12:
Sketch of two sets of deformation fabrics in a road cut in the Çine submassif showing overprinting of pervasive amphibolite-facies structures, shown in grey, by localised greenschist-facies shear zones (shown in black).

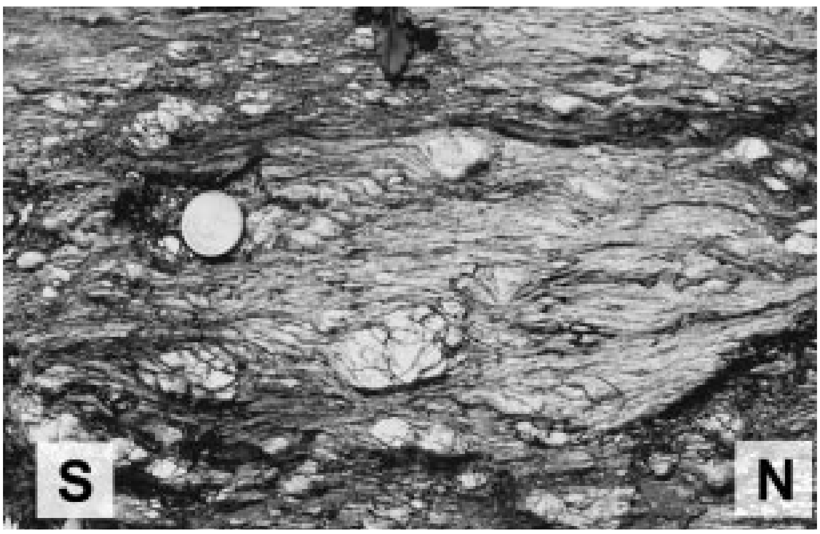

Fig. 2.13:
Greenschist-facies granitic mylonite with brittlely deformed mantled porphyroclasts of magmatic K-feldspar. Shear sense is top-to-S, as interpreted from claststs and shear bands. Note that foliation has a steep southerly dip in the outcrop (180/72) Location of outcrop: 37°29'27N; 27°32'13E.

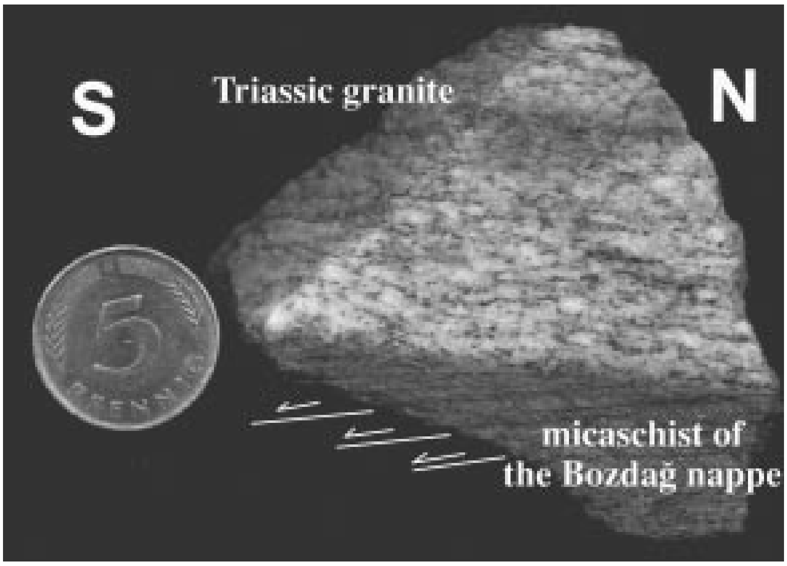

Fig. 2.14:
Polished section of the contact between the Mesozoic granite and the Bozdag nappe mica schist in a road-cut in Derbent. An asymmetric shear-band cleavage, only developed in the mica schist, indicates top-to-S sense of shear, whereas in the granite only a weak fabric with σ-type porphyroclasts is visible.

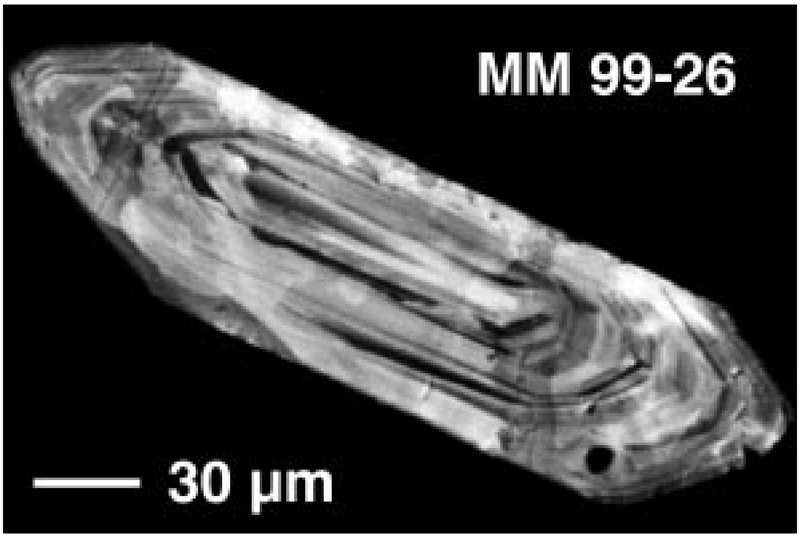

Fig. 2.15:
Cathodoluminiscence image of a typical long-prismatic igneous zircon from sample MM99-26 used for $^{207}Pb/^{206}Pb$ dating.

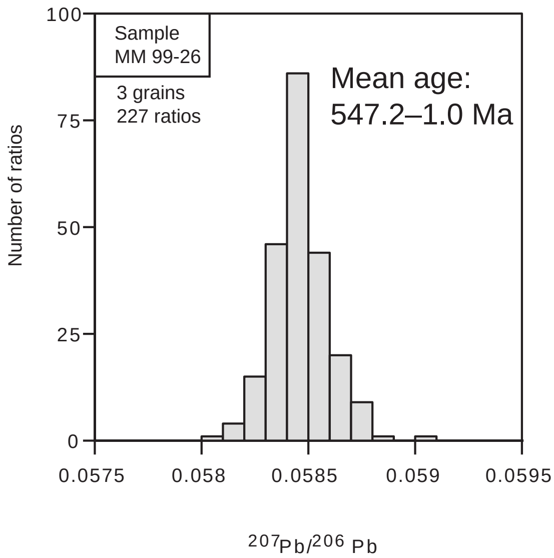

Fig. 2.16:
Histogram showing the distribution of radiogenic lead isotope ratios derived from evaporation of single zircons from metagranite sample MM 99-26 that crosscuts a mylonitically deformed orthogneiss in an outcrop SW of Çine, at 2.4 km on the road from Akçaova to Eskiçine. The spectrum plotted has been integrated from 227 ratios. Mean age is given with 2σ mean error.

2.6 Discussion

A striking feature of the granitoid rocks throughout the Menderes nappes is the difference in composition and the nature of the internal deformation. Ductile deformation fabrics vary according to their metamorphic grade and the type of shear zones in which they occur, and show overprinting relationships. The granitoids of the Çine and Bozdag nappe show two sets of ductile structures, which show consistent overprinting relationships and developed during different metamorphic conditions. The first set of structures (D_{PA}) formed during amphibolite-facies metamorphism and occur exclusively in orthogneisses of the Çine nappe and not in the metagranites and the mid-Triassic granites. One crosscutting metagranite yields a zircon age of 547.2±1.0 Ma, which is likely to be an intrusion age. Orthogneisses dated at 550-570 Ma by *Reischmann and Loos* [1997] are deformed by D_{PA} structures. The consistent crosscutting relationships as well as zircon dating of the crosscutting metagranite provide a robust and important time constraint demonstrating that D_{PA} is of Proterozoic age.

D_{PA} fabrics with top-to-NE kinematics in orthogneisses and metapelites of the Çine nappe and mica schists and amphibolites of the Bozdag nappe in the Ödemis submassif are considered to result from a tectonic event that originally affected the Çine and Bozdag nappes. This is in accordance with the observation that D_{PA} structures can be traced across the nappe contact between the Çine and Bozdag nappes in the eastern Ödemis submassif.

An important feature seems to be the regional variation in kinematics of D_{PA} fabrics. In the Ödemis submassif, where the structurally lower parts of the Çine nappe are exposed, the D_{PA} kinematic indicators are consistently top-to-NE in the Bozdag nappe and in the overlying Çine nappe. In the Çine submassif, where structurally higher parts are exposed, symmetric, top-to-SW and top-to-NE kinematic indicators have been mapped. Folding of top-to-NE fabrics with axes parallel to the stretching lineation, as locally observed, may be one reason for the local reversal in shear sense. The symmetric fabrics may testify that non-coaxial deformation during D_{PA} was mainly concentrated at the nappe contact between the Çine and Bozdag nappes. In the middle and upper parts of the Çine nappe the D_{PA} deformation is likely to have been close to coaxial, producing symmetric fabrics and, at least in part, kinematic indicators with opposite kinematics.

A critical aspect of the tectonic interpretation of D_{PA} is the relation between D_{PA} deformation and metamorphism. In garnet-bearing orthogneisses in the higher parts of the Çine nappe in the Ödemis submassif, the D_{PA} structures formed during the breakdown of garnet to biotite, suggesting that D_{PA} occurred during retrograde amphibolite-facies conditions. However, *Lackmann* [1997] showed that in metapelites of the basal Çine nappe and the directly underlying Bozdag nappe north of Birgi, prograde growth of garnet from biotite occurred synkinematically with the formation of the S_{PA} and L_{PA}. This suggests that D_{PA} occurred during prograde Barrovian metamorphism. The D_{PA} deformation juxtaposed the Çine and Bozdag nappes and both nappes show largely similar peak-metamorphic conditions of about 600-700°C and 9-11 kbar [*Lackmann*, 1997; *Gessner et al.*, 1998]. Because D_{PA} proceeded during prograde metamorphism in the metapelites of the Çine and Bozdag nappes, it is likely that D_{PA} fabrics formed during crustal thickening and resulted from horizontal crustal shortening. The discrepancy between the prograde and the retrograde fabrics may be explained by internal imbrication within the Çine nappe under higher-grade metamorphic conditions than those related to the emplacement of the Çine nappe on top of the Bozdag nappe. During nappe emplacement, reactivation of the tectonic contacts within the Çine nappe may have caused retrogression of the fabrics. Another explanation might be that the breakdown and growth of garnet occurred simultaneously under the same metamorphic conditions due to different bulk chemistries.

During the D_{A3} event, the granitoids of the Çine and Bozdag nappe were deformed heterogeneously by greenschist-facies metamorphism. D_{A3} caused regionally consistent top-to-S tectonic transport. Because D_{A3} affected the mid-Triassic granites, it must be of post-middle Triassic age. Structural mapping in Cretaceous metasediments of the middle unit indicates that D_{A3} is also present there and must therefore be of Alpine age. It will be shown in Chapter 3 that D_{A3} represents a complex deformation causing the assembly of the present nappe pile of the Anatolide belt in the Eocene.

Another important question is whether or not D_{A3} formed during an extensional or a contractional event. It has been shown that brittle-ductile and brittle extensional structures formed during the late Alpine tectonic history of the Menderes nappes [*Hetzel et al.*, 1995a, 1995b; *Hetzel et al.*, 1998; *Emre and Sözbilir*, 1997] (see also Chapter 4). However, not all greenschist-facies shear zones are compatible with the bivergent orogenic extension model suggested by *Hetzel et al.* [1995a] and *Hetzel et al.* [1998]. *Collins and Robertson* [1998] and *Ring et al.* [1999a] proposed that the D_{A3} Selimiye shear zone formed in response to crustal shortening. As noted by *Hetzel and Reischmann* [1996] and *Collins and Robertson* [1998], structure and metamorphic gradient of the Selimiye shear zone are in marked contrast to typical core-complex-type extensional shear zones. Furthermore, deformation/metamorphism relationships indicate that D_{A3} structures formed during prograde greenschist-facies metamorphism or at the peak of the latter (see Chapter 3). Collectively, these observations suggest that D_{A3} is related to crustal shortening.

The widespread occurrence of rocks of the Çine nappe on top of the Bayındır nappe, especially north of Aydin, has been attributed to thrusting by *Candan et al.* [1992] and *Lips* [1998]. In the Ödemis area, however, the Çine nappe occurs above the Bozdag nappe, which in turn rests upon the Bayındır nappe. This nappe pile, together with the overlying middle and upper units, was finally assembled during greenschist-facies metamorphism [*Ring et al.*, 1999a]. The contact between the Çine and Bayındır nappe north of Aydin is a cataclastic fault zone. Collectively, these observations indicate that the cataclastic fault zone must be a relatively late, i.e. Miocene or Pliocene structure. Furthermore, there is no indication of thrusting or reverse faulting in the Neogene sediments. In accord with *Emre and Sözbilir* [1997], it is feasible to assume that the Güney detachment cut out the entire Bozdag nappe and placed the Çine nappe above the Bayındır nappe in this area.

2.7 Concluding remarks

Granitoids of the Çine and Bozdag nappes show two distinct sets of structures, which formed during different orogenies. The first set of structures formed during amphibolite-facies metamorphism in the latest Proterozoic and caused, at least in part, internal imbrication in the Menderes nappes. During the Alpine orogeny, the second set of structures formed during greenschist-facies metamorphism. This second set of structures is attributed to horizontal crustal shortening and caused the final juxtaposition of the Menderes nappes with the overlying units of the Cycladic blueschist unit, the Izmir-Ankara suture zone and the Lycian nappes during collision of Anatolia with the Sarakaya continent to the north.

Chapter 3

The Eocene post-high-pressure emplacement of the Cycladic blueschist unit onto the Menderes nappes

This Chapter is largely identical with a manuscript entitled ‘The Cyclades in Turkey: Evidence for Eocene post-high-pressure emplacement of the Cycladic blueschist unit onto the Menderes nappes, Anatolide belt, western Turkey’, which has been submitted to ‘Tectonics’ in March 2000. Co-authors are Uwe Ring, Cees W. Passchier and Talip Güngör.

3.1 Abstract

Structural analysis reveals that the Anatolide belt of western Turkey was assembled in the Eocene by top-to-S out-of-sequence thrusting of the Cycladic blueschist unit onto the Menderes nappes during greenschist-facies metamorphism. The Cycladic blueschist unit in western Turkey contains relics of a prograde Alpine D_{A1} fabric, which was overgrown by poikiloblastic kyanite and chloritoid during high-pressure metamorphism. This high-pressure mineral growth stage temporally overlapped with the onset of the D_{A2} deformation, which was associated with top-to-NE shearing during initial decompression. The subsequent greenschist-facies D_{A3} deformation has been the first event to affect the Cycladic blueschist unit and the Menderes nappes together. The thrust contact between the Cycladic blueschist unit and the Menderes nappes is a D_{A3} shear zone, the Cycladic-Menderes thrust (CMT). Along the CMT, the Cycladic blueschist unit was juxtaposed with different thrust sheets of the Menderes nappes and defines an out-of-sequence ramp structure, which cuts up-section towards the south. In the Cycladic blueschist unit, deformation fabrics associated with the CMT crosscut high-pressure structures. In the Menderes nappes in the footwall, D_{A3} induced a regionally coherent deformation fabric with top-to-S kinematic indicators in the internal parts of the nappes and in shear zones, which define the nappe boundaries. The CMT overprinted pre-Alpine structures in the Bozdag nappe and is likely to be coeval with the first deformation event in the Bayındır nappe. The lack of Alpine high-pressure fabrics below the CMT implies ~35 km of exhumation of the Cycladic blueschist prior to its Eocene emplacement on top of the Menderes nappes. The substantial differences in the pre-assembly tectonometamorphic histories of the Cycladic blueschist unit and the Menderes nappes contradict the model of a laterally continuous orogenic zone, in which the Menderes nappes are interpreted as the eastern continuation of the Cycladic blueschist unit.

3.2 Introduction

Traditionally the Hellenide-Anatolide orogen in the eastern Mediterranean (Fig. 3.1) is regarded as an arcuate array of tectonic units, which are laterally continuous over large distances [e.g. *Brunn*, 1956; *Aubouin*, 1959; *Dürr et al.*, 1978; *Jacobshagen et al.*, 1978]. A fundamental assumption of this hypothesis is that the Pelagonian zone [*Aubouin*, 1959], the Cycladic zone and the Menderes Massif [*Paréjas*, 1940] can be grouped together as a continuous 'Median Crystalline Belt' [*Dürr et al.*, 1978]. Following this 'classical' interpretation, the Median Crystalline Belt is assumed to represent Carboniferous basement and Permo-Mesozoic cover of the partly subducted Adriatic plate. *Ring et al.* [1999a] recently questioned the long-standing view that the Menderes Massif is correlative with the Cycladic zone and suggested significant along-strike differences in the Alpine nappe pile of the Hellenide-Anatolide orogen (Fig. 3.1). *Ring et al.* [1999a] proposed that the Menderes Massif is made up by two different units: the Cycladic blueschist unit and the underlying Menderes nappes.

The exhumation of the Cycladic blueschist unit is largely attributed to normal faulting caused by rollback of the subducting Hellenic slab [e.g. *Lister et al.*, 1984; *Buick*, 1991]. The onset of normal faulting is placed into the middle Oligocene [*Raouzaios et al.*, 1996]. However, based on geologic relationships on the islands of Evvia and Samos, *Avigad et al.* [1997], and *Ring et al.* [1999b] were able to show that up to 30-40 km of the exhumation of the Cycladic blueschist unit occurred before the middle Oligocene.

At the beginning of this Chapter a review is given addressing aspects of the tectonic development of the Cycladic blueschist unit in the Aegean and the Menderes nappes in western Turkey. The consecutive sections comprise a detailed structural study of the Cycladic blueschist unit in western Turkey and the tectonic boundary between the Cycladic blueschist unit and the Menderes nappes. Substantial differences in the tectonometamorphic history of both units will be outlined, which imply important along-strike differences in the Hellenic-Anatolide orogen. It will further be shown that the Cycladic blueschist unit in western Turkey was considerably exhumed by middle Eocene times and it will be discussed how this early exhumation might have been achieved.

3.3 Overview

3.3.1 The nappe pile in the Aegean and western Turkey

The Hellenides in the Aegean can be subdivided from top (interides) to bottom (externides) into (1) the internal zone, (2) the Vardar-Izmir-Ankara zone, (3) the Lycian nappes, (4) the Cycladic zone, and (5) the external Hellenides (Fig. 3.1). A major difference between the Aegean and western Turkey is that in the latter the Menderes nappes, instead of the external Hellenides, form

the lowermost tectonic unit (Fig. 3.1).
The internal zone is considered part of Eurasia and Sakarya underneath which oceanic crust of the northern Neotethys was subducted. The related suture is the Vardar-Izmir-Ankara zone [*Sengör and Yilmaz*, 1981], parts of which were metamorphosed under blueschist-facies conditions in the late Cretaceous [*Okay*, 1998; *Sherlock et al.*, 1999] (Fig. 3.1c). The Lycian nappes [*de Graciansky*, 1972] are a thin-skinned thrust belt, which is assumed to root in the Vardar-Izmir-Ankara zone [*Collins and Robertson*, 1997]. Within the Lycian nappes, top-to-S displacement occurred from the late Cretaceous to the early Miocene [*Collins and Robertson*, 1998]. Parts of the Lycian nappes were metamorphosed under incipient high-pressure conditions [*Bernoulli et al.*, 1974; *Franz and Okrusch*, 1992].
The Cycladic zone can be subdivided into three units [*Altherr and Seidel*, 1977; *Avigad et al.*, 1997; *Ring et al.*, 1999b], which are from top to bottom: (i) The heterogeneous Cycladic ophiolite nappe, consisting of unmetamorphosed to greenschist-facies ophiolitic and sedimentary rocks containing high-grade metamorphic blocks of Jurassic and Cretaceous age. (ii) The Cycladic blueschist unit, which is made up of a high-pressure nappe stack comprising from top to bottom an ophiolitic mélange, a Permo-Mesozoic shelf sequence, and a Carboniferous basement. (iii) The basal unit is exposed in at least four windows (Fig. 3.1). It is probably part of the external Hellenides, which are a thrust pile of Permian to Paleogene rocks. The structurally highest units of the external Hellenides are unmetamorphosed, and are tectonically separated from high-pressure rocks on the Peleponnesos and Crete [*Seidel et al.*, 1982; *Thomson et al.*, 1999].
Overall, the nappe pile in the Aegean displays a temporal progradation of nappe emplacement and associated high-pressure metamorphism towards the south. Southward propagating high-pressure metamorphism mimics the southward retreat of the Hellenic subduction zone.
In contrast to parts of the External Hellenides, the Menderes nappes, which also occur tectonically below the Cycladic zone, do not show Alpine high-pressure metamorphism [*Ring et al.*, 1999a; *Okay*, 2000]. Another important difference is that the basement of one of the Menderes nappes (Çine nappe, see Chapter 2) is of Proterozoic/Cambrian age [*Kröner and Sengör*, 1990; *Hetzel and Reischmann*, 1996; *Hetzel et al.*, 1998; *Reischmann and Loos*, 1999]. This basement preserved deformation fabrics of latest Proterozoic age (the D_{PA} event introduced in Chapter 2). The absence of Alpine high-pressure metamorphism in the Menderes nappes and the lack of a well-defined subduction zone to the south of western Turkey suggests that subduction ceased after the collision of the exotic Anatolide microcontinent in the Eocene [*Hetzel et al.*, 1995a; *Ring et al.*, 1999a]. Figure 3.2 shows a schematic map, which illustrates the supposed pre-convergence palaeogeographic situation of the eastern Mediterranean in the early Cretaceous.

3.3.2 Lithology and tectonometamorphic evolution of the Cycladic blueschist unit in the Aegean

Aspects of the tectonometamorphic evolution of the Cycladic blueschist unit in the Aegean are reviewed here to allow comparisons with the development of the Cycladic blueschist unit in western Turkey. *Ring et al.* [1999b] showed that the Cycladic blueschist unit on Samos Island is represented by three high-pressure nappes, which are from top to bottom: (1) the Selçuk nappe (ophiolitic mélange), (2) the Ampelos nappe (Permo-Mesozoic shelf sequence), and (3) the Agios Nikolaos nappe (Carboniferous basement).

The Selçuk nappe contains blocks of metagabbro in a matrix of serpentinite and phyllite. *Ring et al.* [1999b] tentatively correlated the Selçuk nappe with the ophiolitic mélanges on the Cycladic islands of Syros and Tinos [*Okrusch and Bröcker*, 1990; *Bröcker and Enders*, 1999], where a rock unit similar in lithology and tectonic position is exposed. Metamorphic conditions are in the range of 10-15 kbar and 400-500°C [*Ring et al.*, 1999b].

The Ampelos nappe, as well as correlative tectonic units across the entire Cyclades consist of quartzite, metapelite and metabasite overlain by metabauxite-bearing marble [*Dürr et al.*, 1978]. This succession has been interpreted as a former passive-continental-margin sequence [*Altherr and Seidel*, 1977]. The underlying Agios Nikolaos nappe contains garnet-mica schist intruded by Carboniferous orthogneiss and represents part of the former basement of the shelf sequence. P-T conditions of the shelf/basement unit are on the order of 12-19 kbar and 450-550°C [e.g., *Okrusch and Bröcker*, 1990; *Avigad et al.*, 1991; *Will et al.*, 1998].

The basal unit below the Cycladic blueschist unit largely consists of marbles capped by Eocene flysch. It was also subjected to high-pressure metamorphism, which reached about 8-10 kbar and 350-400°C [*Avigad et al.*, 1997; *Ring et al.*, 1999b]. A subsequent Barrovian metamorphism overprinted all high-pressure units and reached greenschist to amphibolite-facies conditions.

Age data for high-pressure metamorphism show a consistent pattern across the Aegean. In the ophiolitic mélanges of Syros and Tinos, *Bröcker and Enders* [1999] dated zircons, which overgrew high-pressure minerals, at 78 Ma and 63-61 Ma. High-pressure metamorphism in the underlying shelf/basement unit is usually placed into the Eocene (53-40 Ma) and cooling during decompression below ~350-400°C took place between 40-35 Ma. The Barrovian-type overprint occurred at about 25-15 Ma [e.g. *Altherr et al.*, 1979, 1982; *Wijbrans and McDougall*, 1986, 1988; *Wijbrans et al.*, 1990; *Bröcker et al.*, 1993]. Scarce age data from high-pressure rocks of the basal unit suggest an age of ~40-35 Ma [*Schermer et al.*, 1990], which is concurrent with decompression and cooling in the Cycladic blueschist unit.

The tectonometamorphic evolution of the Cycladic blueschist unit in the Aegean involved structures developing during prograde high-pressure metamorphism. The structures young structurally downwards and were poikiloblastically overgrown by glaucophane, chloritoid and kyanite [*Lister and Raouzaios*, 1996 for Sifnos Island; *Ring et al.*, 1999b for Samos Island]. During subsequent decompression, thrusting of the Cycladic blueschist unit onto the basal unit was associated with moderate high-pressure metamorphism in the latter [*Avigad et al.*, 1997; *Ring et al.*, 1999b]. Succeeding middle Oligocene to Recent crustal-scale extension occurred before, during a

b

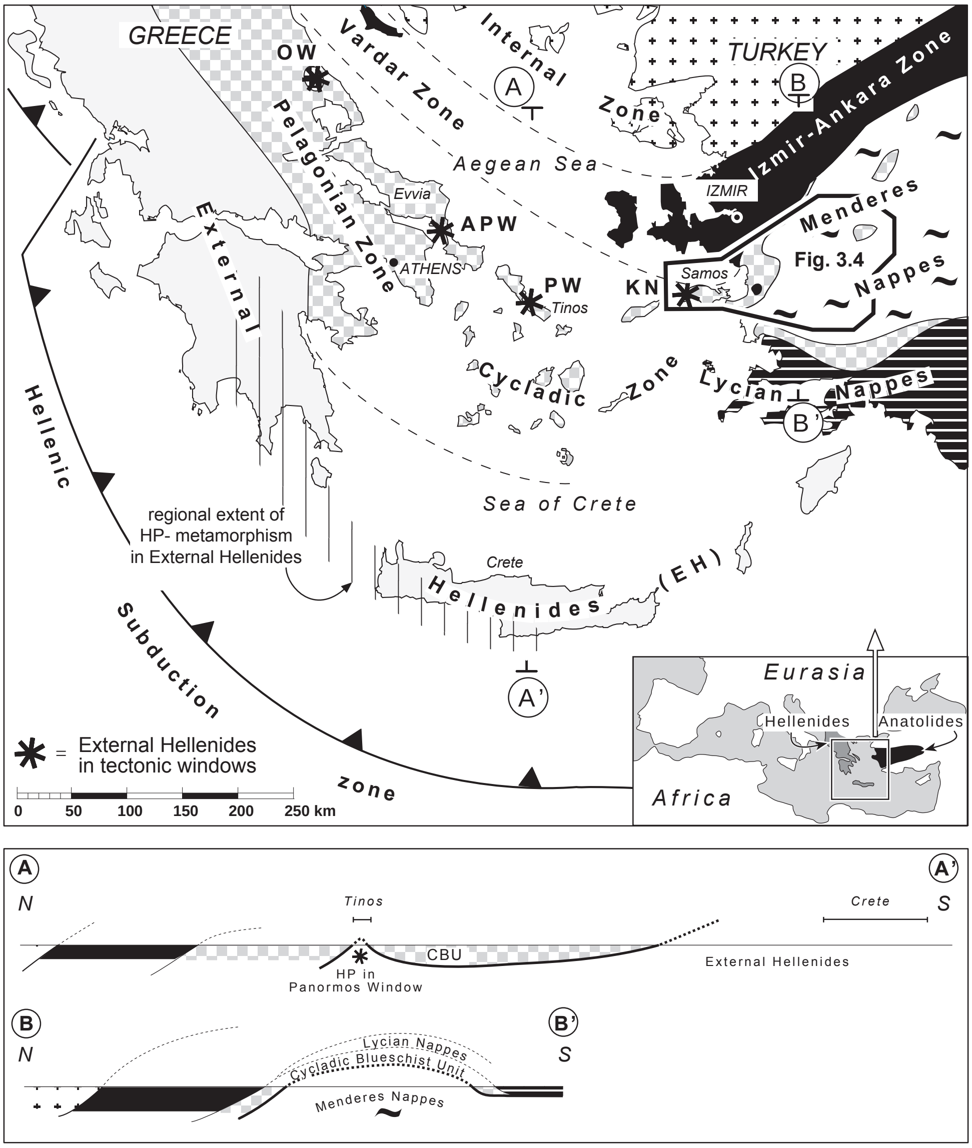

c

	Tectonometamorphic unit	HP Metamorphism Cret.	Pal.	Eoc.	Olig.	Mio.	Time [Ma]	P / T [kbar/°C]	Authors
	Vardar-Izmir-Ankara Zone	■					~80	20 / 430	Sherlock et al. 1999
	Lycian Nappes	?					?	7 / ~400	Franz and Okrusch 1992, Oberhänsli et al. 1998
	Cycladic zone (CZ)	■					75-65	~12-19 / 450-550	Altherr et al. 1979, Wijbrans and McDougall 1986, Wijbrans et al. 1988, Wijbrans et al. 1990, Bröcker et al. 1993, Bröcker and Enders 1999
				■			50-43		
*	External Hellenides in tectonic windows in CZ			■			40-35	≤10 / ≤400	Schermer et al. 1990, Avigad et al. 1997
	HP in External Hellenides					■	24-19	8-14 / 350-450	Seidel et al. 1982, Theye and Seidel 1993, Thomson et al. 1999
	External Hellenides						—	—	—
~	Menderes nappes						—	—	—

Figure 3.1:
Map and cross-sections showing the major tectonometamorphic units of the Hellenide-Anatolide orogenic belt. Pelagonian and Cycladic zones are shown together for their common architecture and metamorphic history. The Cycladic blueschist unit makes up the largest part of the Cycladic zone, where it occurs below the heterogeneous Cycladic ophiolite nappe and above Eocene metasediments of the External Hellenides. Windows of External Hellenides below Pelagonian and Cycladic zones are marked with an asterisk and abbreviated OW = Olympus window, APW = Almyropotamos window, PW = Panormos window and KN = Kerketas nappe. Cross sections A-A' and B-B' show different units in the footwall of the Cycladic blueschist unit: the External Hellenides in the Aegean and the Menderes nappes in western Turkey. Box indicates location of Fig. 3.4. Modified after *Schermer et al.* [1990], *Seidel et al.* [1982], *Avigad et al.* [1997], *Walcott* [1998], *Bröcker and Enders* [1999] and *Ring et al.* [1999b]. Inset shows location of main map in the Mediterranean and regional extent of the Hellenides and the Anatolides.

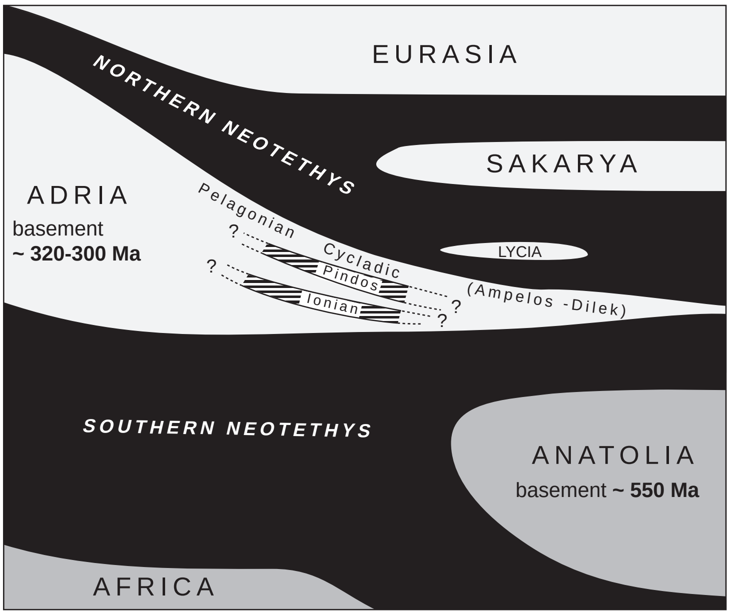

Figure 3.2:
Palaeogeographic sketch map for the early Cretaceous modified from *Sengör et al.* [1981] and *Robertson et al.* [1996] illus-trating the supposed spatial arrangement of continents and continental fragments and their basement ages. Adria is shown to pinch out to the east; its crust is in part highly thinned as indicated by the Ionian and Pindos zones; the latter may even have been oceanic. Ana-tolia is interpreted as a micro-continent which rifted off from Africa in the early Mesozoic and, unlike Adria, consisted of 'nor-mal' thickness continental crust.

and after the Barrovian metamorphic event. Extension is manifest by greenschist-facies shear zones and brittle normal faults, which are inferred to represent different generations of linked detachment systems [*Forster and Lister*, 1999].

3.3.3 Lithology and tectonometamorphic evolution of the Menderes nappes

The tectonometamorphic development of the Menderes nappes will now be summarised in order to demonstrate the substantial differences between the latter and the Cycladic blueschist unit. Overall three Alpine deformation events, abbreviated D_{A3}-D_{A5}, have been recognised in the Menderes nappes (the Alpine deformations, indicated by suffix 'A', D_{A1} and D_{A2} only occur in the Cycladic blueschist unit, see below). Parts of the Menders nappes were affected by a pre-Alpine event (D_{PA}) (Figure 3.3), as outlined in Chapter two.

The Menderes nappes consist from top to bottom of (1) the Selimiye nappe, (2) the Çine nappe, (3) the Bozdag nappe, and (4) the Bayındır nappe [*Ring et al.*, 1999a] (Figs. 3.4 and 3.5). The Selimiye nappe contains a metasedimentary sequence, the basal part of which is of Precambrian age [*Hetzel and Reischmann*, 1996; *Reischmann and Loos*, 1999]. Preliminary structural work suggests that an amphibolite-facies fabric of as yet unresolved kinematics and age was overprinted by the Alpine D_{A3} top-to-S Selimiye shear zone, which separates the Selimiye nappe from the underlying Çine nappe. The Selimiye shear zone formed during prograde greenschist-facies metamorphism and related structures were overgrown by garnet at temperatures >450°C [*Hetzel and Reischmann*, 1996]. *Hetzel and Reischmann* [1996] showed that $^{39}Ar/^{40}Ar$ white-mica ages of 43-37 Ma constrain slow cooling below 350-400°C (assumed closure temperature for Ar diffusion in white mica) after D_{A3}.

The Çine and Bozdag nappes are characterised by a distinct overprinting sequence of ductile fabrics. The structurally higher Çine nappe consists of amphibolite to granulite-facies ortho- and paragneiss with intercalated metabasite [*Dora et al.*, 1995; *Lackmann*, 1997], while the Bozdag nappe is composed of amphibolite-facies garnet-mica schist and metabasite. In Chapter 1 it has been shown that the D_{PA} event in the Bozdag and Çine nappes occurred during amphibolite-facies metamorphism at ~550 Ma and caused top-to-NE shear. D_{PA} was overprinted by a D_{A3} greenschist-facies tectonometamorphic event. The corresponding S_{A3} foliation crosscuts S_{PA} and produced a variably spaced shear-band foliation and a well-defined stretching lineation associated with top-to-S kinematic indicators in both nappes and also in Triassic metagranite (cf. Fig. 2.8b and 3.4). Exact P-T conditions for Alpine greenschist-facies metamorphism during D_{A3} are unknown.

The Bayındır nappe at the base contains shelf sediments of inferred Permo-Carboniferous age [*Osman Candan*, pers. comm., 1998], which were metamorphosed under lower greenschist-facies conditions at ~37 Ma [*Lips*, 1998]. The absence of biotite in rocks of suitable bulk composition suggests temperatures <~400°C [*Yardley*, 1989]. The Bayındır nappe was deformed by the synmetamorphic D_{A3} event, which is the first deformation event in the Bayındır nappe. The corresponding S_{A3} foliation is penetrative and associated with a fine-grained N-trending stretching lineation (L_{A3}) (Fig. 3.6). L_{A3} is expressed by stretched quartz, albite and chlorite aggregates and aligned tourmaline. In the structurally highest parts of the Bayındır nappe north of Aydın, D_{A3} ductile shear bands and sigma-type objects [*Passchier and Simpson*, 1986] indicate a top-to-S shear sense. However, north of Bozdag Mountain, a mylonite that formed during the intrusion of the Middle Miocene Turgutlu and Salihli granodiorites (Fig. 3.4) yields a consistent top-to-N shear sense associated with ductile extensional deformation [*Hetzel et al.*, 1995a]. Because the structures north of Bozdag Mountain formed in the middle Miocene, they are about 15-20 Ma younger than the D_{A3} fabrics, which are more or less coeval with the lower greenschist-facies metamorphism at ~37 Ma [*Lips*, 1998]. Therefore, the structures north of Bozdag Mountain is considered to represent a separate D_{A4} ductile extensional event.

Late-Alpine brittle extension (D_{A5}) is expressed by normal-fault systems of Miocene to Recent age. In the Miocene, two symmetrically arranged normal-fault systems formed and were subsequently rotated into a low-angle position by differential exhumation of the footwall. These are the Kuzey detachment in the north and the Güney detachment in the south, which delimit the Central Menderes metamorphic core complex [*Hetzel et al.*, 1995b; *Emre and Sözbilir,* 1997; *Ring et al.*, 1999a] (Figs. 3.4 and 3.5), which will be the subject of Chapter 4.

This summary reveals two important aspects: (1) There is no evidence for Alpine high-pressure metamorphism in the Menderes nappes, and (2) the grade and age of metamorphism associated with D_{A3} apparently decreases structurally downward. Temperatures in the Selimiye nappe were >450°C and occurred before 43-37 Ma [*Hetzel and Reischmann*, 1996], whereas in the Bayındır nappe temperatures barely reached 400°C and occurred later at ~37 Ma [*Lips*, 1998].

3. 4 The Cycladic blueschist unit in western Turkey

3.4.1 Lithology and metamorphism

The Cycladic blueschist unit in western Turkey is made up by the Selçuk mélange and the underlying Dilek nappe [*Erdogan and Güngör*, 1992; *Candan et al.*, 1997; *Güngör*, 1998; *Ring et al.*, 1999a]. The Selçuk mélange consists of blocks of metagabbro and metabauxite-bearing marble, which are surrounded by a matrix of serpentinite and garnet-mica schist. The Dilek nappe is a Permo-Mesozoic shelf sequence, which includes a quartzite conglomerate with interlayered kyanite-chloritoid schist, metabasite, phyllite and marble, the latter of which in part contains metabauxite. Rudists in some marbles indicate that deposition continued at least into the late Cretaceous. The Selçuk mélange correlates with the Selçuk nappe and the Dilek nappe is correlative with the Ampelos nappe in Samos [*Candan et al.*, 1997; *Ring et al.*, 1999a]. No Carboniferous basement is exposed below the Dilek nappe in western Turkey.

Candan et al. [1997] reported P-T conditions of >10 kbar and <470°C for high-pressure metamorphism in the Dilek nappe, which are slightly different from the ~15 kbar and 500°C in the Ampelos nappe in Samos [*Will et al.*, 1998]. 39Ar/40Ar ages for phengite were interpreted to date high-pressure metamorphism at ~40 Ma in the Dilek nappe [*Oberhänsli et al.*, 1998].

3.4.2 Deformation history

Because parts of the Dilek nappe have late Cretaceous protolith ages, regional deformation in the Cycladic blueschist unit in western Turkey has to be Alpine in age and has been abbreviated D_{A1}, D_{A2} and D_{A3}. D_{A1} fabric elements occur exclusively as microscopic relics in the Dilek nappe; mesoscopic D_{A2} and D_{A3} fabrics are present in both the Selçuk mélange and the Dilek nappe.

D_{A1} is manifest as an internal foliation (S_{A1}) in millimetre- to centimetre-sized chloritoid and kyanite porphyroclasts in intercalated kyanite-chloritoid schist in quartzite conglomerate. S_{A1} inclusion trails can be straight, curved or even tightly crenulated (Fig. 3.7a-c). In some porphyroclasts, a diffuse opaque banding oriented at a small angle to S_{A1} can be observed and may represent a sedimentary or a pre-D_{A1} deformation fabric (Figs. 3.7c, 3.8a and 3.8b).

The second foliation (S_{A2}) developed heterogeneously in rocks of the Selçuk mélange. Serpentinite and metapelite display a penetrative foliation, which is associated with a well-defined NE- to E-trending stretching lineation. Some metabasic and ultrabasic lithologies occur as massive, largely unfoliated blocks. In the Dilek nappe, D_{A2} fabrics are best preserved in marble, quartzite and kyanite-chloritoid schist, whereas in phyllite only relics of D_{A2} occur. In quartzite and marble, the arrangement of quartz, calcite, white mica and chlorite defines a pervasive S_{A2} foliation parallel to lithologic layering. In kyanite-chloritoid schist, S_{A2} is the dominant foliation, which is expressed by the preferred orientation of white mica and flattened quartz. The angle bet-

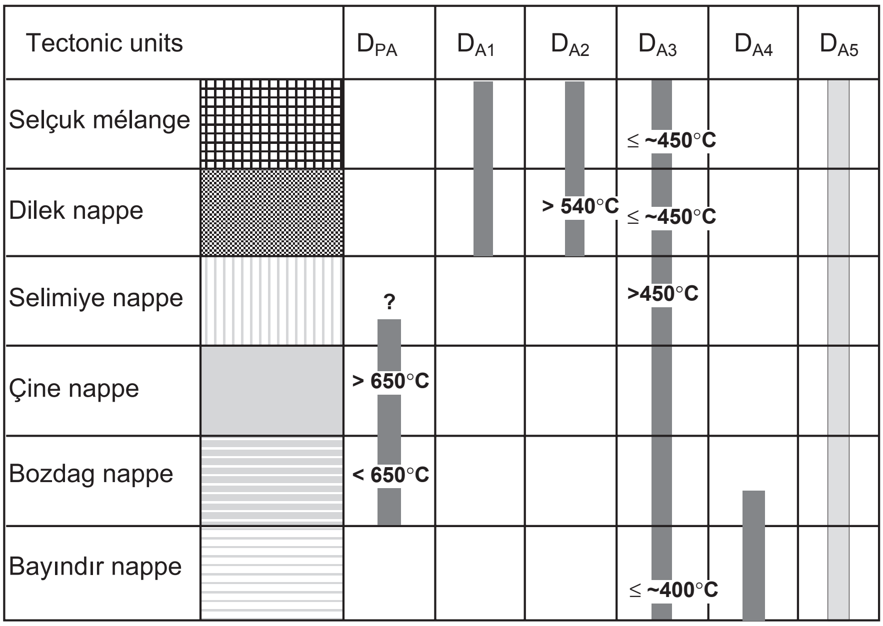

Figure 3.3:
Diagram showing the distribution of pre-Alpine and Alpine events D_{PA} and D_{A1-5} in the tectonic units of the Anatolide belt. Temperature estimates after own observations, except for the Çine and Bozdag nappes [*Ring et al.*, 2000]. The diagram indicates that the anatolide belt was assembled during D_{A3}. D_{A5} is outlined for its brittle deformation style; suffix 'PA' denotes pre-Alpine and 'A' Alpine deformation age.

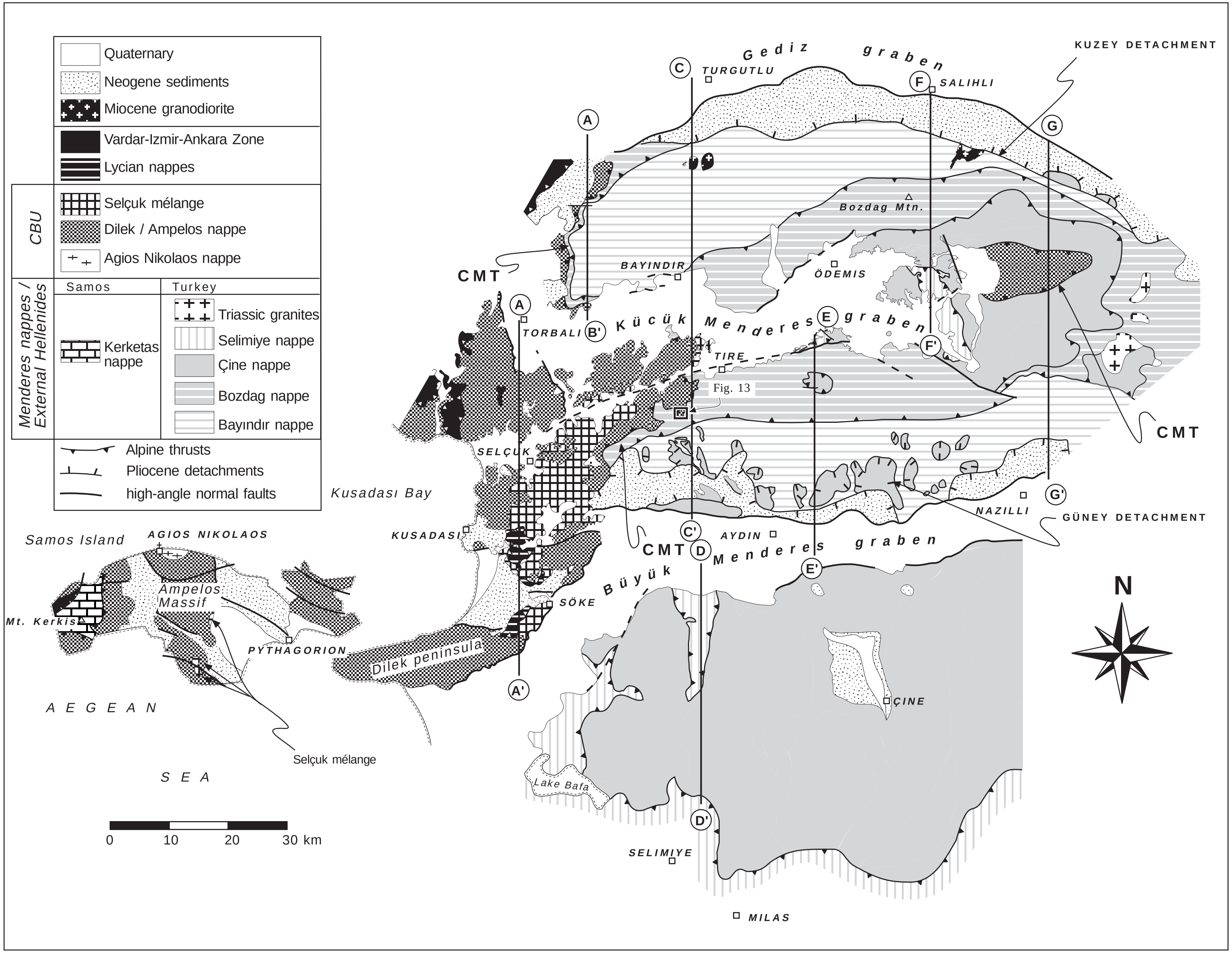

Figure 3.4: Tectonic map of western Turkey and Samos Island after *Hetzel et al.* [1995a], *Hetzel* [1995b], *Dora et al.* [1995], *Candan* and *Dora* [1998], *Güngör* [1998], *Ring et al.* [1999a], *Ring et al.* [1999b] and own observations. Lines for cross-sections A-A' to G-G' (Figure 3.4) and location of Figure 3.13 are indicated. Abbreviations: CBU = Cycladic blueschist unit, CMT = Cycladic-Menderes thrust.

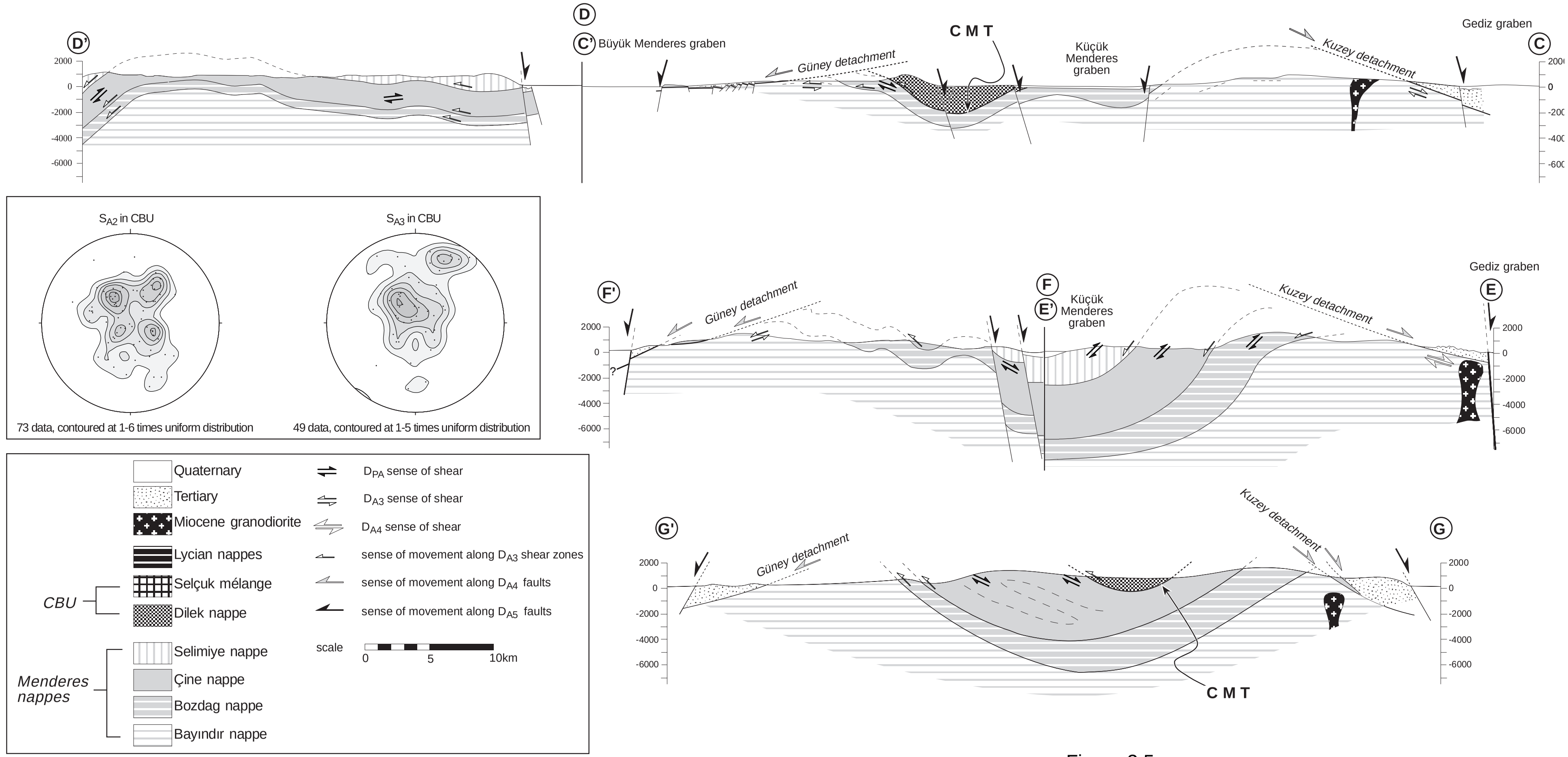

Figure 3.5:
Cross sections A-A' to G-G' (for position of coss-section lines refer to Fig. 3.4). Section A-A' shows that the CMT cuts up-section towards the south in the direction of tectonic transport. For geometric viability section planes are oriented parallel to the mean orientation of L_{A3}. Trace of foliation is projected into the section plane and used to infer the geometry of sub-surface structures.

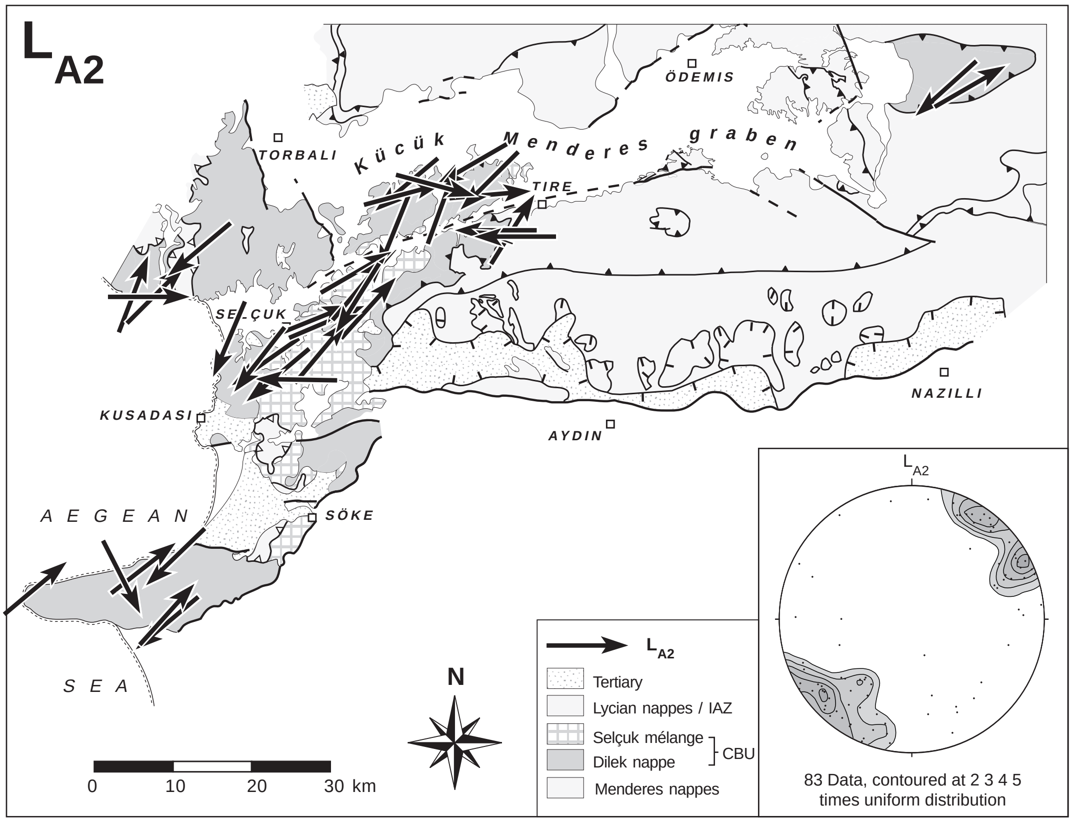

a

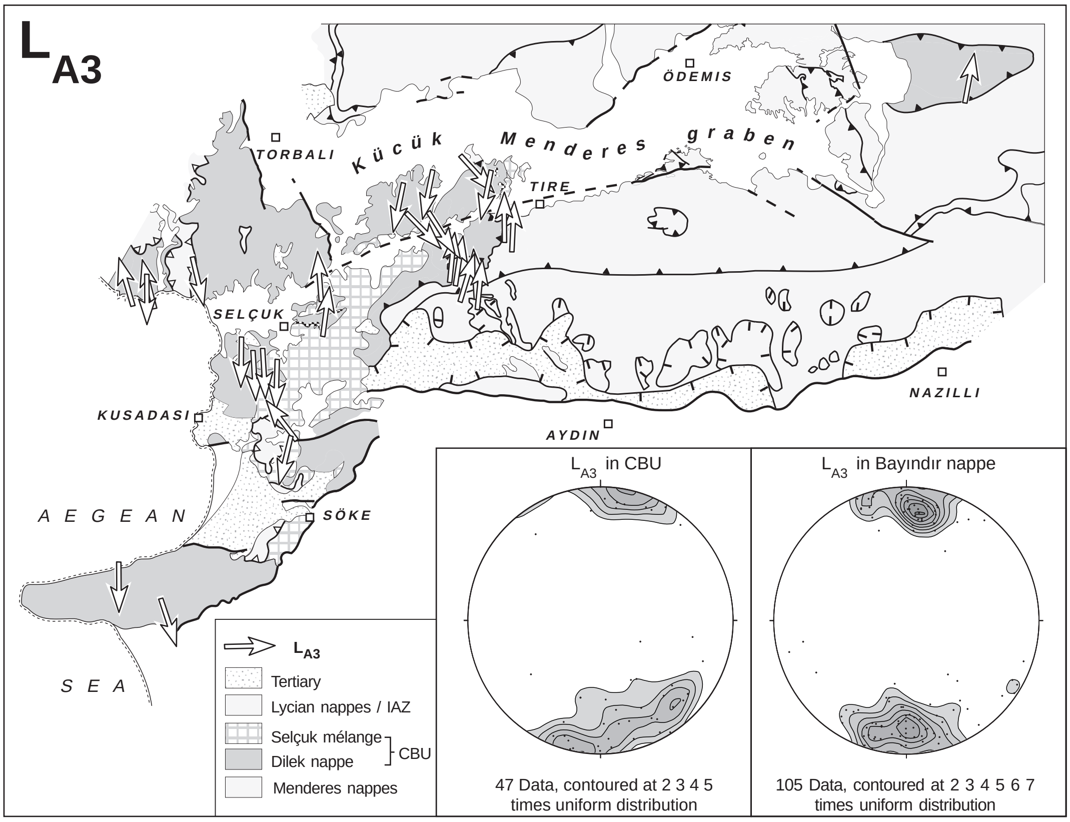

b

Figure 3.6:
Orientations of stretching lineations L_{A2} (a) and L_{A3} (b) in map view and stereograms (equal-area lower-hemisphere projections). In (b), a stereogram of L_{A3} in the Bayındır nappe is shown for comparison.

ween the internal S_{A1} foliation in the porphyroclasts and the external S_{A2} foliation in the matrix is variable, but angles of up to 90° occur. (Fig. 3.7b). On S_{A2}, a L_{A2} stretching lineation is expressed by elongated quartz pebbles and quartz-fibre aggregates in quartzite, kyanite-chloritoid schist and phyllite and by elongated aggregates of white mica in marble (Fig. 3.9a). Stretched L_{A2} quartz-fibre aggregates commonly occur as folded rods or in microlithons between later S_{A3} shear bands. Locally, kyanite laths (Fig. 3.9b), epidote and blue amphibole are aligned subparallel to L_{A2}. In zones where a D_{A3} fabric is weak or absent, L_{A2} generally trends NE (Fig. 3.6a). In zones of strong D_{A3} shear, the orientation of L_{A2} scatters around the N direction.

In zones of pronounced D_{A3} shear, L_{A2} appear to be reoriented into subparallelism with L_{A3}. The present difference in the azimuths of the L_{A2} and L_{A3} stretching lineations of ~45° in rocks which are not or only weakly deformed by D_{A3} is probably close to the original angular separation between L_{A2} and L_{A3} (Fig. 3.10). Therefore, it can be assumed that the original orientation of L_{A2} was about NE-SW.

The shear sense associated with D_{A2} is difficult to detect mesoscopically and aside from rare, directionally inconsistent shear bands, hardly any asymmetries were observed. Nonetheless, at the microscopic scale, asymmetric fabrics in kyanite-chloritoid schist yield a consistent D_{A2} shear sense. D_{A2} top-to-NE shear bands are abundant in the matrix. Between S_{A2} shear bands, chloritoid and kyanite porphyroclasts form σ-shaped objects (Fig. 3.7a and 3.7b, 3.8a and 3.8c) with strain shadows containing recrystallised quartz. The asymmetries displayed by the external and internal foliations of kyanite and chloritoid porphyroclasts can be explained by two kinematic models which imply opposing shear directions [Passchier and Trouw, 1996; their Fig. 7.34(a)] (Figure 3.11a and 3.11b). In the first model (Fig. 3.11a), the asymmetries are caused by dextral (i.e. top-to-SW in this specific case) rotation of the clast with respect to the flow eigenvectors and the external foliation. In the second model (Fig. 3.11b), the external foliation rotates sinistrally (i.e. top-to-NE) with respect to the flow eigenvectors, while the clast is rotating little or not because it is coupled with the strain shadows. The latter model is likely to apply to the kyanite and chloritoid porphyroclasts described here, because of the asymmetric, stair-stepping shape of the strain shadows. Moreover, the top-to-NE displacement along dilational shear bands in the matrix independently point to the same conclusion. If this interpretation is accepted, the vast majority of the kinematic indicators yield a top-to-NE sense of shear during D_{A2}.

The contact between the Selçuk mélange and the Dilek nappe is exposed west of Tire. There, garnet-mica schist of the Selçuk mélange overlies kyanite-bearing calcschist of the Dilek nappe. At the contact, D_{A2} structures are pervasive. S_{A2} layering is parallel to the contact and is associated with a NE-trending L_{A2}, defined by stretched calcite-mica aggregates and up to 30 mm long kyanite laths (Fig. 3.9b).

D_{A3} structures deformed the D_{A2} fabrics in the Selçuk mélange and the Dilek nappe. These overprinting relations and differences in structural style allow for a distinction between D_{A2} and D_{A3} fabrics in many places. D_{A3} is well documented in phyllite and greenschist of the Dilek nappe, whereas in the Selçuk mélange, D_{A3} structures are rare. A S_{A3} foliation is expressed as a penetrative cleavage in phyllosilicate-rich lithologies, in which S_{A2} is strongly transposed and S_{A3} usually forms the dominant foliation. In marble and quartzite, S_{A3} is mostly absent. In composite lithologies like phyllite-quartzite alternations and calcschist, S_{A3} represents a heterogeneous shear-band foliation, in which D_{A2} fabrics are offset by S_{A3} shear bands. In microlithons between the S_{A3} shear bands, crenulation of S_{A2} is frequently observed. A N-trending L_{A3} stretching lineation (Fig. 3.6b) is expressed by fine-grained white mica-chlorite-quartz aggregates. In zones of high D_{A3} strain, folding of S_{A2} and L_{A2} is common with F_{A3} axes oriented subparallel to L_{A3} (Fig. 3.9c and d). D_{A3} high-strain zones within the Dilek nappe are well exposed in phyllite and albite-bearing greenschist at the northern and southern shores of Kusadası Bay. There, S_{A2} and S_{A3} are at such a small angle that L_{A2} and L_{A3} virtually occur on the same foliation plane (Fig. 3.9e). Folding of L_{A2} quartz rods produced F_{A3} sheath folds (Fig. 3.9f). Shear bands, σ-type objects and asymmetric folds associated with D_{A3} fabrics are abundant in the Dilek nappe and yield a uniform top-to-S shear sense (Fig. 3.12).

3.5 The Cycladic-Menderes thrust

The Cycladic-Menderes thrust (CMT) cuts through several nappes of the underlying Menderes nappe pile (Figs. 3.4 and 3.5). In the Selçuk-Tire region, the CMT separates the Dilek nappe from the Bozdag nappe. East of Ödemis, the Dilek nappe overlies para- and orthogneiss of the Çine nappe. South of Selimiye, the CMT is obscured by a series of imbrications, but most likely separates the Dilek nappe from the Selimiye nappe.

The CMT has been studied in detail in the Selçuk-Tire region, where it is well exposed along a ridge crest northwest of Yemisler village (Fig. 3.13). There, the base of the Dilek nappe consists of quartzite and marble, which make up the twin peaks Ballikkayası Tepe and Bozkaya Tepesi. The southern slope of the ridge consists of garnet-mica schist and amphibolite of the Bozdag nappe in the footwall of the CMT. South of Yemisler, amphibolite-facies D_{PA} structures dominate the fabric in the Bozdag nappe. The S_{PA} foliation is expressed by flattened potassium feldspar and quartz and by the preferred orientation of white mica and biotite. S_{PA} is associated with a NE-trending L_{PA} stretching lineation made up by elongated biotite-white mica and quartz-potassium feldspar aggregates. Shear bands indicate a top-to-NE sense of shear. North of Yemisler, in a section several hundred meters thick, the amphibolite-facies D_{PA} structures in the Bozdag nappe are progressively destroyed within a greenschist-facies shear zone. Overprinting criteria, style and metamorphic grade of the foliation and fold axes, as well as the orientation of the stretching lineation and associated kinematic indicators allow to correlate these greenschist-facies structures with D_{A3} structures in the overlying Dilek nappe. D_{A3} structures start to develop ~400 m below the Dilek nappe, where the deformation of D_{PA} structures is characterised by the development of occasional shear bands, in which biotite is retrogressed to chlorite, and narrow quartz veins. D_{A3} structures become penetrative ~300 m below the contact. An increase in D_{A3} intensity is documented by (1) an increased retrogression of biotite and garnet to chlorite (Fig. 3.14a); (2) a conspicuous increase in the number of quartz veins; (3) an increase in the number of cm- to dm-scale asymmetric folds of the D_{PA} fabric associated with a pervasive D_{A3} axial-plane foliation (Fig. 3.10d); and (4) progressively closer spacing of phyllonitic shear bands consisting of sericitic white mica and chlorite. Associated with the narrowly spaced D_{A3} shear bands is a fine-grained N-trending L_{A3} stretching lineation expressed by strongly elongated chlorite-white mica aggregates. In a ~100 m thick zone below the CMT, biotite and garnet are nearly completely retrogressed to chlorite (Fig. 3.14b) and greenschist-facies mylonite shows only D_{A3} structures, which include a penetrative, top-to-S displacing shear-band foliation. The pervasive D_{A3} shear bands can be traced across the CMT. Above the CMT, quartzite of the Dilek nappe displays a narrowly spaced mylonitic S_{A3} with SC'-type shear bands (Fig. 3.14c and d) indicating top-to-S sense of shear. Associated with S_{A3} is a N-trending L_{A3} stretching lineation expressed by stretched quartz, chlorite and white-mica aggregates. Within a ~100 m thick mylonitic D_{A3} shear zone at the base of the Dilek nappe, no D_{A2} fabrics have survived. Above this zone of intense D_{A3} shear, D_{A3} shear bands become less pervasive. About ~250 m above the CMT, D_{A3} shear bands occur as isolated, non-penetrative structures.

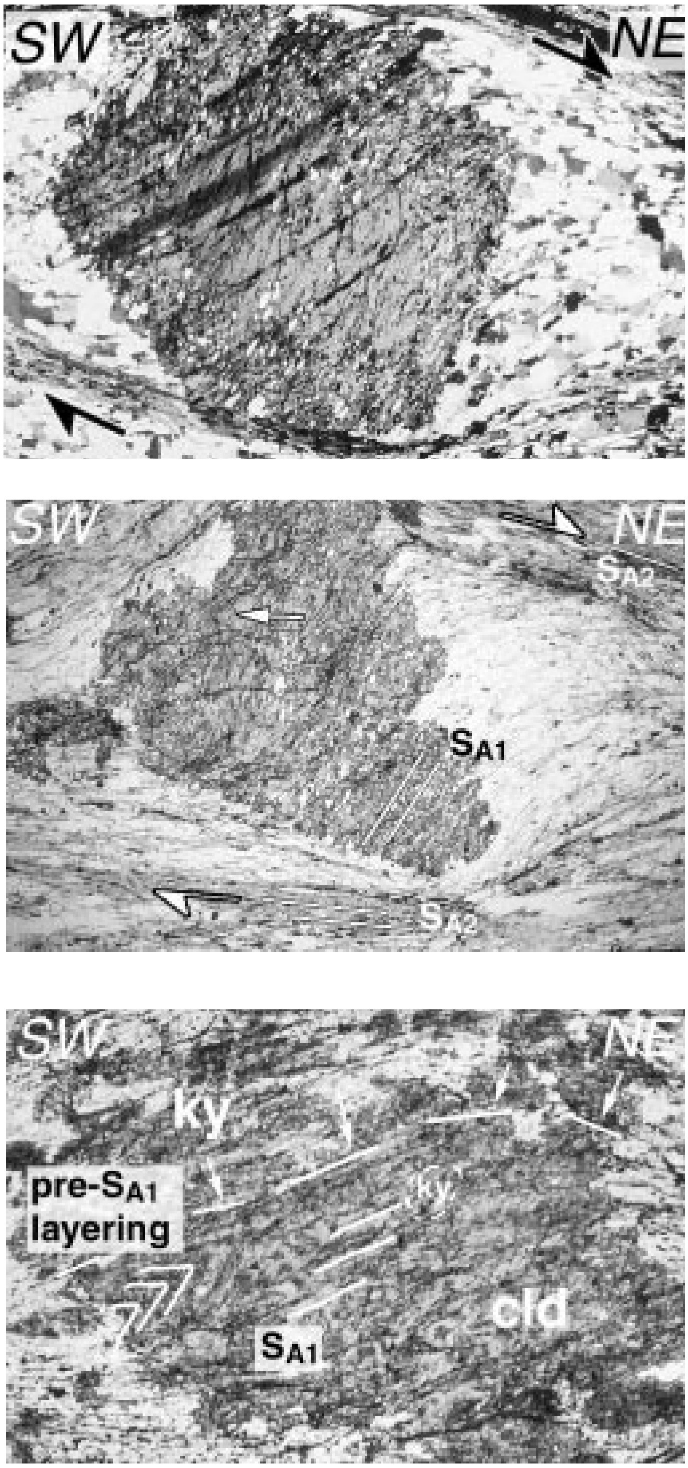

<u>Figure 3.7:</u>
Photomicrographs depicting the relation between foliations S_{A1} and S_{A2} and inferred sense of shear in kyanite-chloritoid schist intercalations in quartzite conglomerate of the Dilek nappe. Mineral abbreviations: ky = kyanite, cld = chloritoid). Location of outcrop where all photomicrographs come from: 37°54.24N, 027°21.92E.
(a) Zoned chloritoid σ–type porphyroclast (*sensu Passchier and Simpson* [1986]) showing faint, straight S_{A1} inclusion trails in the core and slightly curved and more pronounced early D_{A2} inclusion trails in its outer rim. Sense of shear is dextral, i.e. top-to-NE. Field of view is 11 x 16 mm.
(b)Chloritoid σ–type porphyroclast (*sensu Passchier and Simpson* [1986]) with internal foliation S_{A1} oriented at a high angle to S_{A2} in the matrix. Note crenulation of opaque banding indicated by arrow. Sense of shear is top-to-NE. Plane polarised light, field of view is 13 x 18 mm.
(c)Chloritoid and kyanite with crenulated inclusions of pre-S_{A1} opaque banding. Grain boundary between kyanite and chloritoid is outlined by dashed line with arrows. Note that in the strain shadows S_{A1} is stair-stepping upward to the right, indicating top-to-NE sense of shear. Plane polarised light, field of view is 9.5 x 13.5 mm.

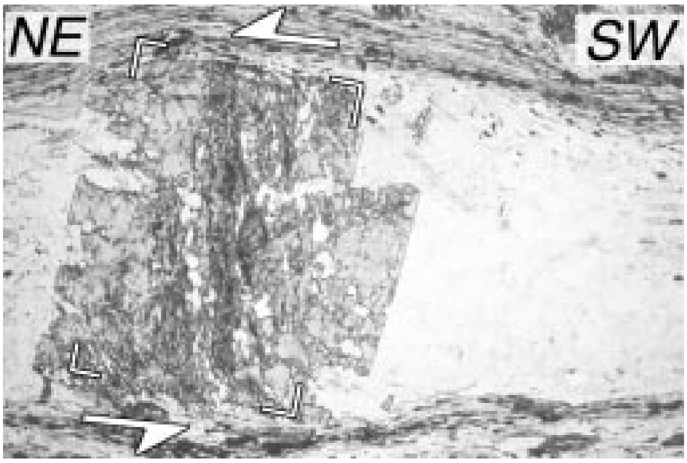

a

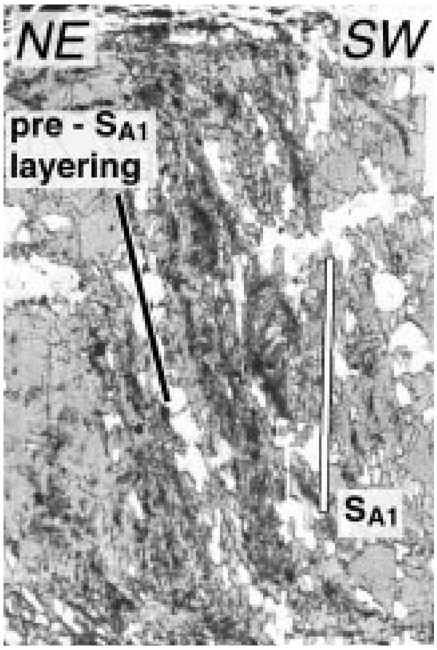

b

c

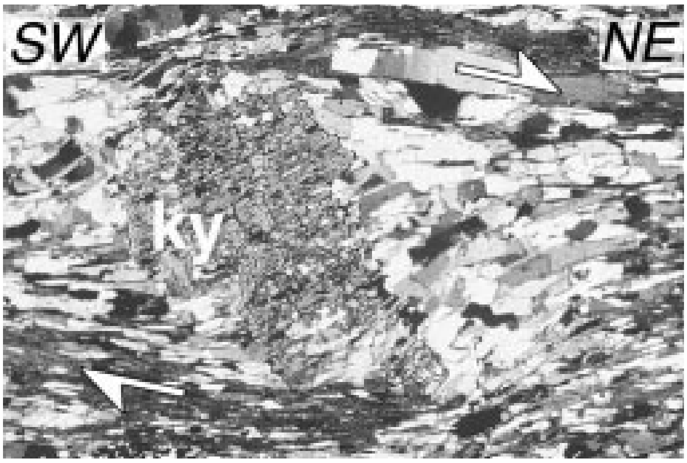

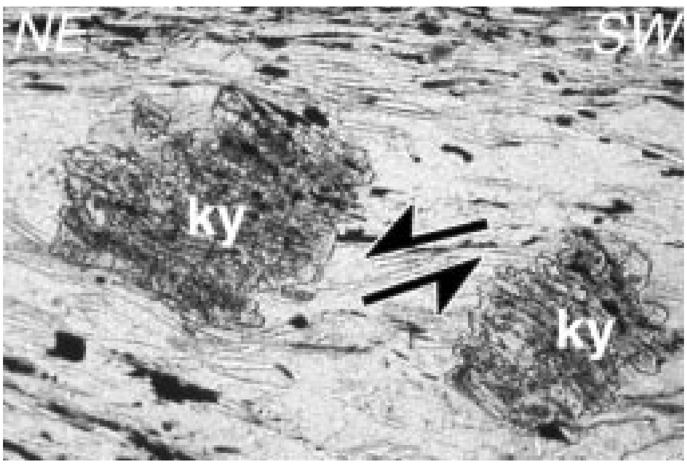

d

<u>Figure 3.8:</u>
Photomicrographs depicting the relation between S_{A1} and S_{A2} and inferred sense of shear in kyanite-chloritoid schist of the Dilek nappe (same location as Fig. 3.6).
(a) Chloritoid porphyroclast with curved inclusion trails illustrating the angular relationship between pre-S_{A1} opaque banding, internal foliation S_{A1}, and foliation S_{A2} in the matrix. Sense of shear is top-to-NE. Note that white box in (a) indicates the location of Fig. 3.7(b). Plane polarised light, field of view is 9 x 13.5 mm in (a) and 8 x 5.5 mm in (b).
(c) Kyanite porphyroclast with σ–type geometry indicating top-to-NE sense of shear. Field of view is 1.8 x 2.7 mm.
(d) Asymmetrically boudinaged kyanite grains with the dilational shear band indicating top-to-NE sense of shear; crossed nicols, field of view is 4.1 x 6.3 mm

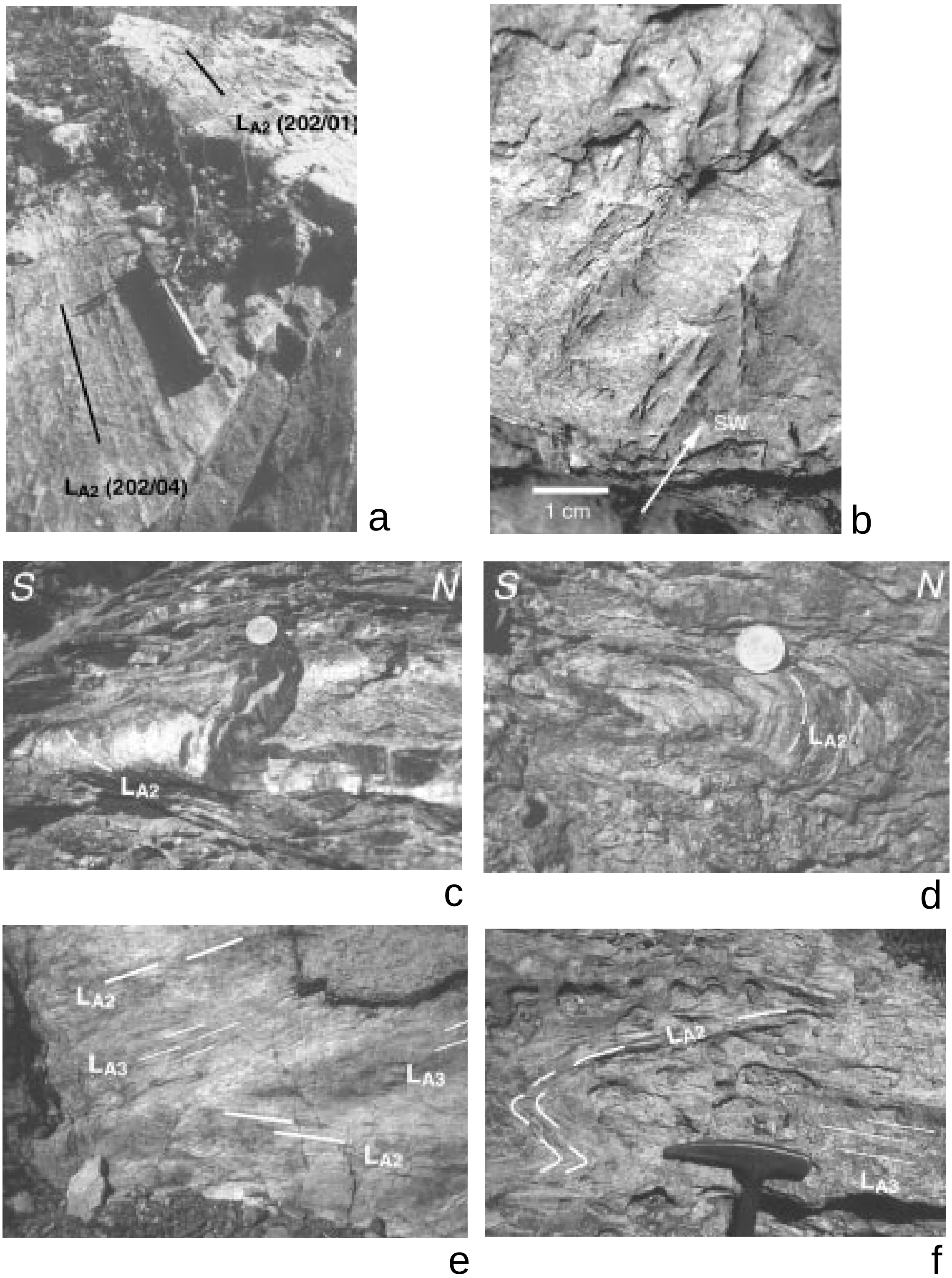

Figure 3.9:
Outcrop photographs showing D_{A2} fabrics.
(a) Subhorizontal S_{A2} in marble of the Dilek nappe with typically 'coarse' L_{A2} mica-aggregate lineation. Orientation of lineations is illustrated; view is to the east, outcrop location is 38°03.12N, 27°31.65E.
(b) Aligned kyanite laths on S_{A2} in kyanite-chloritoid schist of the Dilek nappe in plan view. Location of outcrop is 37°54.24N, 027°21.92E.
(c) and (d) Folding of S_{A2} and L_{A2} about N-trending F_{A3} fold axes in calcschist-phyllite intercalation. Same outcrop as in(b).
(e) Coarse-grained relic L_{A2} expressed by stretched quartz and fine grained L_{A3} mica-aggregate lineations on S_{A3}. Location of outcrop is 37°59.36N, 27°10.96E; field of view 45 x 30 cm. (f) Sheath-like folding of L_{A2} quartz rod in albite-epidote greenschist of the Dilek nappe. L_{A3} is expressed by a N-trending fine-grained white-mica-aggregate lineation; plan view, outcrop is located at 38°00.76N 027°06.23E.

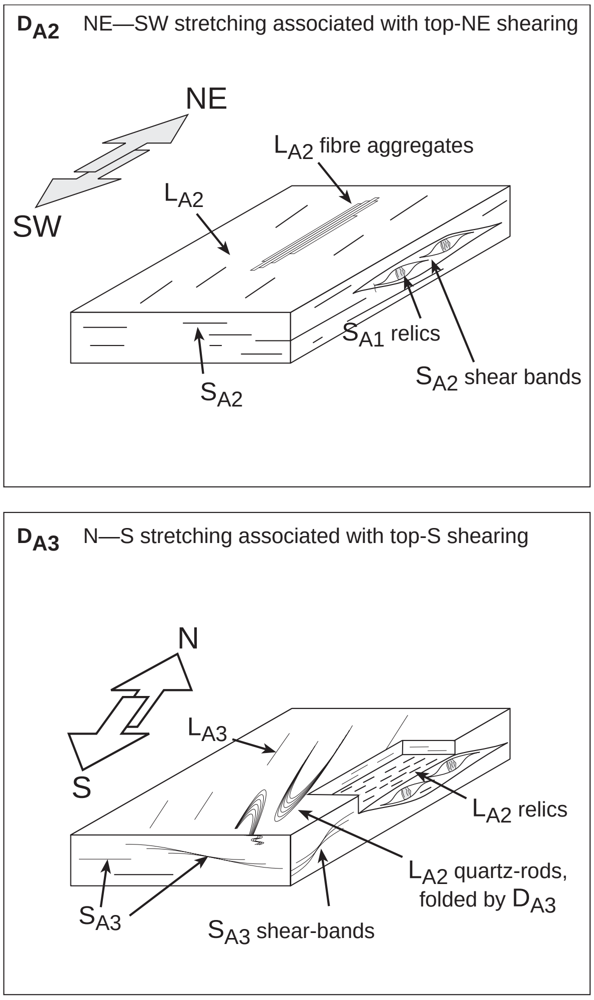

Figure 3.10:
Schematic illustration of the different regional stretching directions during D_{A2} and D_{A3}, as inferred by the mean orientations of L_{A2} and L_{A3}. Kyanite-chloritoid schists, which preserve D_{A1} relics occur in large lenses of quartz conglomerates which show little if any D_{A3} overprint.

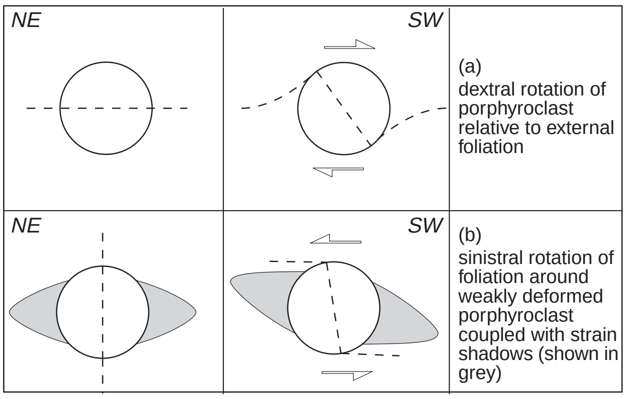

Figure 3.11:
Schematic model for the development of porphyroclasts displaying a high angle bewteen internal and external foliation during non-coaxial deformation. (a) Porphyroclast rotates freely with respect to flow eigenvectors causing steepening of the internal foliation; internal and external foliation in this case would belong to the same generation (i.e. S_{A2} as described in this paper) and the inferred sense of shear would be dextral, i.e. top-to-SW. (b) Case, in which foliation rotates sinistrally (i.e. top-to-NE) with respect to porphyroclast which largely remains stationary because it is coupled with the strain shadows. Because the foliation rotates relative to the porphyroclast new cleavage domains (S_{A2}) form between the strain shadows. Case (b) is preferred because it is in agreement with the sense of shear indicated by shear bands in the matrix. The internal foliation within the porphyroclast is S_{A1}, and its steep dip is close to the original attitude of S_{A1}.

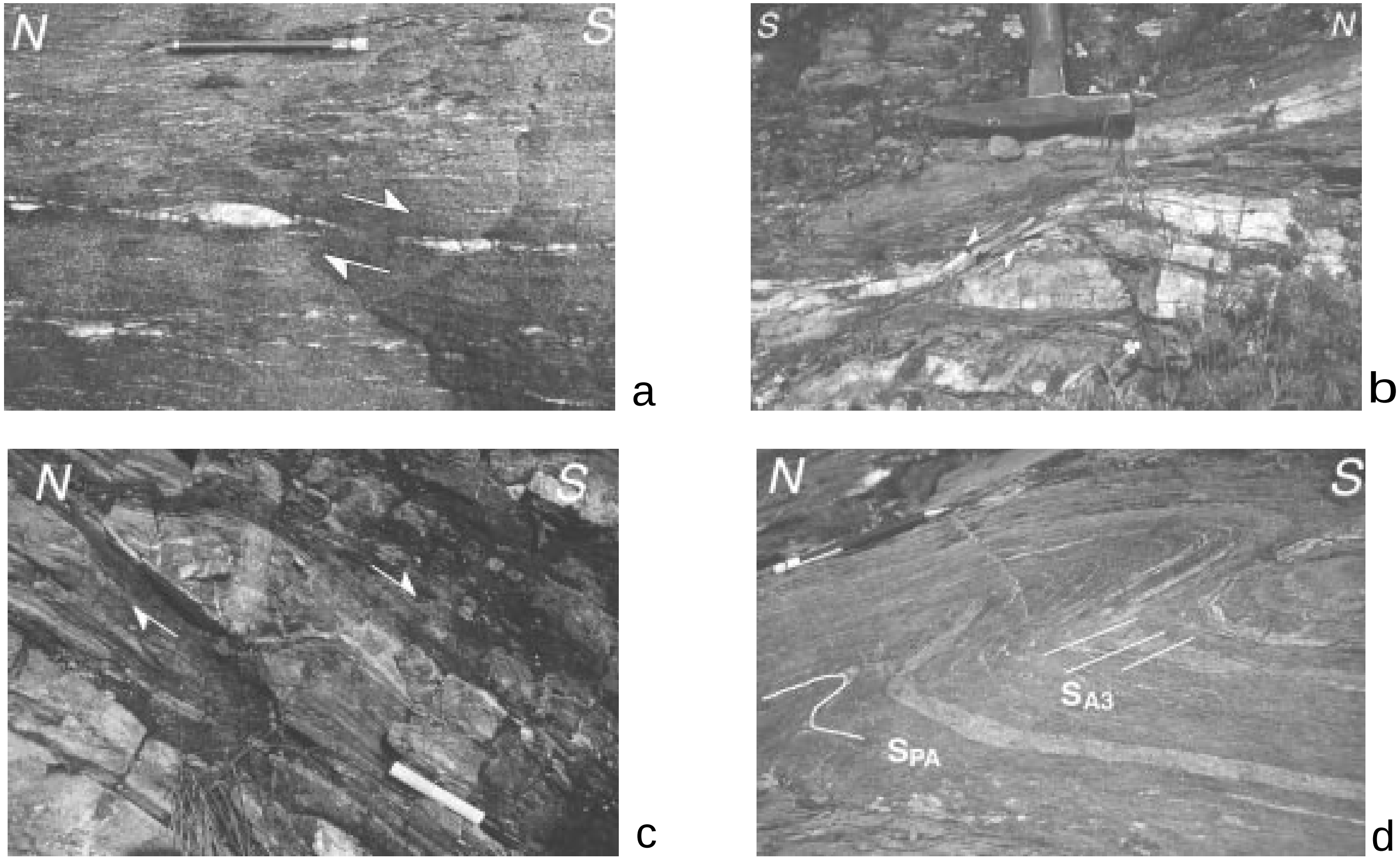

Figure 3.12:
Macroscopic D_{A3} shear-sense indicators. (a) Quartz vein offset by D_{A3} dilational shear band indicating top-to-S shear sense in albite-epidote greenschist. Section view; same outcrop as Fig. 3.9(f). (b) D_{A3} dilational shear band displacing S_{A2} in calcschist-phyllite intercalation of the Dilek nappe. Inferred shear sense is top-to-S; location is at 38°037.8N, 027°31.43E. (c) D_{A3} shear zone in calcschist of the Dilek nappe with a σ–type object of marble indicating top-to-S sense of shear; location is at. 37°55.01N, 027°20.12E (d) Asymmetric D_{A3} fold in quartzite of the Bozdag nappe with a closely spaced axial-planar S_{A3} cleavage. Outcrop is located at 38°01.75N, 27°41.11E.

3.6 Interpretation of deformation / metamorphism / timing relationships

3.6.1 D_{A1} and D_{A2}

Chloritoid and kyanite form a peak-high-pressure assemblage in the Ampelos nappe in Samos [Will *et al.*, 1998] and the correlative Dilek nappe in western Turkey. The temporal relation between the formation of S_{A1} and S_{A2} and the growth of chloritoid and kyanite reveals aspects of the tectonometamorphic history of the Dilek nappe during high-pressure metamorphism. An interpretative sequence of the relationship between the development of structures and mineral growth is shown in Figure 3.15a-f. Growth of chloritoid and kyanite porphyroblasts occurred after the formation of S_{A1} and overlapped with the onset of D_{A2} structures. Early during D_{A2}, chloritoid and kyanite ceased to grow (Fig. 3.15d-e). This can be explained by D_{A2} decompression.

3.6.2 D_{A3}

Deformation/metamorphism relations during D_{A3} are complex and heterogeneous. In the Selimiye nappe, *Hetzel and Reischmann* [1996] reported growth of garnet (i.e. temperatures exceeding 450°C) after the formation of the D_{A3} Selimiye shear zone. Accordingly, $^{40}Ar/^{39}Ar$ white-mica ages from the Selimiye shear zone were interpreted to constrain cooling after shearing [*Hetzel and Reischmann*, 1996]. In the Bayındır nappe at the base of the Menderes nappes, D_{A3} fabrics formed at peak-metamorphic temperatures of ≤400°C (Fig. 3.2). Hence, the $^{40}Ar/^{39}Ar$ white-mica ages of *Lips* [1998] closely date D_{A3} in the Bayındır nappe. As suggested above, downward propagation of D_{A3} thrusting was associated with decreasing temperatures.
Deformation/metamorphism relations across the CMT indicate that the breakdown of garnet and biotite to chlorite at temperatures ≤ ~ 400°C [*Yardley*, 1989] is a consequence of D_{A3} mylonitisation. It follows that temperatures at the CMT were >50°C lower than in the Selimiye shear zone and that the inverted metamorphic gradient in the Menderes nappe pile is likely to be older than the CMT. Therefore the CMT can be regarded as a late D_{A3} structure. In concert with geometric constraints (Figs. 3.5 and 3.16), the age data suggest that the emplacement of the Cycladic blueschist unit was by out-of-sequence thrusting.

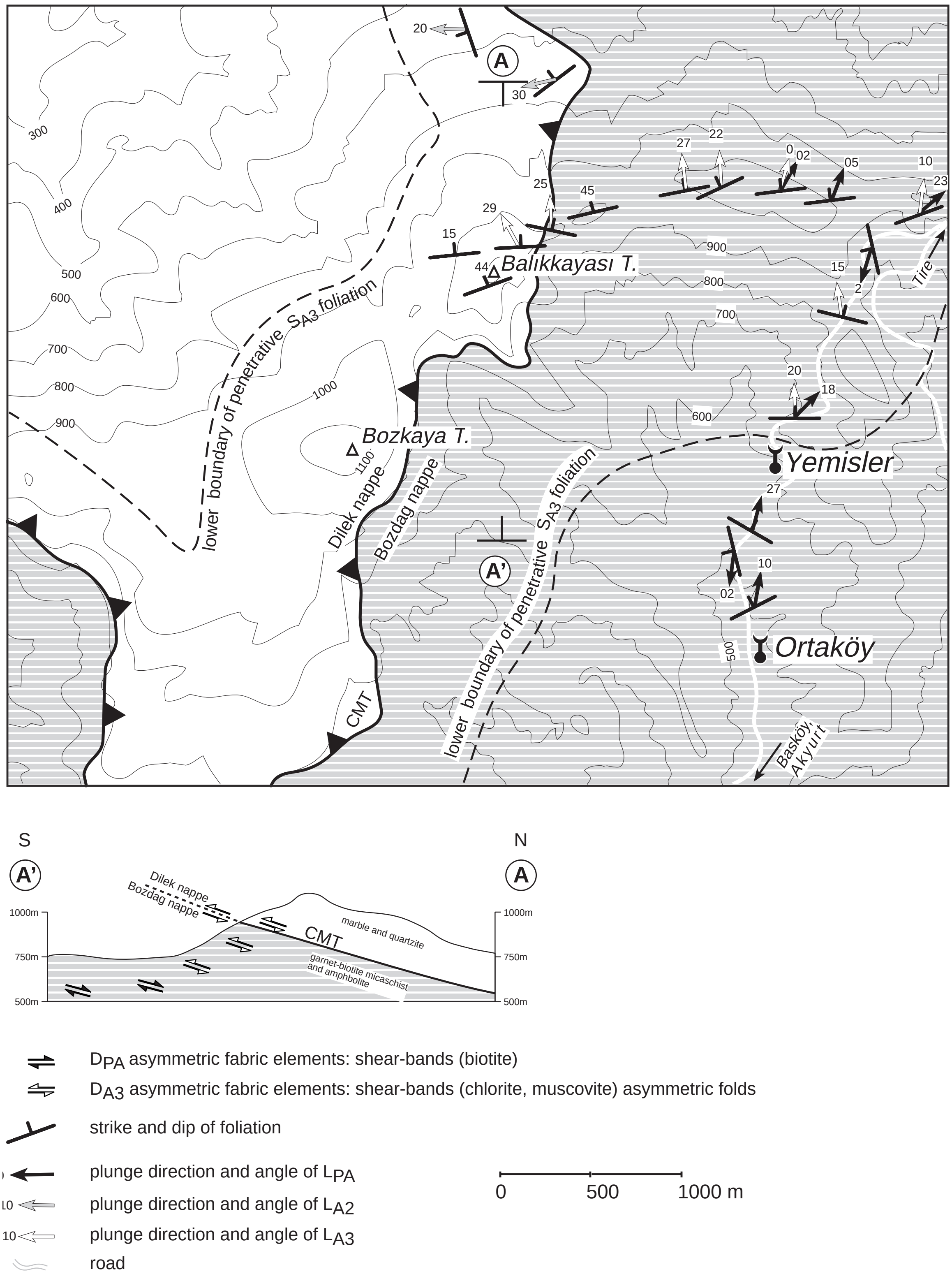

Figure 3.13:
Structural map and cross-section from the area southwest of Tire, where the CMT separates the Dilek nappe from the underlying Bozdag nappe (refer to Fig. 3.4 for location of the map). The extent of the D_{A3} shear zone separating the nappes is indicated; also shown are D_{A3} structures as well as those structures which were deformed by D_{A3}. Fill pattern in Dilek nappe has been omitted for clarity of illustration; elevations shown in meters.

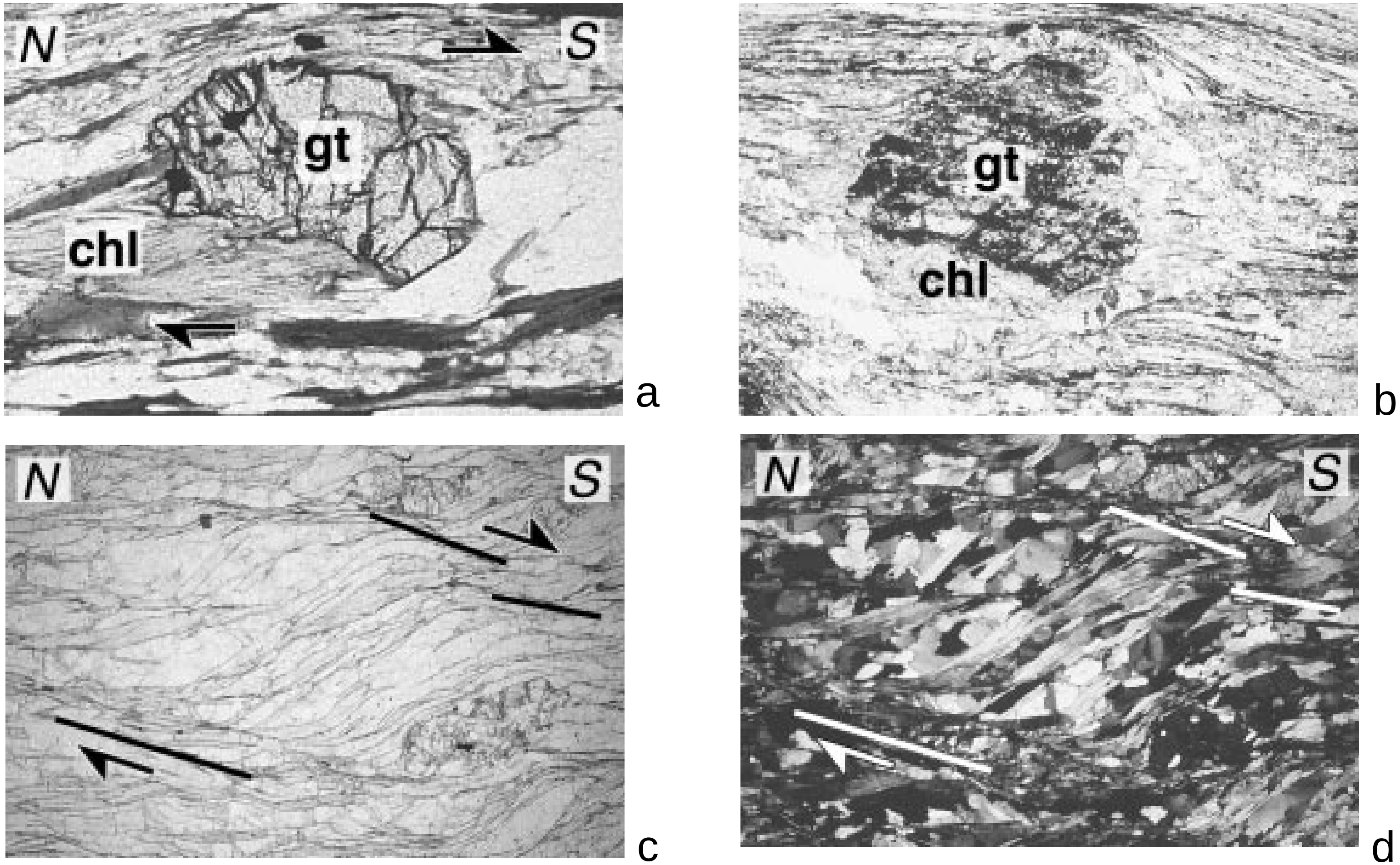

Figure 3.14:
Microstructures from the CMT. (a) Photomicrograph showing the retrograde growth of chlorite (chl) at the expense of garnet (gt) in garnet-biotite schist of the Bozdag nappe. Asymmetric tails of chlorite indicate top-to-south directed shearing during retrogression; plane polarised light, field of view 3.5 x 5.3 mm, location of outcrop is 38°01.94N, 27°41.22E. (b) Strong retrogression of garnet in sericitic micaschist of the CMT mylonite zone; plane polarised light, field of view 11 x 16 mm, location of outcrop is at 38°05.46N, 27°40.33E. (c) and (d) Photomicrograph of quartzite mylonite of the Dilek nappe in the hangingwall of the CMT with shear bands showing top-to-S displacement; plane polarised light (c) and crossed nicols (d), field of view 11 x 16 mm, location of outcrop is at 38°02.59N, 27°40.58E.

3.7 Discussion

3.7.1 Tectonic implications

Detailed structural work across the contact of the Dilek nappe with the underlying Bozdag nappe reveals that this contact is a late D_{A3} greenschist-facies shear zone, the CMT, along which the Cycladic blueschist unit was emplaced on top of the Menderes nappes by out-of-sequence thrusting. Significant differences in pre-CMT histories in the hanging- and footwall imply large displacements along the CMT. In the Cycladic blueschist, the CMT overprinted a two-phase Alpine high-pressure history; in the footwall, the CMT crosscuts pre-Alpine structures. During mylonitisation along the CMT the temperature was relatively low at least in the upper portion of the Menderes nappe pile, if compared to the temperature at which D_{A3} fabrics formed in the Selimiye nappe. This implies that the Menderes nappes had been assembled early during D_{A3}, before the Cycladic blueschist unit was emplaced.
The reason why it is proposed that D_{A3} and the associated CMT resulted from crustal shortening is that the Cycladic blueschist unit ramped upwards relative to the Earth' surface in the direction of D_{A3} transport. As illustrated in Figure 3.5a and 3.5b, the CMT cuts up-section through the Menderes nappe pile, which was assembled during an earlier stage of D_{A3}. Within the Menderes nappes, the inverted metamorphic gradient suggests crustal shortening. Even if the original attitude of the Menderes nappe contacts had been subhorizontal, the CMT would still have had to be somewhat steeper in order to cut up-section in the direction of transport. This geometry is displayed in Figure 3.16, which illustrates the proposed thrust sequence and the albeit scarce thermochronologic data. The mylonitic rocks in the Selimiye shear zone cooled below 350-400°C between 43-37 Ma [*Hetzel and Reischmann*, 1996] (thrust 5 in Fig. 3.16). D_{A3} thrusting in the Menderes nappes progressed structurally downwards and affected the Bayındır nappe at ~37 Ma [*Lips*, 1998] (thrusts 6 and 7 in Fig. 3.16). If this interpretation is correct, phengite $^{40}Ar/^{39}Ar$ ages of 40 Ma reported by *Oberhänsli et al.* [1998] from the Dilek nappe would constrain cooling of the latter below ~350-400°C after greenschist-facies emplacement of the Cycladic blueschist unit. The available age data do not allow a clear statement whether or not deformation of the Bayındır nappe occurred before, during or after motion at the CMT.
Overall, the tectonic evolution in western Turkey as outlined in Figure 3.16 is in striking contrast to the orogenic development in the Aegean, where the Cycladic blueschist unit rests on the External Hellenides. The latter show early Oligocene high-pressure metamorphism in some windows and early Miocene high-pressure metamorphism in Crete and the Peleponnesos (Fig. 1.1). The downward propagating high-pressure metamorphism in the Aegean was probably controlled by progressive southward retreat of the Hellenic subduction zone, which most likely commenced in the Eocene [*Thomson et al.*, 1998]. In western Turkey, subduction-zone retreat was probably halted when the exotic Anatolide microcontinent (Fig. 3.2) entered the subduction zone in the Eocene [*Hetzel et al.*, 1995b; *Ring et al.*, 1999a]. It could be speculated that the overall continental

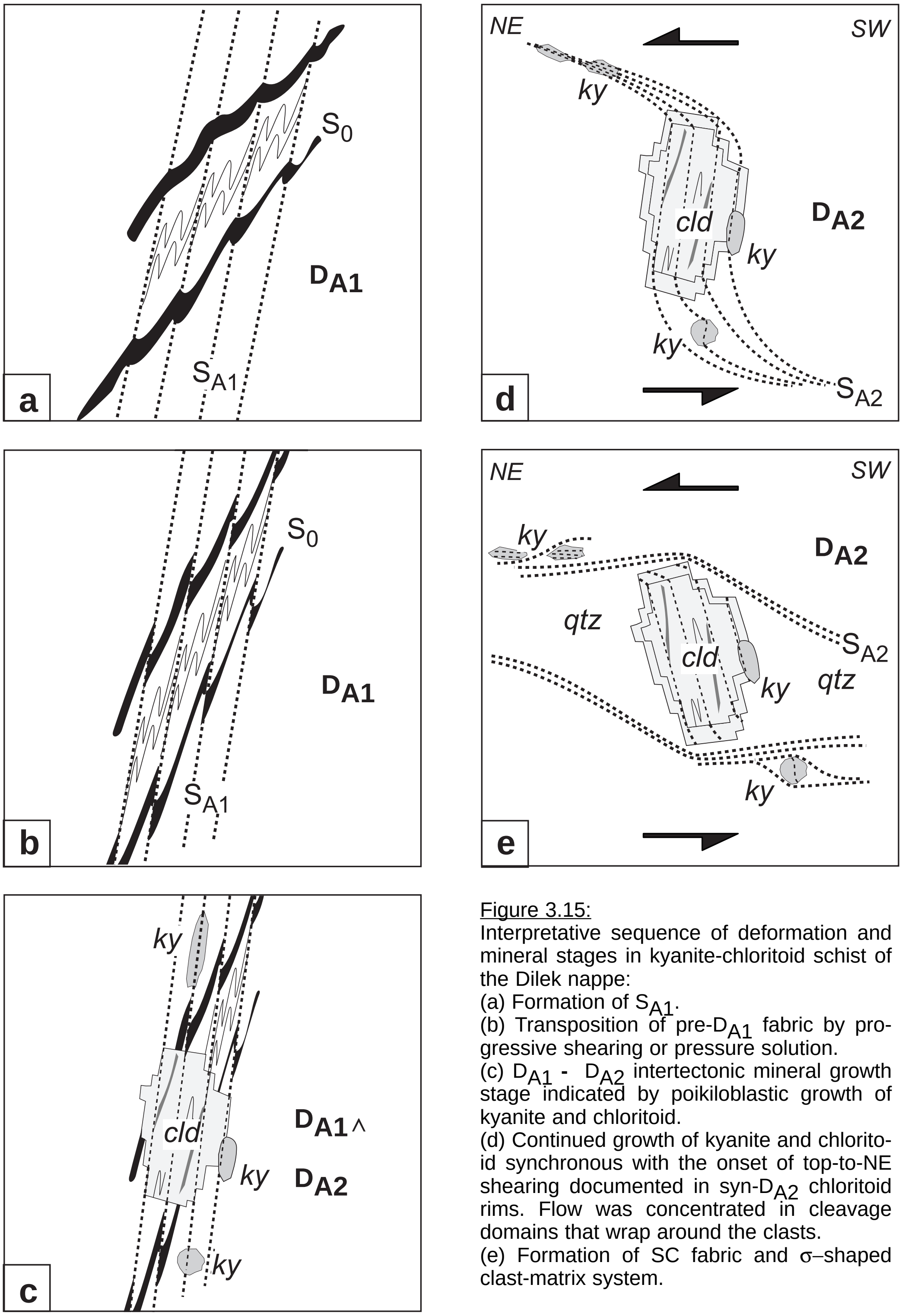

Figure 3.15:
Interpretative sequence of deformation and mineral stages in kyanite-chloritoid schist of the Dilek nappe:
(a) Formation of S_{A1}.
(b) Transposition of pre-D_{A1} fabric by progressive shearing or pressure solution.
(c) D_{A1} - D_{A2} intertectonic mineral growth stage indicated by poikiloblastic growth of kyanite and chloritoid.
(d) Continued growth of kyanite and chloritoid synchronous with the onset of top-to-NE shearing documented in syn-D_{A2} chloritoid rims. Flow was concentrated in cleavage domains that wrap around the clasts.
(e) Formation of SC fabric and σ–shaped clast-matrix system.

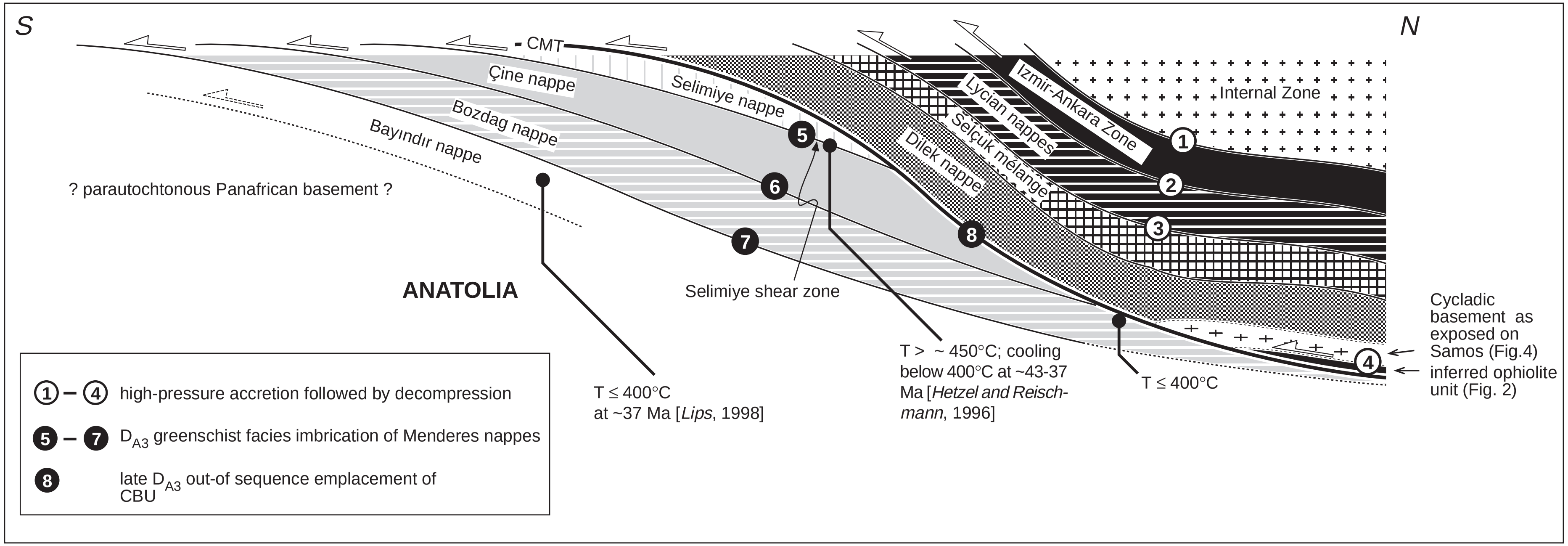

Figure 3.16:
Interpretative thrust sequence in the Anatolide belt of western Turkey. Late Cretaceous to early Eocene imbrication of the Vardar-Izmir-Ankara zone and the Cycladic blueschist unit during high-pressure metamorphism (thrusts 1-4). Collision of Anatolia caused greenschist-facies imbrication within Menderes nappes (thrusts 5-7). The initiation of the out-of-sequence CMT is may be due to the collision of the evolving thrust wedge with the Bayındır nappe (and its concealed basement), which is thought to have caused additional shortening and supposedly a change in wedge taper, which may have triggered backstepping of thrusting and emplacement of the Cycaldic blueschist unit onto the Menderes nappes. In this case the collision had forced the basal thrust of the wedge to steepen as it climbed over the colliding terrane. The predicted result would be to shift deformation rearward into the wedge with the formation of out-of-sequence thrust faults. Note that this model does allow simultaneous in-sequence motion of the Bozgag nappe onto the Bayındır nappe and out-of-sequence movement at the CMT. Because of the rare thermochronologic data, the proposed thrust sequence remains speculative but provides a testable working hypothesis.

architecture of the Anatolide microcontinent was different from that of easternmost Adria. The crust of the latter was, at least in part, highly thinned (Pindos) or even oceanic (Ionian basin), and had probably been easier to subduct than the crust of Anatolia. There is no indication that the crust of Anatolia was thinned before entering the subduction zone. *Wijbrans and McDougall* [1988] made a similar proposition by speculating that the Cycladic zone was formerly a collage of small fragments of easily subductable continental crust. The accretion of Anatolia may have caused early D_{A3} thrusting in the upper Menderes nappes (thrusts 5 and 6 in Fig. 3.16). Accretion of the Bayındır nappe may have caused a change in wedge taper triggering additional shortening, backstepping of thrusting towards the hinterland and emplacement of the Cycaldic blueschist unit onto the Menderes nappes.

The observation that the Cycladic blueschist unit sits on top of the Menderes nappes has also implications for the Lycian nappes above the Cycladic blueschist unit. Because early orogenic development progressed structurally downward, high-pressure metamorphism in the Lycian nappes should be older than that in the Cycladic blueschist unit and therefore be late Cretaceous in age. Such an inference fits well into the recently proposed tectonic model for the Lycian nappes by *Collins and Robertson* [1998]. The tectonic position of the Lycian nappes above the Cycladic blueschist unit implies that the Lycian nappes were once part of Adria or Sakarya, or a continental fragment rifted off from Adria or Sakarya, rather than part of Anatolia, as is generally assumed [*Sengör and Yilmaz*, 1981; *Sengör et al.*, 1984; *Collins and Robertson*, 1998].

3.7.2 Exhumation of the Cycladic blueschist unit

The overgrowth of S_{A1} by a blueschist-facies mineral assemblage suggests that D_{A1} occurred during prograde high-pressure metamorphism and is probably related to nappe stacking in the Cycladic blueschist unit (see *Lister and Raouzaios* [1996] for Sifnos Island and *Ring et al.* [1999b] for Samos Island). The subsequent D_{A2} event occurred during initial decompression, i.e. exhumation, and may have reactivated the nappe contact of the Dilek nappe and the Selçuk mélange. The Cycladic blueschist unit must have been exhumed by ~35 km before Eocene greenschist-facies emplacement onto the Menderes nappes during late D_{A3}. How this pronounced exhumation was accomplished is largely unknown. *Avigad et al.* [1997, their Fig. 3.13] inferred an early extensional event and placed it into the Oligocene. *Ring* [1998] argued that vertical ductile thinning associated with a subhorizontal foliation and erosion aided 30-40 km of Eocene/early Oligocene exhumation of the Cycladic blueschist unit in Samos.

There are two possibilities for the tectonic interpretation of D_{A2} top-to-NE shear. (1) D_{A2} is related to backthrusting of the Cycladic blueschist unit onto its hinterland. Backthrusting in an accretionary wedge might be due to the development of topographic gradients [e.g., *Willett et al.*, 1993]. Accordingly, S_{A2} should have originally dipped towards the SW, but pervasive D_{A3} shearing may have rotated S_{A2} into subparallelism with the N-dipping penetrative S_{A3} foliation. The

~35 km of exhumation would then be due to vertical ductile thinning and erosion. (2) D_{A2} is related to normal faulting, which aided exhumation of the Cycladic blueschist unit during D_{A2} in the Eocene. An initially high angle between S_{A1} and the instantaneous stretching axis of D_{A2} can be inferred from S_{A1} and S_{A2} in those porphyroclasts which retained their initial position between the strain shadows during shearing (Fig. 3.11). The high angle between S_{A1} and S_{A2} may reflect a pronounced change of the flow field, i.e. a strain reversal, and would lend strong support into an extensional interpretation of D_{A2}. If D_{A2} reworked the contact between the Dilek nappe and the Selçuk mélange, the Dilek nappe should have decompressed faster in the Eocene than the Selçuk mélange. Further work is needed to resolve this issue, which has important implications for exhumation processes in the eastern Mediterranean.

3.8 Conclusions

The Anatolide belt of western Turkey was assembled by top-to-S thrusting of the Cycladic blueschist unit onto the Menderes nappes during greenschist-facies metamorphism in the Eocene. The different tectonometamorphic histories of both units preclude the model that the Menderes nappes are the eastern continuation of the Cycladic blueschist unit. The Cycladic blueschist unit displays a prograde Alpine D_{A1} fabric, which was overgrown by a high-pressure mineral assemblage. The onset of D_{A2} occurred during initial decompression of this high-pressure event and is associated with top-to-NE shearing. A subsequent top-to-S greenschist-facies D_{A3} event affected the Cycladic blueschist unit and the Menderes nappes together. Late during D_{A3} the contact between the Cycladic blueschist unit and the Menderes nappes, the Cycladic-Menderes thrust, formed. The CMT defines an out-of-sequence ramp structure, which cuts up-section through Menderes nappes towards the south. In the Cycladic blueschist unit, late D_{A3} fabrics associated with the CMT crosscut high-pressure D_{A2} structures. In the footwall, D_{PA} structures in the Bozdag nappe were deformed by the CMT. The Cycladic blueschist unit was exhumed by ~35 km before the CMT formed in the Eocene. D_{A2} structures aided this early exhumation, either by vertical ductile thinning, normal faulting, or a combination of both.

Chapter 4

Late Alpine extension and core complex formation

4.1 Abstract

A large syncline structure in the central part of the Anatolide belt of western Turkey occurs between a symmetrically arranged detachment system. The bivergent detachment system delimits the Central Menderes metamorphic core complex (CMCC). The regional pattern of apatite fission-track ages shows that the CMCC started to form in the middle Miocene. Back-rotation of time lines of the apatite-fission track ages and the regional foliation shows that the detachments rotated from an initially steep to a presently shallow orientation by a rolling-hinge mechanism. Associated upwarping of the footwalls to the detachments produced the syncline structure. Detachment faulting caused considerable topography across the CMCC, which suggests that the upper mantle was involved in this process.

4.2 Introduction

Metamorphic core complexes form when continental lithosphere stretches at high rates and strain within the upper crust becomes localised in detachment faults which can accommodate tens of kilometers of displacement [*Buck*, 1991]. Detachment faults are exposed as low-angle to horizontal shear zones, along which sedimentary or low-grade metamorphic rocks of a brittlely deforming upper plate are placed against medium- to high-grade rocks of a ductily deforming lower plate. The Basin and Range province in the western U.S. [*Wernicke*, 1981] and the Aegean Sea in the Mediterranean [*Lister et al.*, 1984] are classic examples of lithospheric stretching and core-complex formation.

Controversial views exist about the initial angle and incremental development of the detachment faults and the nature of strain partitioning within different layers of the stretching lithosphere during core-complex formation. While some authors infer low-angle normal fault geometries for the basal cutoff throughout core-complex formation [*Davis and Lister*, 1988; *Wernicke*, 1995] (Fig. 4.1a), others claim that the low dip angles are not original [*Buck*, 1988; *Lavier et al.*, [1999] (Fig. 4.1b). The latter authors infer that flat-lying detachments are produced by a so-called rolling-hinge mechanism [*Axen et al.*, 1995], by which initially high-angle normal faults are rotated into a low-angle orientation by upward flexing of the footwall as an isostatic response to unloading. For this setting, the deforming lithosphere is generally assumed to be mechanically stratified with a brittle-elastic upper crust being decoupled from a viscous lower crust [*Gans*, 1987; *Buck*, 1991; *Axen et al.*, 1998]. However, to what extent regional unloading and the resulting horizontal stress gradient affect the deeper layers of the lithosphere remains unknown. Is flow limited to the lower crust [*Block and Royden*, 1990; *Buck*, 1991] or is the upper mantle also deforming [*Spencer*, 1984; *Buck*, 1988; *Wernicke and Axen*, 1988]? If the former is the case, a decoupled, weak lower crust is likely to accommodate most of the strain by lateral inflow of material, thus leaving the Moho and topography flat across the detachments as observed in the core complexes of the Basin and Range province [*Block and Royden*, 1990; *Buck*, 1991]. If the lower crust is cooler and stronger, viscous flow occurs at lower rates and may not be able to compensate the lateral stress gradient. In this case, the Moho may become upwarped and topography builds up. Because there is little topography across the core complexes in the Basin-and-Range province and the Moho beneath it is flat, it has been argued that a weak decoupled lower crust may be a general requirement for core-complex formation [*Gans*, 1987; *Block and Royden*, 1990; *Buck*, 1991]. In contrast, *Lavier et al.* [1999] presented a self-consistent numerical model in which a pronounced topographic gradient develops across a large offset detachment with a rolling-hinge geometry.

This Chapter deals with the structure and cooling history of the Central Menderes metamorphic core complex (CMCC) in western Turkey, which is a field example for a still active bivergent rolling-hinge detachment system with a large topographic gradient.

4.3 The Central Menderes Metamorphic core complex

The CMCC is located in the Anatolide belt of western Turkey, which formed during late Eocene thrusting of Cycladic high-pressure units onto the Anatolian microcontinent [*Ring et al.*, 1999b]. The CMCC extends for about 100 km in E-W direction and 50 km in N-S direction. It is bounded by two E-striking symmetrically arranged detachment systems (Fig. 4.2a and 4.2b): The N-down Kuzey detachment in the north [*Hetzel et al.*, 1995] and the S-down Güney detachment in the south [*Emre and Sözbilir*, 1997], both of which cut the upper levels of the Alpine nappe pile for a distance of approximately 80 km. The Kuzey detachment dips at 15-20°N. The hanging wall consists of S-dipping Miocene alluvial sediments underlain by small volumes of amphibolite-grade orthogneiss. The footwall exposes a greenschist-facies mylonitic shear zone of early Miocene age [*Hetzel et al.*, 1995].

The Güney detachment is exposed along the northern shoulder of the Büyük Menderes graben as a 0-15°S-dipping cataclastic shear zone, which constitutes the basal cut-off to a Neogene supra-detachment basin system. Asymmetric fabric elements like Riedel composite structures [*Chester and Logan*, 1987; *Cowan and Brandon*, 1994] yield slip vectors that indicate top-to-S displacement (Fig. 4.3) In an array of tilted blocks, metamorphic rocks are exposed as the substratum of nonconformably overlying Miocene alluvial sediments. Both, basement and sediments are cut by brittle shear zones, which in their present orientation display low-angle normal and reverse fault geometries.

Down-dip displacement along the detachments is largest in the central part of the CMCC; laterally the faults either die out or terminate against small-offset high-angle normal faults. At the Kuzey detachment, a distinct high-grade orthogneiss, which occurs in the internal part of the CMCC and above the detachment suggests a minimum down-dip displacement of ~12 km (Fig. 4.4). Displacement-to-length relationships [*Cowie and Scholz*, 1992] suggest a roughly similar displacement at the Güney detachment.

The Kuzey and the Güney detachments root in Plio-Pleistocene to Recent half-graben, which separate the CMCC from adjacent plateau-like areas. These are the Gediz graben and the Büyük Menderes graben. Both graben were seismically active in historic times. In, 1969, two earthquakes of surface magnitude 6.5 and 5.9 occurred in the Gediz and Simav graben and involved N-down normal faulting [*Eyidogan and Jackson,* 1985] (Fig. 4.2a). No sense of motion is known from the large-magnitude event of 1899 in the Aydin-Nazilli area of the Büyük Menderes graben [*Schaffer*, 1900]. There is no record of seismic activity for the Plio-Pleistocene Kücük Menderes graben, which is oriented parallel to the axial trend of the CMCC syncline and has a N-facing half-graben geometry (Fig. 4.4a). The Gediz and Büyük Menderes graben are associated with a number of geothermal fields and Miocene to Recent volcanic activity, both of which phenomena have been associated with the emplacement of mantle-derived melts into the lower crust [*Seyitoglu et al.*, 1997; *Özgür et al.*, 1998].

In the internal part of the CMCC, the regional foliation, which formed in ductile flow, defines a map-scale E-trending symmetric syncline with a wavelength of ~45 km and an amplitude of ~10 km. The syncline is limited to the CMCC; in the Gördes Massif to the north and the Çine Massif to the south, the regional foliation is basically flat-lying (Fig. 4.4a).

4.4 Cooling history of the CMCC

Samples for apatite fission-track thermochronology were collected along a N-S transect across the Anatolide belt, from Milas in the south to Simav in the north (Figs. 4.2 and 4.4b). The transect parallels the regional displacement direction during exhumation of the belt [*Hetzel et al.*, 1995]. Sampling in this fashion results in a less ambiguous integration and interpretation of thermochronologic and structural data than would otherwise be the case [*Gallagher et al.*, 1998].

Analysis of the samples was undertaken using the external-detector and zeta-calibration approach [*Hurford and Green*, 1982] and the ages were calculated by the central-age method of *Galbraith* [1992]. Twenty-nine apatite-fission-track analyses yielded apparent ages ranging between 27.9±1.2 Ma and 1.8±0.6 Ma . Accompanying apatite track length data is for the most part unimodal and is >14µm. This indicates a simple cooling history in which most samples cooled rapidly with respect to the period over which tracks accumulated (their apparent age) to temperatures below which little or no track annealing occurred (<60°C). In addition to the apatite results, three zircon fission-track analyses yielded central ages of 24.7±0.9 Ma, 24.2±1.1 Ma and 5.2±0.3 Ma. The apatite fission-track analyses have been used to produce cooling curves using the quantitative modeling approach of Gallagher [1995]. These cooling curves summarise the

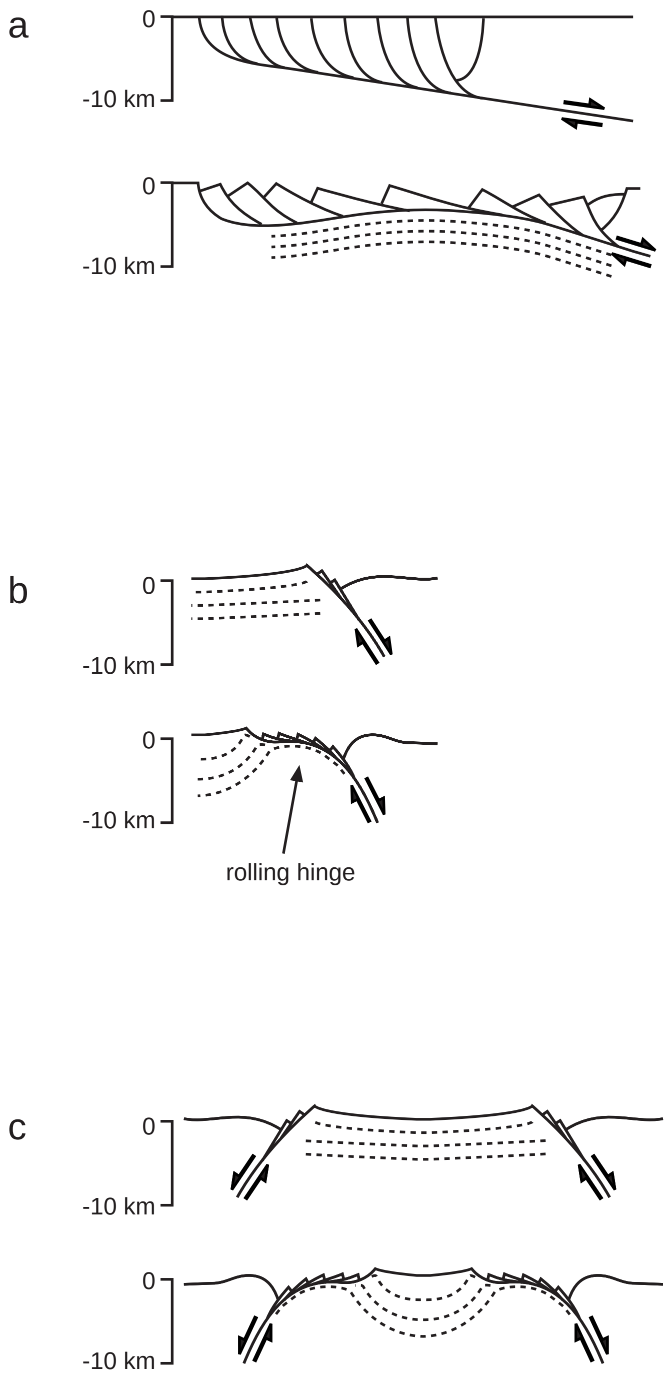

Figure 4.1:
Schematic cross sections for the development of detachment faults. (a) Listric detachment system with steep normal faults merging in a flat basal cutoff, which evolves into a gently domed structure (from *Wernicke* [1981]. (b) Rolling-hinge model in which the footwall of a steep normal fault is deformed by flexural uplift. Because the active fault plane becomes too flat to accommodate further brittle strain, new faults form in the hanging wall. Note how planar fabrics in the footwall become increasingly exhumed towards the detachment (from *Buck* [1988]). The term rolling hinge [*Axen et al.*, 1995] refers to the migration of the flexure towards the direction of displacement. (c) Conceptual model for the CMCC, with a symmetric array of two rolling-hinge detachment systems. Note thata syncline structure is superimposed on an initially flat-lying planar fabric.

variation that has been identified in cooling history along the transect, for different sections of the Anatolide belt. Where possible, these cooling curves have been further constrained with the additional zircon fission-track data and $^{39}Ar/^{40}Ar$ data from *Hetzel et al.* [1995] and *Hetzel and Reischmann* [1996] (Fig. 4.4c-f).

The cooling curves reveal a two-stage cooling history for the Anatolide belt. (1) The earliest phase of cooling occurred during the late Oligocene and ended in the early to middle Miocene. It affected the Gördes and Çine Massifs (Fig. 4.4c) and the higher levels of the nappe pile in the present-day Kücük Menderes graben (Fig. 4.4e). During this period, temperatures within much of the CMCC remained above ~110°C. A potential constraint on the timing for the youngest possible cessation of this cooling phase is provided by the analysis of three samples collected from a klippen above the Güney detachment. This klippen belongs structurally to the Çine Massif from below which the CMCC emerged. Unlike the other samples from the Çine Massif, all of which had cooled to below ~60°C by the early Miocene, quantitative modeling of the fission-track data reveals that these three samples remained above ~110°C until ~15 Ma at which time they cooled to ~90°C. (2) The second phase of cooling is restricted to the CMCC and is marked by cooling in the footwall of the two detachments to temperatures below ~60°C (Fig. 4.4d and f). Initial cooling is moderately well constrained by the $^{39}Ar/^{40}Ar$ and zircon fission-track analyses from the footwall to the Kuzey detachment. These data indicate accelerating cooling from ~15 Ma onwards. Final cooling to below ~60°C, defined by the apatite fission-track data from the footwall of the Kuzey detachment, occurred during the Plio-Pleistocene. This is coincident with final cooling in the klippen from above the Güney detachment. Since it is physically reasonable to suppose that cooling in the footwall of this structure did not predate the cooling in the overlying klippen, this timing is taken to be the same for the footwall rocks.

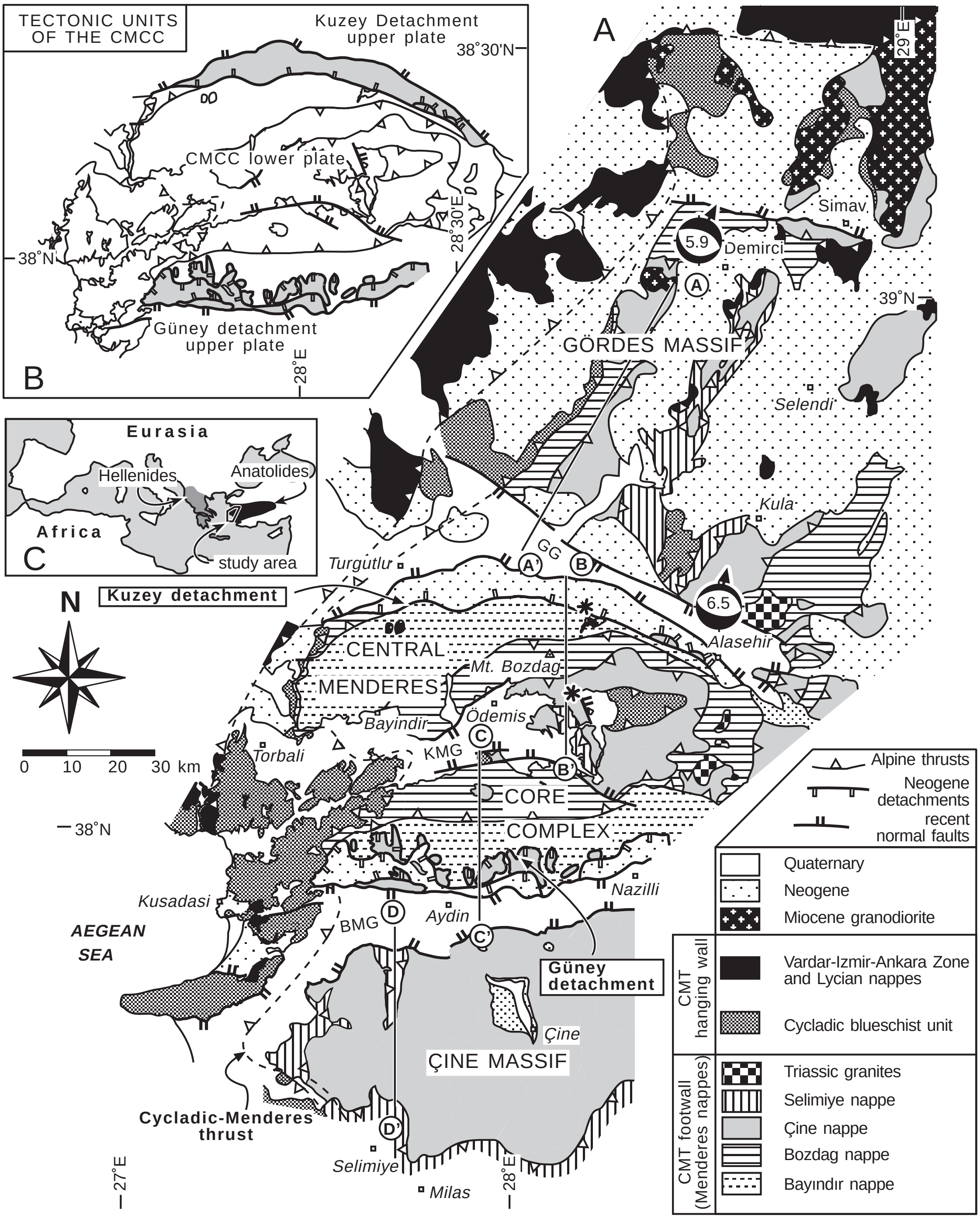

Figure 4.2:
(a) Tectonic map of the Anatolide belt in western Turkey. Circled letters refer to cross sections A-A' to D-D' in Figure 3A; asterisks refer to a high-grade orthogneiss used as a marker to estimate down-dip displacement at the Kuzey detachment; location, fault-plane solutions (lower-hemisphere focal projections with compressional quadrants shaded), surface magnitude and slip vectors of the March, 1969 Demirci and Alasehir earthquakes [*Eyidogan and Jackson*, 1985]. Abbreviations: GG = Gediz graben, KMG = Küçük Menderes graben, BMG = Büyük Menderes graben.
(b) Area of the upper plate of the Kuzey and Güney detachments.
(c) Location of the study area in the Mediterranean.

4.5 Discussion

The controls on exhumation of the Çine and Gördes Massifs and the processes responsible for the observed cooling cannot be adequately addressed with the available structural and thermochronologic data. What the data does provide, however, is a point of comparison between these two massifs, whose presently outcropping surfaces were at, or close to, the Earth's surface by the early Miocene, and the subsequent exhumation of the CMCC. In effect, the Çine and Gördes Massifs can be viewed as being 'pinned' to the Earth's surface, providing a fixed framework in time and space to consider the subsequent emergence of the CMCC.

Since the middle Miocene, the age pattern in the axial part of the CMCC was modified by a second stage of exhumation. Related cooling ages become progressively younger towards the detachment faults and jump to older ages in their hanging walls. This is because breakaway along both detachment faults brought successively deeper and hotter portions of the nappe pile of the CMCC from beneath the Çine and Gördes Massifs as illustrated by the converging cooling curves in Figure 4.4 (the Earth's surface acts as a near-isothermal boundary to the system).

The syncline structure and the brittle detachment systems are likely to be related structures. Unloading along the detachments induced upward flexuring of the upper crust and thus the presently exposed detachment surfaces were rotated to lower angles during progressive exhumation. One consequence of the rolling-hinge model described by *Lavier et al.* [1999] is the creation of significant relief in the footwall of the modeled fault. The creation of relief tends to promote erosion [*Ahnert*, 1970; *Summerfield*, 1991] and this leads to isostatic readjustment in the footwall. The denudational unloading acts together with the tectonic unloading, as predicted from the rolling-hinge model, to first flatten and then fold the footwall rocks. As these mechanisms act in concert along the emerging northern and southern margins of the CMCC, they

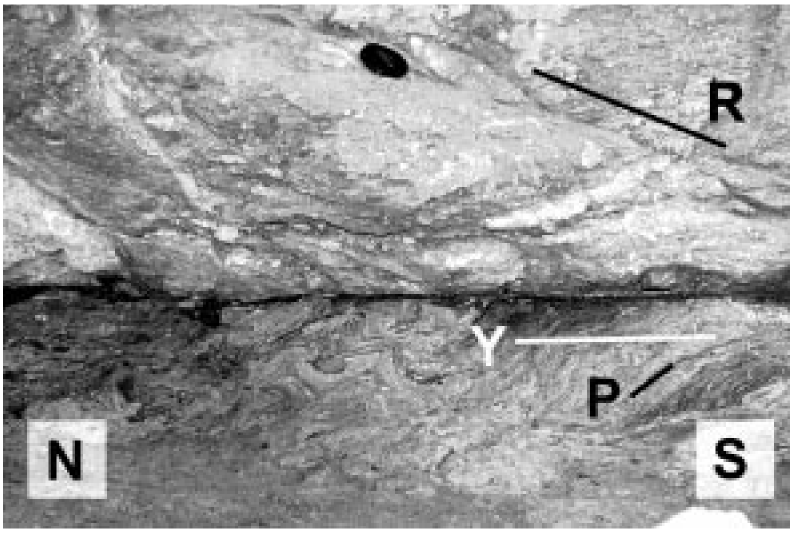

Figure 4.3: (a) Cataclastic shear zone at the base of the Güney detachment system NW of Aydın. In the outcrop both the hanging-wall rock unit, consisting of orthogneisses, and the phyllitic mica schist of the Bayındır nappe forming the footwall show pronounced brittle deformation. A metre-thick zone of asymmetrically folded cataclasite (lower part) is cut by a discrete centimetre-thick gouge zone. The brittle shear plane fabrics in the orthogneiss costitute a composite planar fabric [*Chester and Logan*, 1987; *Cowan and Brandon*, 1994], where the gouge zone represents the Y–plane parallel to the shear-zone boundaries. There is also a set of south-dipping synthetic Riedel or R planes. The shear-sense is top-to-S. Location of outcrop: 37°57'48N; 27°40'39E.

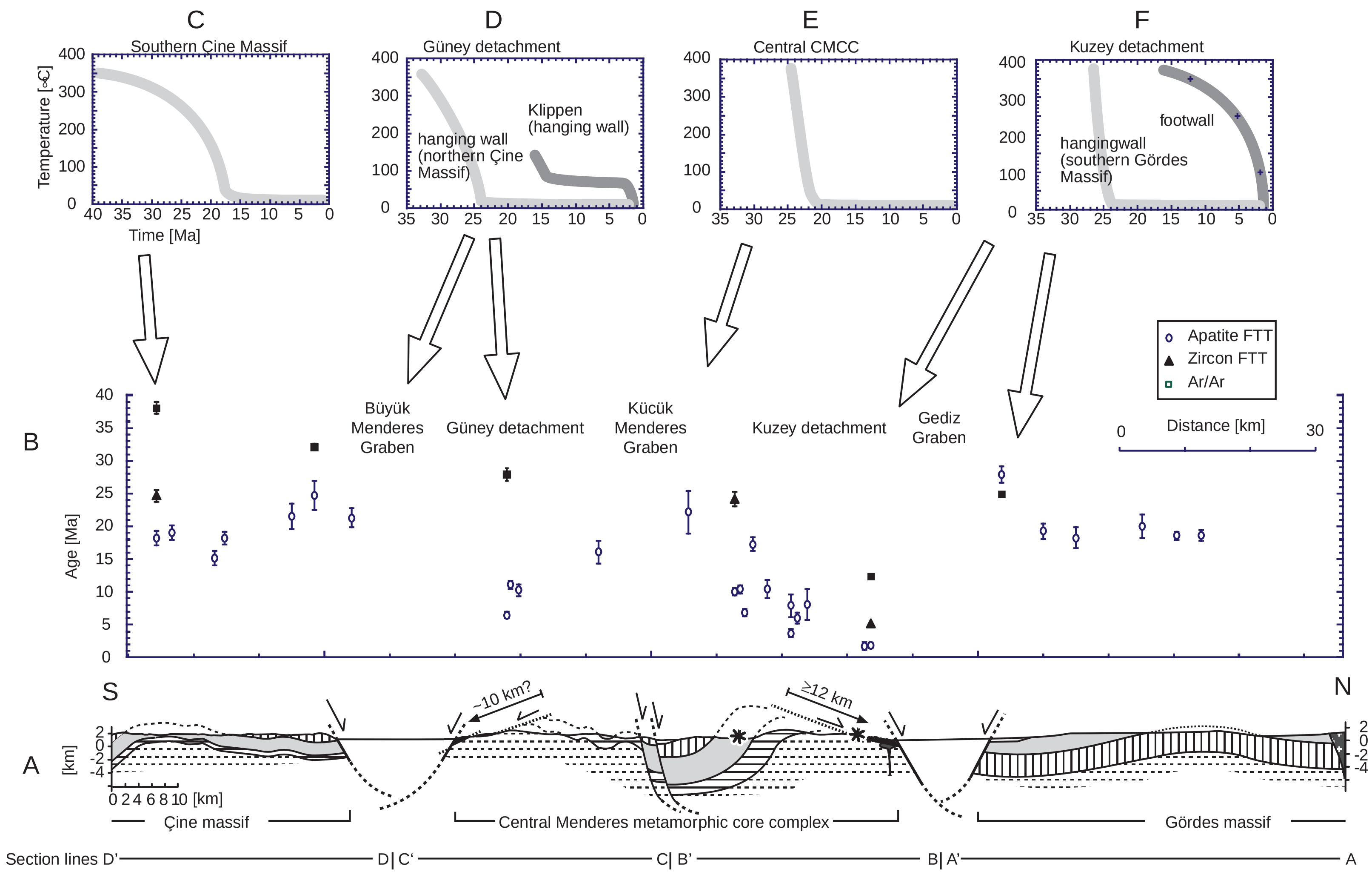

Figure 4.4:
Structural cross sections (a) (for position refer to Fig. 4.2) and cooling ages (b) in relation to elevation and position along this section of the CMCC (FTT = fission-track thermochronology). C-F: Cooling history from four areas along the cross section based on apatite- and zircon fission-track data and Ar/Ar data [*Hetzel et al.*, 1995; *Hetzel and Reischmann*, 1996]. The Çine and Gördes Massifs and also the central part of the CMCC cooled in the early and middle Miocene, therefore the Çine and Gördes Massifs can be viewed as being 'pinned' to the Earth's surface, providing a fixed framework in time and space to consider the subsequent emergence of the CMCC.

together cause the development of an intervening syncline. This feature is defined by both the regional foliation and the apparent apatite fission-track age time lines (Fig. 4.5a). The time lines may be viewed as successive positions of the ~110°C crustal isotherm for rapidly cooled rocks. The time lines end at the detachments and when the syncline is retro-deformed, the time lines straighten out and the detachment fault is equally rotated back into its steeper initial orientation (Fig. 4.5b). In the case of the CMCC, the initial angles are ~60° for the Kuzey and ~40° for the Güney detachment. The space between the faults with their restored dips and the trace of the present-day Earth's surface through the time lines represents the missing section of the footwall that has been removed by erosion. Even though this graphic approach to restoring the pre-flexure geometry of the rolling hinge is simplified, it shows that a low-angle origin of the detachments bounding the CMCC is unlikely. Furthermore, the amount of displacement and the overall footwall geometry of the Kuzey and Güney detachments are in agreement with the numerical rolling-hinge model of Lavier *et al.* [1999]. This is also true for the large topographic gradient, which has formed across the CMCC detachments. The maximum topography of ~3000 m between Bozdag mountain (2159 m) and the maximum basement depth in the Gediz graben (~1 km; Cohen *et al.*, [1995], suggest that flow in the lower crust has not been sufficient to accommodate the lateral pressure gradient across the normal faults. Nevertheless, the crust below the CMCC is unlikely to be cool and strong. A high regional upper crustal temperature gradient must be assumed by the low flexural rigidity of the upper crust, the Neogene volcanic activity, and the geothermal fields in the graben. Therefore, the structure and cooling history of the CMCC cannot be reconciled with models of lithospheric extension that limit compensation of topography to a mechanically decoupled lower crust. It is therefore suggest that lithospheric deformation associated with the rolling-hinge detachment systems in the CMCC also involves the upper mantle, which below the Gediz and Büyük Menderes graben may have been upwarped enough to allow localised decompression melting.

This model implies that the faults, which bound the Gediz and Büyük Menderes graben, formed as the two detachments were rotated into shallower orientations, i.e., detachment and graben faults are related. Thermal modeling suggests that cooling related to core-complex formation started at ~15 Ma and seismic data suggests that this process is still active. The inferred displacement of ~10-12 km suggest that the detachments operated at average slip rates of ~0.7-0.8 km Ma^{-1}.

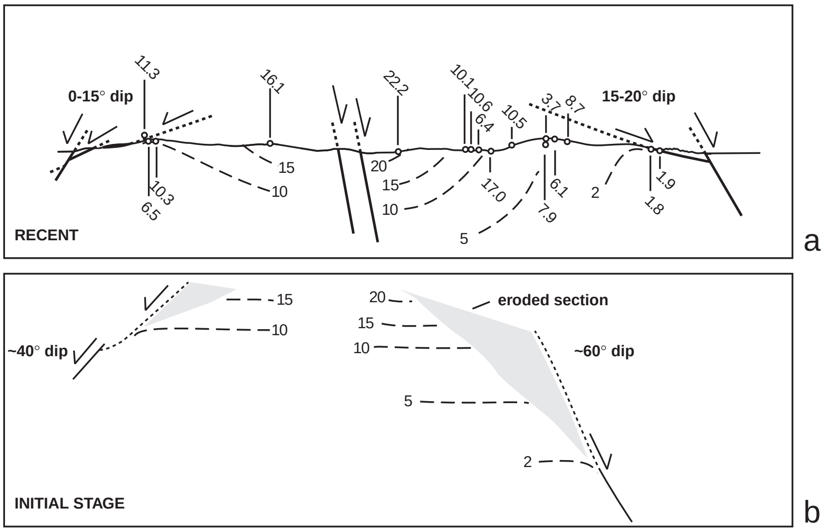

Figure 4.5:
Graphic reconstruction of the relation between cooling ages and the initial orientation of the detachment faults. (a) Projection of apatite fission-track data from Fig. 4.4 onto the cross-section plane. Dashed lines refer to extrapolated time lines subparallel to the regional foliation. (b) Retro-deformed cross section, where the detachment faults have been rotated together with the time lines to a flat pre-flexure orientation of the regional fabric. The grey-shaded areas represent the eroded section from the footwall of the detachments whose removal has contributed to the flexing and folding of the CMCC into its current synclinal form

4.6 Conclusions

The synthesis of the structure and cooling history of the CMCC suggests that its present-day geometry is controlled by a Miocene to Recent bivergent system of detachment faults. Each of the detachments shows a rolling-hinge geometry, which induced a large-scale syncline structure defined by the trace of the regional foliation. The topography across the CMCC detachments shows a gradient of up to 3 km, which suggests that deformation induced by the detachments is of lithospheric scale.

Chapter 5

General conclusions

The Anatolide belt of western Turkey consists of two distinct tectonic domains: the Menderes nappes, and the overlying Cycladic blueschist unit. Deformation-metamorphism relationships, fabric overprint and kinematic analysis outline a distinctly different tectonometamorphic history of both units prior to their D_{A3} juxtaposition during Eocene greenschist-facies metamorphism. The Cycladic blueschist unit displays a prograde Alpine D_{A1} fabric, which was overgrown by a high-pressure mineral assemblage. The onset of D_{A2} occurred during initial decompression of this high-pressure event and is associated with top-to-NE shearing. The subsequent top-to-S greenschist-facies D_{A3} event affected the Cycladic blueschist unit and the Menderes nappes together. Within the Menderes nappes D_{A3} is well constrained by overprinting relations and cross-cutting of deformation fabrics within the Granitoids of the Çine and Bozdag nappes. A first set of structures (D_{PA}) formed during amphibolite-facies metamorphism in the Proterozoic and is likely to be related to internal imbrication in the Menderes nappes. The second set of structures overprints D_{PA} and is interpreted to be identical with D_{A3} in the Cycladic blueschist unit, because it is similar in orientation, kinematics and metamorphic grade.

Late during D_{A3} the contact between the Cycladic blueschist unit and the Menderes nappes, the Cycladic-Menderes thrust, formed. The CMT defines an out-of sequence ramp structure, which cuts up-section through Menderes nappes towards the south. In the Cycladic blueschist unit, late D_{A3} fabrics associated with the CMT crosscut high-pressure D_{A2} structures. In the footwall, D_{PA} structures in the Bozdag nappe were deformed by the CMT. The Cycladic blueschist unit was exhumed by ~35 km before the CMT formed in the Eocene. D_{A2} structures aided this early exhumation, either by vertical ductile thinning, normal faulting, or a combination of both.

The different tectonometamorphic histories of the Cycladic blueschist unit and the Menderes nappes units preclude the model that both domains belonged to the same continent prior to the Alpine orogeny. This not only contradicts that the 'Median Aegean crytalline belt' of *Dürr et al.* [1978] extends into Turkey, but also questions a connection of the Anatolide-Tauride platform with Apulia [*Sengör and Yilmaz*, 1981]. The observation that the Cycladic blueschist unit is situated on top of the Menderes nappes further has implications for the age of metamorphism and for the palaeogeographic position of the overlying Lycian nappes. High-pressure metamorphism in the Lycian nappes should be older than in the Cycladic blueschist unit and therefore be late Cretaceous in age because orogenic development progressed structurally downward. The tectonic position of the Lycian nappes above the Cycladic blueschist unit further implies that the Lycian nappes originated from a position towards the hinterland of the Cycladc blueschists. The Lycian nappes could thus have been part of Adria or Sakarya or part of a continental fragment rifted off from Adria or Sakarya. They cannot, however, have been part of a continuous Anatolide-Tau-

ride platform as proposed by *Sengör and Yilmaz* [1981].
Incipient cooling of the Alpine nappe pile after D_{A3} contraction occurred in the Eocene along the southern margin of the Anatolide belt [Hetzel and Reischmann, 1996]. By the early Miocene the upper levels of the Alpine nappe pile, which today are exposed in the Çine and Gördes Massifs, slowly had cooled to earth surface temperature.
Since the middle Miocene, the cooling age pattern obtained by low-temperature thermochronology and the structure of the central Anatolide belt were modified by a second stage of exhumation governed by a D_{A5} bivergent detachment system, which formed the Central Menderes metamorphic core complex. The syn-extensional ductile fabrics exposed in the footwall of the Kuzey detachment [*Hetzel et al*., 1995b] predate this second cooling stage by at least four million years and are therefore interpreted to represent a separate extensional event D_{A4}.
Breakaway along the N-down Kuzey detachment and the S-down Güney detachment brought successively deeper and hotter portions of the nappe pile of the CMCC from beneath the Çine and Gördes Massifs, while several hundred meters of alluvial sediments were accomodated in supra-detachment basins. Each of the detachments shows a rolling-hinge geometry, which by the symmetrical arrangement of the detachments resulted in a large-scale syncline structure defined by the trace of the D_{A3} foliation. Thermal modeling suggests that cooling related to core-complex formation started at ~15 Ma and seismic data suggests that this process is still active. The inferred displacement of ~10-12 km implies that the detachments operated at average slip rates of ~0.7 to 0.8 km Ma^{-1}. Topography across the CMCC detachments shows a high relief of up to 3 km, which suggests that deformation induced by the detachments is of lithospheric scale.

Chapter 6

References

Ahnert, F., Functional relationships between denudation, relief and uplift in large mid-latitude drainage basins, Amer. J. Sci., 268, 243-263, 1970.

Altherr, R., and E. Seidel, Speculations on the geodynamic evolution of the Attic-Cycladic crystalline complex during alpidic times, in Geology of the Aegean region, Proceedings VI Colloq, Athens., edited by Kallergis, G., pp. 347-351, Institute of Geology and Mineral Exploration, 1977.

Altherr, R., M. Schliestedt, M. Okrusch, E. Seidel, H. Kreuzer, W. Harre, H. Lenz, W. I., and G.A. Wagner., Geochronology of high-pressure rocks on Sifnos (Cyclades, Greece), Contrib. Mineral. Petrol., 70, 245-255, 1979.

Altherr, R., H. Kreuzer, I. Wendt, H. Lenz, G.H. Wagner, J. Keller, W. Harre, and A. Höhndorf, A late Oligocene/early Miocene high temperature belt in the Attic-Cycladic crystalline complex (SE Pelagonian, Greece), Geol Jb, E23, 97-164, 1982.

Aubouin, J., Contribution a l'étude de la Grèce septrionale; les confins de l'Epire et de la Thessalie, Ann. géol. Pays Hellèn., 10, 1-483, 1959.

Avigad, D., and Z. Garfunkel, Uplift and exhumation of high-pressure metamorphic terrains: the example of the Cycladic blueschist belt (Aegean Sea), Tectonophys., 188, 357-372, 1991.

Avigad, D., A. Matthews, B.W. Evans, and Z. Garfunkel, Cooling during the exhumation of a blueschist terrane: Sifnos, Greece, Eur. J. Mineral., 4, 619-634, 1992.

Avigad, D., Z. Garfunkel, J. Jolivet, and J.M. Azañón, Back arc extension and denudation of Mediterranean eclogites, Tectonics, 16, 924-941, 1997.

Axen, G.J., J.M. Bartley., and J. Selverstone, Structural expression of a rolling hinge in the footwall of the Brenner Line normal fault, eastern Alps, Tectonics, 14, 1380-1392, 1995.

Axen, G.J., J. Selverstone, T. Byrne, and J.M. Fletcher, If the strong crust leads, will the weak crust follow?, GSA today, 8/12, 1-8, 1998.

Bernoulli, D., P.C. de Graciansky, and O. Monod, The Extension of the Lycian nappes (SW Turkey) into the southeastern Aegean islands, Eclogae geol. Helv., 67, 39-90, 1974.

Berthé, D., P. Choukroune and P. Jegoutzo, Orthogneiss, mylonite and non-coaxial deformation of granites: the example of the South Armorican shear zone, J. struct. geol., 1, 31-42, 1979.

Block, L., and L. Royden, Core complex geometries and regional scale flow in the lower crust, Tectonics, 9, 557-567, 1990.

Bozkurt, E., Metamorphism of Palaeozoic schists in the southern Menderes Massif: filed, petrographic, textural and microstructural evidence, Tr. J. Earth. Sci., 5, 105-121, 1995.

Bozkurt, E., and G.R. Park, Southern Menderes massif: an incipient metamorphic core complex in western Anatolia, Turkey, J. Geol. Soc. London, 151, 312-216, 1994.

Bozkurt, E., G.R. Park, and J.A. Winchester, Evidence against the core/cover interpretation of the southern sector of the Menderes massif, west Turkey, Terra Nova, 5, 445-451, 1993.

Bozkurt, E., and R.G. Park, Evolution of a mid-Tertiary extensional shear zone in the southern Menderes Massif, western Turkey, Bull. Soc. géol. France, 168, 3-14, 1997a.

Bozkurt, E., and R.G. Park, Microstructures of deformed grains in the augengneiss of southern Menderes massif (western Turkey) and their tectonic significance, Geol. Rdsch., 86, 103-119, 1997b.

Bröcker, M., H. Kreuzer, A. Matthews, and M. Okrusch, 40Ar/39Ar and oxygen isotope studies of polymetamorphism from Tinos Island, Cycladic blueschist belt, Greece, J. met. Geol., 11, 223-240, 1993.

Bröcker, M., and M. Enders, U—Pb zircon geochronology of unusual ecglogite-facies rocks from Syros and Tinos (Cyclades, Greece), Geol. Mag., 136, 111-118, 1999.

Brunn, J.H., Contribution a l'étude géologique du Pinde septentrional et d'une partie de la Macédonie Occidentale, Ann. géol. Pays Hellèn., 7, 1-358, 1956.

Buck, W.R., Flexural rotation of normal faults, Tectonics, 7, 959-973, 1988.

Buck, W.R., Modes of continental lithosperic extension, J. Geophys. Res., 96, 20161-20178, 1991.

Buick, I.S., The late-Alpine evolution of an extensional shear zone, Naxos, Greece, J. geol. Soc. London, 152, 639-654, 1991.

Candan, O., Blueschist relics in the Mesozoic cover series of the Menders Massif and correlations with Samos Island, Cyclades, Schweiz. Mineral. Petrogr. Mitt., 77, 95-99, 1997.

Candan, O., and Ö.O. Dora, The generalised map of the Menderes Massif, Department of Geological Engineering, Dokuz Eylül University Bornova, Izmir, 1998.

Candan, O., O.Ö. Dora, N. Kun, C. Akal, and E. Koralay, Aydın dagları (Menderes Masifi) güney kesimindeki allokton metamorfik birimler (Allochtonous metamorphic units at the southern part of Aydin Mountains, Menderes Massif, in turkish}, Bull. Tur. Assoc. Petrol. Geol., 93-110, 1992.

Candan, O., O.Ö. Dora, S. Dürr, and R. Oberhänsli, Erster Nachweis von Granulit- und Eklogit-Relikten im Menderes-Massiv / Türkei, Göttinger Arb. Geol. Paläont., Sb1, 217-220, 1994.

Chen, G., M. Okrusch, and W. Sauerschell, Polymetamorphic evolution of high-pressure rocks on Samos, Greece., Greece. Ann. Géol. Pays. Hell., 36, 799-915, 1995.

Chester, F.M., and J.M. Logan, Composite planar fabric of gouge from the Punchbowl Fault, California, J. Struct. Geol., 9, 612-634, 1987.

Cocherie, A., C. Guerrot, and P.H. Rossi, Single zircon dating by step-wise Pb-evaporation: Comparison with other geochronological techniques applied to the Hercynian granites of Corsica, Chem. geol., 101, 131-141, 1992.

Cohen, H.A., C.J. Dart, H.S. Akyüz, and A. Barka, Syn-rift sedimentation and structural development of the Gediz and Büyük Menderes graben, western Turkey, J. Geol. Soc . London, 152, 629-638, 1995.

Collins, A.S., and A.H.F. Robertson, Lycian mélange, southwest Turkey: An emplaced Cretaceous accretionary complex, Geology, 25, 255-258, 1997.

Collins, A.S., and A.H.F. Robertson, Process of late Cretaceous to late Miocene episodic thrust-sheet translation in the Lycian Taurides, J. Geol. Soc. Lond., 155, 759-772, 1998.

Cowan, D.S., and M.T. Brandon, A symmetry-based method for kinematic analysis of large-slip brittle fault zones, Amer. J. Sci., 294, 257-306, 1994.

Cowie, P.A., and C.H. Scholz, Displacement-lenght scaling relationships for faults: data synthesis and discussion, J. Struct. Geol., 14, 1149-1156, 1992.

Dannat, C., Geochemie, Geochronologie und Nd-Sr-Isotopie der granitoiden Kerngneise des Menderes-Massivs, SW-Türkei, PhD thesis, Johannes Gutenberg-Universität Mainz, 1997.

Davis, G.A., and G.S. Lister, Detachment faulting in continental extnsion; perspectives from the southwestern U.S. Cordillera, in Processes in continental lithosperic deformation, Spec. P. Geol. Soc. Amer., 218, edited by S.P. Clark Jr. et al., 133-159, 1988.

Dixon, J.E., and A.H.F. Robertson, The geologocal evolution of the eastern Mediterranean, Geol. Soc. Spec Publ, 17, 1984.

Dora, O.Ö., O. Candan, S.H. Dürr, and R. Oberhänsli, New evidence of the geotectonic evolution of the Menderes Massif, Proc. Int. Earth Sci. Colloq. Aegean Reg., 1995.

Dürr, S.H., R. Altherr, J. Keller, M. Okrusch, and E. Seidel, The Median Aegean Crystalline belt: stratigraphy, structure, metamorphism, magmatism, in Alps, Appenines, Hellenides, edited by Cloos, H., D. Roeder, K. Schmidt, 455-477, Schweitzerbart, Stuttgart, 1978.

Emre, T., and H. Sözbilir, Field evidence for metamorphic core complex, detachment faulting and accomodation faults in the Gediz and Büyük Menderes Grabens, Western Anatolia, Proc. Int. Earth Sci. Colloq. Aegean Reg., 1995, 1, 73-94, 1997.

Engel, M., and T. Reischmann, Single zircon geochronology of orthogneisses from Paros, Greece, Bull. Geol. Soc. Greece, 32/1, 91-99, 1998.

Erdogan, B., and T. Güngör, Stratigraphy and tectonic evolution of the Northern Margin of the Menderes Massif, Bull. Tur. Assoc. Petrol. Geol., 4, 9-34, 1992.

Eyidogan, H., and J. Jackson, A seismological study of normal faulting in the Demirci, Alasehir and Gediz earthquakes of 1969-70 in western Turkey: implications for the nature and geometry of deformation in the continental crust, Geophys. J. R. Astron. Soc-, 81, 569-607, 1985.

Forster, M.A., and G.S. Lister, Detachment faults in the Aegean core complex of Ios, Cyclades, Greece, in Exhumation Processes: Normal Faulting, Ductile Flow and Erosion, vol. 154, Spec. Publ. geol. Soc., edited by Ring, U., M. T. Brandon., G. S. Lister and S. D. Willett, London, 1999.

Franz, L., and M. Okrusch, Aragonite-bearing blueschists on Arki Island, Dodecanese, Greece, Eur. J. Mineral., 4, 527-537, 1992.

Galbraith, R.F., Statistical models for mixed ages, in 7th International Workshop on Fission Track Thermochronology, Abstr. with Programs, Philadelphia, 1992.

Gallagher, K., Evolving temperature histories from apatite fission track data, Earth Planet. Sci. Lett., 136, 421-435, 1995.

Gallagher, K., R. Brown, and C. Johnson, Fission track analysis and its applications to geological problems, Ann. Rev. Earth Planet. Sci., 26, 519-572, 1988.

Gans, P.B., An open-system, two-layer crustal stretching model for the eastern Great Basin, Tectonics, 6, 1-12, 1987.

Gautier, P., J.-P. Brun, R. Moriceau, J. Van den Driessche, D. Sokoutis, J. Martinod, and L. Jolivet, Gravity spreading of the Aegean lithosphere during the Neogene: geological constraints and physical models, Proc. Mediterranean basins, Inst. Petrole, Cérgy-Pontoise, 1, 1996.

Gessner, K., T. Güngör, U. Ring, and C.W. Passchier, Structure and crustal thickening of the Menderes massif, southwest Turkey, and consequences for large-scale correlations between Greece and Turkey, Bull. Geol. Soc. Greece, 32/1, 145-152, 1998.

Graciansky, P.C.de, Recherches géologiques dans le Taurus lycien occidental (Turquie du SW)., Thèse Univ. Paris-Sud (Orly), 896, 1-762, 1972.

Güngör, T., Stratigraphy and tectonic evolution of the Menderes Massif in the Söke-Selçuk Region, PhD thesis, Dokuz Eylül University, Izmir, 1998.

Hancock, P.L., and A.A. Barka., Kinematic indicators on active normal faults in western Turkey, J. Struct. Geol., 9, 573-584, 1987.

Hanmer, S., and C.W. Passchier, Shear - Sense Indicators: A Review, Geol. Surv. Can. P., 90/17, 1-72, 1991.

Hatzfeld, D., I. Kassara, D. Panagiotopoulos, D. Amorese, K. Makropoulos, G. Karakaisis, and O. Coutant, Microseismicity and strain pattern in Northwestern Greece, Tectonics, 14, 773-785, 1996.

Hetzel, R., and U. Ring, Extensional collapse of the Menderes Massif, western Turkey: preliminary data, Terra Nostra, 1, 18, 1993.

Hetzel, R., C.W. Passchier, U. Ring, and O.Ö. Dora, Bivergent extension in orogenic belts: the Menderes massif, southwestern Turkey, Geology, 23, 455-458, 1995a.

Hetzel, R., U. Ring, C. Akal and M. Troesch, Miocene NNE-directed unroofing in the Menderes Massif, southwest Turkey, J. Geol. Soc. London, 152, 639-654, 1995b.

Hetzel, R., and T. Reischmann, Intrusion age of Pan-African augen gneisses in the southern Menderes massif and the age of cooling after Alpine ductile extensional deformation., Geol. Mag., 565-572, 1996.

Hetzel, R., R.L. Romer, O. Candan, and C.W. Passchier, Geology of the Bozdag area, central Menderes massif, SW-Turkey: Pan African basement and Alpine deformation, Geol. Rdsch., 87, 394-380, 1998.

Jacobshagen, V., Geologie von Griechenland, 363 pp., Borntraeger, Berlin, 1986.

Hurford, A.J., and P.F. Green, A users' guide to fission track dating, Earth Planet. Sci. Lett., 59, 343-354, 1982.

Isik, V., and O. Tekeli, Structure of lower plate rocks in metamorphic core complex: Northern Menderes Massif, Western Turkey, Geol. Rdsch., in press.

Jaeckel, P., A. Kröner, S.L. Kamo, G. Brandl, and J.I. Wendt, Late Archean to early Proterozoic granitoid magmatism and high-grade metamorphism in the central Limpopo belt, South Africa, J. Geol. Soc. London, 154, 25-44, 1997.Hetzel, R., U. Ring, C. Akal, and M. Troesch, Miocene NNE-directed extensional unroofing in the Menderes massif, southwestern Turkey, J. Geol. Soc. London, 152, 639-654, 1995.

Karabinos, P., An evaluation of the single-grain zircon evaporation method in highly discordant samples, Geochim. Cosmochim. Acta, 61, 2467-2474, 1997.

Ketin, I., Tectonic units of Anatolia, Bull. Miner. Res. Expl. Inst. Turkey, 66, 23-34, 1966.

Kober, B., Whole-grain evaporation for 207Pb/206Pb-age-investigations on single zircon using a double-filament thermal ion source, Contrib. Mineral. Petrol., 93, 482-490, 1986.

Kober, B., Single-zircon evaporation combined with Pb+-emitter bedding for 207Pb/206Pb-age investigations using thermal ion mass spectroscopy, and implications to zirconology, Contrib. Mineral. Petrol., 96, 63-71, 1987.

Koralay, E., M. Satır, and O.Ö. Dora, Geochronologic evidence of Triassic and Precambrian magmatism in the Menderes Massif, west Turkey, Abstr. 3rd Int. Turk. Geol. Symp. Ankara, 1, 285, 1998.

Kröner, A., C.R. Byerly, and D.R. Lowe, Chronology of early Archaean granite-greenstone evolution in the Barberton Mountain Land, South Africa, based on precise dating by single zircon evaporation, Earth Planet. Sci. Lett, 103, 41-54, 1991.

Kröner, A., and E. Hegner, Geochemistry, single zircon ages and Sm-Nd systematics of granitoid rocks from the Gory Sowie (Owl Mts), Polish West Sudetes: evidence for early Palaeozoic are-related plutonism, J. Geol. Soc. London, 155, 711-724, 1998.

Lackmann, W., P-T Entwicklung von Metapeliten des zentralen Menderes Massivs, Türkei, Diploma thesis, Johannes Gutenberg-Universität Mainz, 1997.

Laslett, G.M., P.F. Green, I.R. Duddy, and A.J.W. Gleadow, Thermal annealing of fission tracks in apatite. 2. A quantitative discription, Chem. Geol., 65, 1-13, 1987.

Lavier, L.L., W.R. Buck, and A.N.B. Poliakov, Self-consistent rolling-hinge model for the evolution of large-offset low-angle normal faults, Geology, 27, 1127-1130, 1999.

Le Pichon, X., N. Chamot-Rooke, S. lallement, R. Noomen, and G. Veis, Geodetic determination of the kinematics of central Greece with respect to Europe: implictions for eastern Mediterranean tectonics, J. Geophys. Res., 100 (B7), 12675-12690, 1995.

Lips, A.L.W., Temporal constraints on the kinematics of the destabilization of an orogen; syn- to post-orogenic collapse of the Northern Aegean region, Geol. Ultraiect., 166, 223 pp, 1998.

Lister, G.S., G. Banga, and A. Feenstra, Metamorphic core complexes of Cordilleran type in the Cyclades, Aegean Sea, Greece, J. Struct. Geol., 12, 221-225, 1984.

Lister, G.S., and A. Raouzaios, The tectonic significance of a porphyroblastic blueschist facies overprint during Alpine orogenesis, Sifnos, Aegean Sea, Greece., J. Struct. Geol., 18, 1996.

McKenzie, D.P., Active tectonics of the Mediterranean Region, Geophys. J. R. Astron. Soc., 30, 109-185, 1972.

McKenzie, D.P., Active tectonics of the Alpine-Himalaya Belt, the Aegean sea and surrounding regions, Geophys. J. R. Astron. Soc., 55, 217-254, 1978.

Oberhänsli, R., P. Monié, O. Candan, F.C. Warkus, J. Partzsch, and O.Ö. Dora, The age of blueschist metamorphism in the Mesozoic cover series of the Menderes Massif, Schweiz. Mitt. Mineral. Petrol., 78, 309-316, 1998.

Özgür, N., A. Pekdeger, M. Wolf, W. Stichler, K.P. Seiler, and M. Satir, Water-Rock Interaction, in 9th International Symposium on Water-Rock Interaction, edited by G.B. Arehart and J.R. Hulston, Balkema, Rotterdam, 1998.

Okay, A.I., Stratigraphic and metamorphic inversions in the central Menderes Massif: a new structural model, Int. J. Ea. Sci., (in press).

Okay, A., N.B.W. Harris, and S.P. Kelley, Exhumation of blueschists along a Tethyan suture in northwest Turkey, Tectonophysics, 285, 275-299, 1998.

Okrusch, M., and M. Bröcker, Eclogite facies rocks in the Cycladic blueschist belt, Greece: A review, Eur. J. Min., 2, 451-478, 1990.

Paréjas, E., La tectonique transversale de la Turquie, Rev. Fac. Sci. Univ. Istanbul Ser. B, 5, 133-244, 1940.

Partzsch, J., R. Oberhänsli, O. Candan, and F.C. Warkus, The evolution of the central Menderes Massif, west Turkey: a complex nappe pile recording 1.0 Ga of geological history, Freiberger Forschungsh., C471, 166-168, 1998.

Passchier, C.W., and C. Simpson, Porphyroclast systems as kinematic indicators, J. Struct. Geol., 8, 831-844, 1986.

Passchier, C.W., and R.A.W. Trouw, Microtectonics, 1-289 pp., Springer, Berlin, 1996.

Raouzaios, A., G.S. Lister, and D.A. Foster, Oligocene exhumation and metamorphism of eclogite-blueschists from the island Sifnos, Cyclades, Greece., Geol. Soc. Austral. abstracts, 41, 358, 1996.

Reischmann, T., Single zircon Pb/Pb dating of tectonic units from the Metamorphic Complex of Naxos, Greece, Terra Nova, 9, 496, 1997.

Reischmann, T., Pre-Alpine origin of tectonic units from the metamorphic complex of Naxos, Greece, identified by single zircon Pb/Pb dating, Bull Geol Soc Greece (Proc 8th Int Congr Patras May 1998), 32, 101-111, 1998.

Reischmann, T., and S. Loos, The Evolution of the southern Menderes Massif in SW Turkey as revealed by Zircon dating, J. Geol. Soc. London, 1999.

Reischmann, T., A. Kröner, W. Todt, S. Dürr, and A.M.C. Sengör, Episodes of crustal growth in the Menderes Massif, W Turkey, inferred from Zircon dating, Terra Abstr., 3, 34, 1991.

Ring, U., S. Laws, and M. Bernet, Structural analysis of a complex nappe sequence and late orogenic basins from the Aegean Island of Samos, Greece, J. Struct. Geol., 1575-1602, 1999.

Ring, U., K. Gessner, T. Güngör, and C.W. Passchier, The Menderes Massif of western Turkey and the Cycladic Massif in the Aegean — do they really correlate?, J. Geol. Soc. London, 155, 3-6, 1999.

Ring, U., A. Willner, and W. Lackmann, Nappe stacking and clockwise versus anticlockwise pressure-temperature paths: an example from the Menderes nappes of western Turkey., J. metam. Geol., 2000.

Robertson, A.H.F., J.E. Dixon, S. Brown, A.S. Collins, A. Morris, E. Pickett, I. Sharp, and T. Ustaömer, Alternative tectonic models for the late Palaeozoic—early Tertiary development of Tethys in the Eastern Mediterranean region, in Palaeomagnetism and Tectonics of the Mediterranean Region, vol. 105, Spec. Publs. Geol. Soc Londo., edited by Morris, A. and D.H. Tarling, pp. 239-263, London, 1996.

Schaffer, F., Das Maeanderthalbeben vom 20. September 1899, Mitteilungen der kaiserlichen und königlichen geographischen Gesellschaft Wien, 43, 221-230, 1900.

Schermer, E.R., D.R. Lux, and B.C. Burchfiel, Temperature-time history of subducted continental crust, Mount Olympos Region, Greece, Tectonics, 9, 1165-1196, 1990.

Scotford, D.M., Metasomatic Augen Gneiss in Greenschist Facies, Western Turkey, Geol. Soc. Am. Bull., 80, 1079-1094, 1969.

Seidel, E., H. Kreuzer, and W. Harre, A late Oligocene/early Miocene high pressure belt in the External Hellenides, Geol. Jb., E 23, 165-206, 1982.

Sengör, A.M.C., and Y. Yilmaz, Tethyan Evolution of Turkey: a plate tectonic approach, Tectonophys., 75, 181-241, 1981.

Sengör, A.M.C., M. Satir, and R. Akkök, Timing of the tectonic events in the Menderes massif, western Turkey: implications for tectonic evolution and evidence for Pan-African basement in Turkey, Tectonics, 3, 693-707, 1984.

Seyitoglu, G., D. Anderson, G. Nowell, and B. Scott, The evolution from Miocene potassic to Quaternary sodic magmatism in western Turkey: implications for enrichment processes in the lithospheric mantle, J. Volc. Geotherm. Res., 96, 127-147, 1997.

Sherlock, S., S. Kelley, S. Inger, N. Harris, and A. Okay, 40Ar-39Ar and Rb-Sr geochronology of high-pressure metamorphism and exhumation history of the Tavsanli Zone, NW Turkey, Contrib. Mineral. Petrol., 137, 46-58, 1999.

Spencer, J., Role of tectonic denudation in warping and uplift of low-angle normal faults, Geology, 12, 95-98, 1984.

Stacey, J.S., and J.D. Kramers, Approximation of terrestrial lead isotope evolution by a two-stage model, Earth Planet. Sci. Lett., 207-221, 1975.

Summerfield, M.A., Sub-aerial denudation of passive margins: regional elevation versus local relief models, Earth Planet. Sci. Lett., 102, 460-469, 1991.

Theye, T., and E. Seidel, Uplift-related retrogression history of aragonite marbles in Western Crete (Greece), Contrib. Mineral. Petrol., 114, 349-356, 1993.

Thomson, S.N., B. Stöckhert, H. Rauche, and M.R. Brix, Apatite fission-track thermochronology of the uppermost tectonic unit of Crete, Greece: implications for the post-Eocene tectonic evolution of the Hellenic subduction system, in Advances in Fission-Track Geochronology, edited by Van der Houte, P., De Corte, F., pp. 187-205, Kluwer Academic, Dordrecht, 1998.

Thomson, S.N., B. Stöckhert, and M.R. Brix, Miocene high-pressure metamorphic rocks of Crete, Greece: rapid exhumation by buoyant escape, in Exhumation Processes: Normal Faulting, Ductile Flow and Erosion, vol. 154, Spec. Publs. Geol. Soc London, edited by Ring, U., M. T. Brandon., G. S. Lister and S. D. Willett, London, 1999.

Tullis, J., and R.A. Yund, Dynamic recrystallisation of feldspar: a mechanism for ductile shear zone formation, Geology, 13, 238-241, 1985.

Tullis, J., and R.A. Yund, Transition from cataclastic flow to dislocation creep of feldspar: mechanisms and microstructures, Geology, 15, 606-609, 1987.

Tullis, J., and R.A. Yund, Diffusion creep in feldspar aggregates: experimental evidence, J. Struct. Geol., 13, 987-1000, 1991.

Verge, N., Oligo-Miocene extensional exhumation of the Menderes Massif, western Anatolia, Terra abstracts, 8, 117, 1995.

Voll, G., Recrystallisation of quartz, biotite and feldspars from Erstfeld to the Leventina nappe, Swiss Alps, and its geological significance, Schweiz. Mineral. Petrogr. Mitt., 56, 641-647, 1976.

Walcott, C.R., The Alpine evolution of Thessaly (NW) Greece and late Tertiary Aegean kinematics, Geol. Ultraiect., 162, 1-175, 1998.

Wernicke, B., Low-angle normal faulting in the Basin and Range province: nappe tectonics in an extending orogen, Nature, 291, 645-648, 1981.

Wernicke, B., Low-angle normal fault seismicity: A review, J. Geophys. Res., 100, 20159-20174, 1995.

Wernicke, B., and G.J. Axen, On the role of isostasy in the evolution of normal fault systems, Geology, 16, 848-851, 1988.

Wijbrans, J.R., and I. McDougall, 40Ar/39Ar dating of white micas from an Alpine high-pressure metamorphic belt on Naxos (Greece): resetting of the argon isotopic system., Contrib. Mineral. Petr., 93, 187-194, 1986.

Wijbrans, J.R., and I. McDougall, Metamorphic evolution of the Attic-Cycladic metamorphic belt on Naxos (Cyclades, Greece), J. Met. Geol., 6, 571-594, 1988.

Wijbrans, J.R., M. Schliestedt, and D. York, Single grain argon laser probe dating of phengites from the blueschist to greenschist transition on Sifnos (Cyclades, Greece), Contrib. Mineral. Pet., 104, 582-593, 1990.

Will, T., M. Okrusch, E. Schmädicke, and G. Chen, Phase relations in the greenschist-blueschist-amphibolite-eclogite facies in the system Na_2O-CaO-FeO-MgO-Al_2O_3-SiO_2-H_2O (NCF-MASH), with application to metamorphic rocks from Samos, Greece, Contrib. Mineral. Petrogr., 132, 85-102, 1998.

Will, T.M., Phase Diagrams and their application to determine pressure-temperature paths of metamorphic rocks, N. Jb. Miner. Ahb., 174, 103-130, 1998.

Willett, S.D., C. Beaumont, and P. Fullsack, Mechanical model for the tectonics of doubly vergent compressional orogens., Geology, 21, 371-374, 1993.

Yardley, B.W.D., An introduction to metamorphic petrology, 248 pp., Wiley, New York, 1989.